Null Synthesis and Implementation of Cylindrical Microstrip Patch Arrays

by

Philip Niemand

Submitted as partial fulfilment of the requirements for the degree

Ph.D (Electronic Engineering)

in the

Faculty of Engineering, Built Environment and Information Technology
University of Pretoria
Pretoria

November 2004

Null Synthesis and Implementation of Cylindrical Microstrip Patch Arrays

Philip Niemand

Prof. J. Joubert

Prof. J.W. Odendaal

Department of Electrical, Electronic and Computer Engineering

Ph.D (Electronic Engineering)

As the wireless communications networks expand, the number of both unwanted directional interferences and strong nearby sources increase, which degrade system performance. The signal-to-interference ratio (SIR) can be improved by using multiple nulls in the directions of the interferences while maintaining omnidirectional coverage in the direction of the network users. For the communication system considered, the interferences are static and their spatial positions are known. A non-adaptive antenna array is needed to provide spatial filtering in a static wireless environment. Omnidirectional arrays, such as cylindrical arrays, are the most suitable to provide the omnidirectional coverage and are capable of suppressing interferences when nulls are inserted in the radiation pattern.

In this thesis, a cylindrical microstrip patch antenna array is investigated as an antenna to provide an omnidirectional radiation pattern with nulls at specified angular locations to suppress interference from directional sources. Three null synthesis methods are described and used to provide the omnidirectional array pattern with nulls using the radiation characteristics of the cylindrical microstrip patch antenna elements. The orthogonal projection method is extended to incorporate the directive radiation patterns of the cylindrical microstrip patch elements. Using this method, an optimal pattern that minimises the squared pattern error with respect to the ideal pattern is obtained. Instead of only minimising the array pattern error, a multi-objective optimisation approach is also followed. The objective weighting method is applied in null pattern synthesis to improve the amplitude pattern characteristics of the cylindrical patch arrays. As a third null synthesis technique, a constraint optimisation method is applied to obtain a constrained pattern with the desired amplitude pattern characteristics. The influence of the array attributes on the characteristics of the amplitude patterns obtained from the null synthesis methods, is also studied.

In addition, the implementation of the cylindrical microstrip patch array is investigated. The influence of the mutual coupling on the characteristics of the null patterns of the cylindrical patch arrays is investigated utilising simulations and measurements. A mutual coupling compensation technique is used to provide matched and equal driving impedances for all the patch antenna elements given a required set of excitations. Test cases in which this technique is used, are discussed and the consequent improvements in the bandwidth and reflection coefficient of a linear patch arrays are shown. The characteristics of the resulting null pattern for the cylindrical microstrip patch array is also improved using the compensation technique.

Keywords: antenna, microstrip, array, cylindrical, null, synthesis, orthogonal, projection, coupling, compensation.

Acknowledgements

First of all I would like to dedicate this thesis to my Father in heaven who made it possible through his many blessings.

I would also like to thank my wife, Willemien, for her patience and support.

Special thanks to Johan Joubert and Wimpie Odendaal for their guidance and friendship.

Furthermore, I would like to thank everybody whose support and friendship made this thesis possible.

CONTENTS

CHAPTER 1

INTRODUCTION

1.1 Background

The demand for wireless communications services is growing at an extensive rate all over the world. The intensive development and wide application of new generations of personal communication systems and wireless local systems, have increased the need for new antenna designs [1]. As the wireless communications networks expand, the number of both unwanted directional interferences and strong nearby sources increase, which degrade system performance. Optimal antenna arrays play an important role in the improvement of communications systems by providing increased coverage through antenna gain control and interference rejection [2, 3]. A system consisting of an array and a processor can perform filtering in both space and frequency to reduce the sensitivity of the system to interfering directional sources.

There are many requirements that new communications systems pose on antennas. The most common are low cost, low weight and compact designs with high-performance radiation and impedance characteristics. Therefore uplink and downlink antennas undergo a lot of modifications and performance improvement [1]. In many wireless communications systems, the signal-to-interference ratio (SIR) is improved by using multiple nulls in the directions of the interferences while maintaining omnidirectional coverage in the direction of the network users. The nulls in the radiation pattern may be used to reduce the interference from strong nearby sources as well as co-channel interference by introducing nulls in the directions of surrounding communication sys-

tems.

For the communication system considered in this thesis, the interferences are static and their directions of arrival are known. A non-adaptive antenna array is needed to provide the spatial filtering in a static wireless environment. Multi-path scenarios and space-time filtering via an adaptive array are therefore not addressed.

Omnidirectional arrays, such as cylindrical arrays, are the most suitable to provide the omnidirectional coverage and are capable of suppressing interferences when nulls are inserted in the radiation pattern. Some examples of cylindrical arrays are shown in Figure 1.1.

Microstrip antennas, which the work in this thesis will focus on, are popular components in modern systems, since they are low in profile, light in weight and well suited for integration with microwave integrated circuits. They can also be made conformal to non-planar surfaces such as cylinders to form cylindrical arrays as shown in Figure 1.1(c).

This type of cylindrical array is also classified under conformal arrays of which the analysis and design can be divided into three areas [4]:

1. the analysis of the antenna element radiation pattern,
2. the array pattern analysis and synthesis to obtain the element excitations, and
3. the design of the radiators and the feed network to obtain the desired excitations.

The analysis of cylindrical microstrip patch antennas and arrays have been discussed in many publications [5–31]. The cavity model theory, method of moments, geometric theory of diffraction (GTD) and finite-element method have all been applied to obtain the resonant frequency, impedance behaviour and/or radiation pattern of a rectangular microstrip patch on a conducting cylinder. For electrically thin substrates, the cavity model has been shown to be sufficient to compute the characteristics of the patch antenna [23, 24, 29]. Hybrid modes are excited for electrically thick patches which require more accurate analysis methods [14]. When the radius of the cylinder is much larger than the operating wavelength, the effect of the curvature on the characteristics of the patch antennas may be neglected. For radii comparable to the operating wavelength, the input impedance, resonant frequency and radiation pattern of the patch antenna

are effected by the curvature. The cavity model [13] and a commercial finite difference time domain (FDTD) analysis program have been used during the design of the radiating element to incorporate the influences of the curvature [30]. The FDTD analysis program can also be utilised where electrically thick patches are considered to improve bandwidth and gain performance.

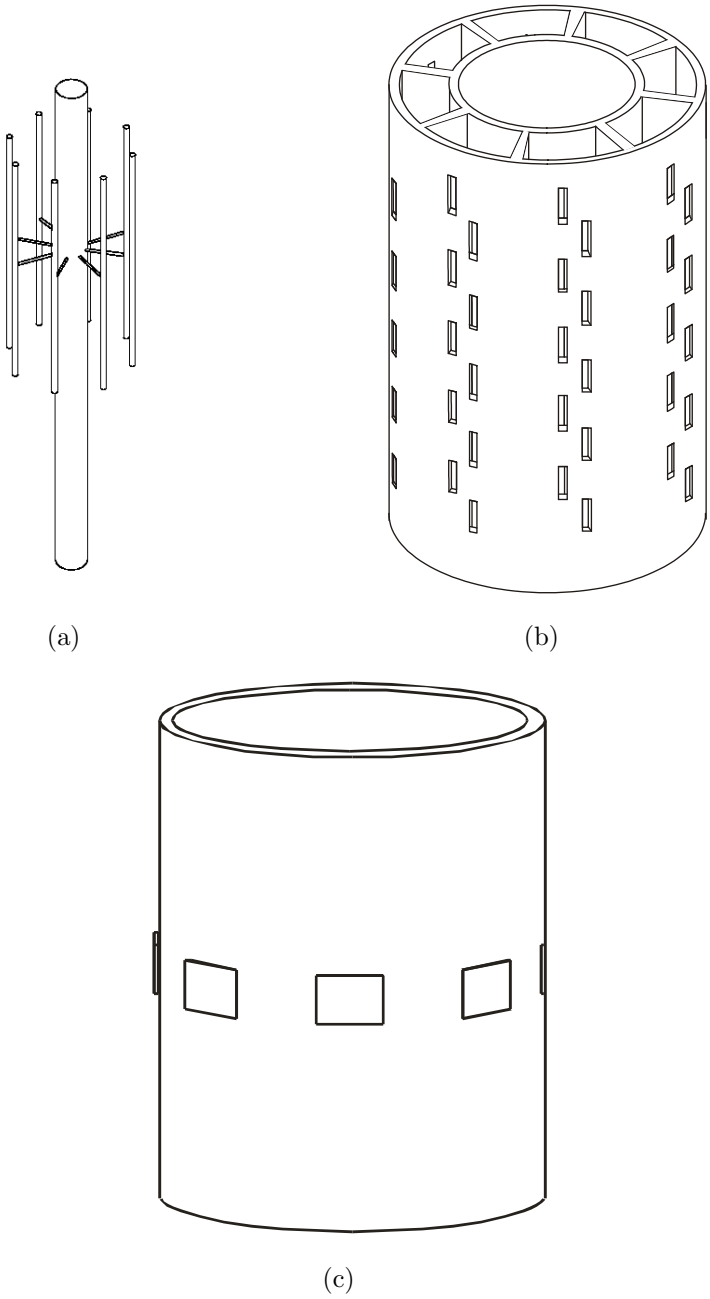

Figure 1.1: Cylindrical arrays: a) dipole array, b) slotted waveguide array and c) microstrip patch array

Previously, cylindrical microstrip patch arrays were extensively used for omnidirecitonal coverage [9,18] and the formation of beams in the far field radiation pattern [1,32–40]. Many techniques for the introduction of nulls in the far field radiation patterns of cylindrical arrays can be found in the open literature [41, 43–55]. Lim [43] proposed the introduction of a single null into an omnidirectional pattern by approximating an abrupt phase reversal in the phase pattern of the array. This phase reversal in the specified direction of the null also minimised the null width. An orthogonal projection method was introduced by Vescovo [50,51] to synthesise a desired radiation pattern for an equally spaced cylindrical array. Abele *et al* [53, 54] combined these two methods to synthesise multiple nulls in the omnidirectional pattern of a cylindrical array. An ideal null pattern with constant amplitude and an abrupt phase reversal at the desired location of each null was used in the orthogonal projection method. The null positions and depths could be controlled independently and some control could be exercised over the gain ripple and null width by utilising windowing functions.

All the above methods use radiating elements that are identical in radiation pattern, polarisation, gain and impedance. In conformal arrays, the elements, and consequently their radiation patterns, point in different directions and the element pattern cannot be factorised out of the array pattern to obtain an array factor [4,56,57]. Vescovo [56] also applied the projection method to an arc array of elements with directional radiation patterns. After a main beam was formed through the projection method, additional nulls were introduced in the pattern with null constraints to reduce the side lobe level.

The effect of mutual coupling between elements in an array is one of the most relevant problems in the synthesis of array antennas. Numerous methods to compute or represent the mutual coupling in linear and cylindrical microstrip patch arrays have been presented [17, 19, 24, 25, 29, 58–71]. The mutual coupling between the antenna elements modifies the element excitations and the driving input impedances of the antenna elements.

For arrays with wide band antenna elements and small mutual coupling between the elements, the measured radiation pattern characteristics may still be within the desired characteristics, although the mutual coupling was not taken into account during the design process of the array [32, 34–37, 39]. On the other hand, the consequent errors in the element excitations due to high mutual coupling may deteriorate the radiation pattern. This is especially true for a shaped or scanned beam, if the mutual coupling

is not compensated for in the design process [72, 73]. For the accurate computation of the sidelobe levels in a beam pattern, the mutual coupling was taken into account by Bartolic *et al* [1].

Null filling and null position errors also occur during null synthesis due to the mutual coupling [53, 74]. Various authors have presented techniques to compensate for the mutual coupling effect on a synthesised array pattern [54, 72–86]. At the array feed port, a mismatch occurs due to coupling [87], which may significantly degrade the performance of narrowband arrays. The driving impedances of the antenna elements resulting from radiation pattern correction methods remain unequal and the design of the feeding and matching network can be complicated. Another solution is to alter the individual element geometries physically in order to have equal driving impedances for the required element excitations [88, 89]. This method causes the feeding network to be much simpler.

1.2 Contributions

In this thesis, a cylindrical microstrip patch antenna array is investigated as an antenna to provide an omnidirectional radiation pattern with nulls at specified angular locations to suppress interference from directional sources. The null synthesis for the cylindrical microstrip patch array is presented by discussing the above three mentioned areas of array analysis and design.

Three null synthesis methods are described and used to provide the omnidirectional array pattern with nulls using the radiation characteristics of the cylindrical microstrip patch antenna elements. The desired element excitations are obtained from:

- the extension of the orthogonal projection method to incorporate the radiation patterns of the cylindrical microstrip patch antenna elements [90–92],
- the implementation of the objective weighting method for null pattern synthesis, and
- the application of a constraint optimisation method for the synthesis of null patterns with specified characteristics [92].

In addition, the implementation of the cylindrical microstrip patch array is investigated by:

- studying the effect of the mutual coupling on the desired null pattern [93, 94], and
- applying a technique to compensate for the mutual coupling between the cylindrical microstrip patch antenna elements to obtain the desired excitations [93,94].

1.3 Methodology

The null synthesis technique of Abele *et al* [53] is extended to incorporate the directive radiation patterns of the cylindrical microstrip patch elements. Using this method, an optimal pattern that minimises the squared pattern error with respect to the ideal pattern is obtained. The orthogonal projection method may not give an amplitude pattern with the desired characteristics (null depth, null width and ripple in the omni-region) for certain array configurations. Instead of only minimising the array pattern error, a multi-objective optimisation approach is followed [95–97]. The objective weighting method, previously applied in other fields of computational electromagnetic problems [96,97], is used to improve the amplitude pattern characteristics of the cylindrical patch arrays.

Previously, constrained optimisation techniques were used to obtain beam patterns for circular and arc arrays [45, 52]. As a third null synthesis technique, a constraint optimisation method is applied to obtain a constrained pattern with the desired amplitude pattern characteristics. The optimal pattern is used as the starting value for the optimisation. The influence of the array attributes, such as the number of array elements and the inter-element spacing, on the characteristics of the amplitude patterns obtained from the null synthesis methods, is also studied.

In the last part of the array synthesis,the implementation of the cylindrical microstrip patch arrays is investigated. The influence of the mutual coupling on the characteristics of the null patterns of the cylindrical patch arrays is investigated utilising simulations and measurements. In a mutual coupling compensation technique, Chen [88,89] varied the lengths and radii of the dipoles in linear and planar arrays to obtain the desired

radiation patterns as well as equal driving impedances for the dipoles. This compensation technique is used to provide matched and equal driving impedances for all the patch antenna elements given a required set of excitations. The driving impedances are corrected by adjusting the lengths and feeding points of the individual patches. Utilising the compensation technique, the impedances of the microstrip patch antennas in both the planar and cylindrical arrays are designed to be 50 Ω for the desired element excitations. The consequent improvements in the bandwidth and reflection coefficient of a linear patch arrays are discussed. The resulting amplitude pattern for the compensated cylindrical microstrip patch array is also compared with the amplitude pattern before the compensation, to observe the improvements in the pattern characteristics.

1.4 Layout of thesis

The relevant background to the null synthesis and mutual coupling compensation for a cylindrical microstrip patch array is given in Chapter 2. An overview of the characteristics of the cylindrical patch antenna element, the null synthesis techniques, the mutual coupling effects and coupling compensation techniques is given. In Chapter 3, a null synthesis technique is adapted and extended for a cylindrical microstrip patch array. Results of the null synthesis techniques are shown and compared for different array geometries. A technique to compensate for the mutual coupling in both planar and cylindrical arrays is discussed and applied in Chapter 4. Both simulated and measured results are shown. Chapter 5 presents the conclusions of the study.

CHAPTER 2

BACKGROUND

Microstrip patch antennas can easily be made to conform to cylindrical surfaces to provide low profile omnidirectional arrays. A specified array pattern can also be obtained by configuring the geometries of the elements, the array and the cylinder. For a design procedure, the radiation patterns of the cylindrical patch elements and the array are needed. The cavity model is well suited to analyse cylindrical patches etched on thin substrates and to demonstrate the characteristics of these patch antennas. Two linear polarisations with different radiation characteristics are available when utilising cylindrical patches. In the first part of this chapter, the characteristics of the radiated fields for both polarisations will be discussed. The radiated fields will also be compared for different substrates and cylinder radii.

Due to the cylindrical configuration of the microstrip patch array, the array is classified as a cylindrical array. An introduction to cylindrical arrays and equally spaced cylindrical arrays, will be given. When the elements are equally spaced around the circumference of the array, the elements can be excited by using phase-sequence excitations. The orthogonal set of excitation vectors resulting from these phase-sequences may be implemented in a pattern synthesis method to obtain an optimal set of excitations for a required radiation pattern.

The objective in this thesis is to provide an omnidirectional radiation pattern with one or more nulls at specified angle locations to suppress directional interferences. Different techniques have been presented which perform null beam forming or null pattern synthesis [41,43–55]. In null beam forming, additional nulls are introduced in the beam

pattern, while null pattern synthesis provide omnidirectional coverage with directional nulls. In this chapter, a discussion on various null synthesis techniques for omnidirectional patterns will be given. These methods determine the element excitations which provide the required array radiation pattern.

The element excitations are applied to the array by setting either the element currents or voltages proportional to the excitations. When the mutual coupling between the antenna elements in the array is not taken into account during the computation of the excitations, the resulting radiation pattern may be distorted [53, 72–74]. Not only does the coupling deform the array imbedded radiation patterns of the individual elements, but also modifies the active impedances at the element ports. Consequently, a technique to compensate for the mutual coupling has to be implemented to obtain the desired array radiation pattern. Different techniques to compensate for the mutual coupling during the synthesis process, will also be discussed.

2.1 Characteristics of a cylindrical microstrip patch

Utilising the cavity model for the cylindrical patch antenna, the characteristics of the patches can be studied. These antennas may be used in two linear polarisations with different radiation characteristics, which will be discussed in the following paragraphs.

2.1.1 Cavity model for cylindrical microstrip patches

The geometry of a typical cylindrical microstrip patch antenna is shown in Figure 2.1. $2b$ and $2\theta_0$ define the dimensions of the patch in the z and ϕ directions, respectively. ϕ_0 indicates the ϕ-position of the patch, while a and h define the radius of the cylinder and height of the substrate, respectively. The position of the coaxial probe feed is indicated by z_f and ϕ_f.

One model for the cylindrical patch can be found by regarding the region underneath the patch as a cavity bounded by four magnetic walls and two electric walls [5, 7]. The E-field in the cavity has only a ρ component, which is independent of ρ if the substrate is thin ($h \ll a$). When the coaxial probe feed is modeled by a current density, with

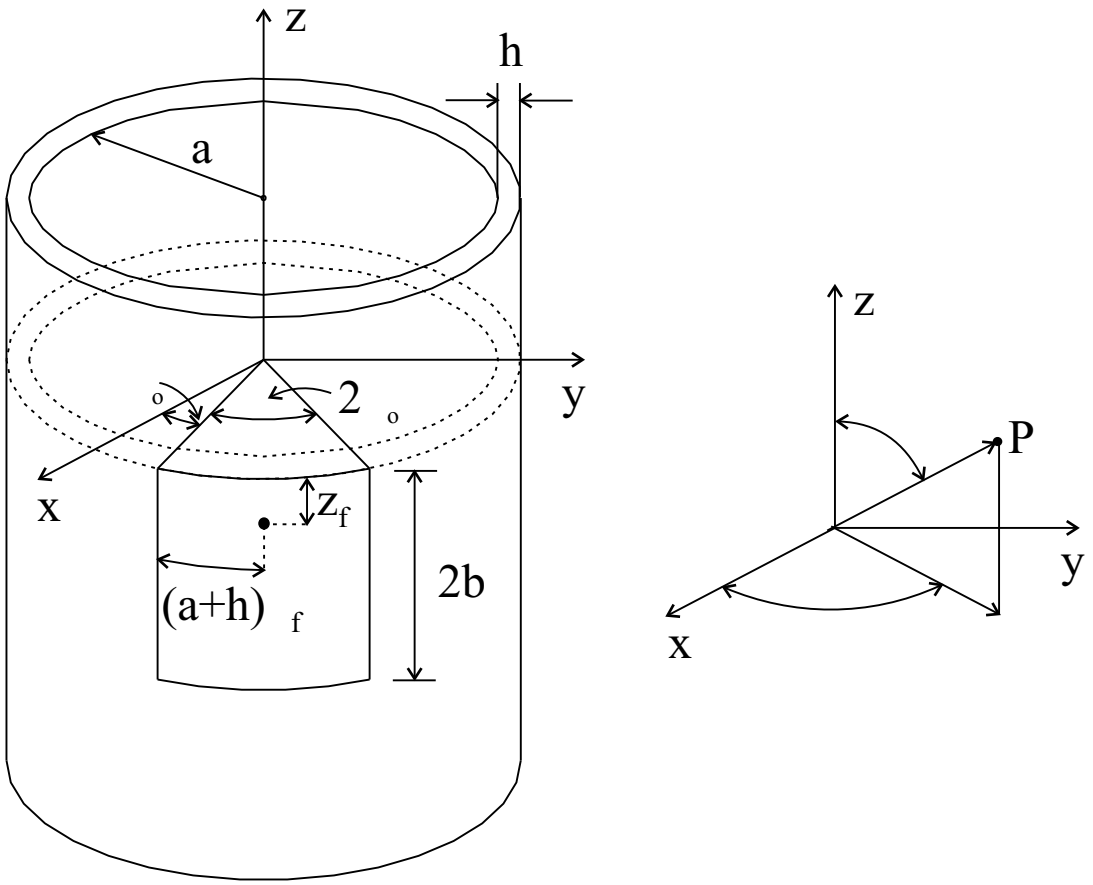

Figure 2.1: Geometry of cylindrical microstrip patch antenna

an effective width w, the field in the cavity can be found by a summation over all the cavity modes [13]:

$$E_\rho = j\omega\mu_0 \sum_{m,n} C_{mn} \cos\left[\frac{m\pi}{2\theta_0}(\phi - \phi_0)\right] \cos\left[\frac{n\pi z}{2b}\right], \tag{2.1}$$

where m and n are the mode indexes. The modal amplitudes C_{mn} are defined as:

$$C_{mn} = \frac{w}{k_{eff}^2 - k_{mn}^2} \frac{\Delta_m \Delta_n}{4(a+h)b\theta_0} \cos\left[\frac{m\pi\phi_f}{2\theta_0}\right] \cos\left[\frac{n\pi z_f}{2b}\right] \operatorname{sinc}\left[\frac{m\pi w}{4(a+h)\theta_0}\right], \tag{2.2}$$

where

$$\Delta_k = \begin{cases} 1, & k = 0 \\ 2, & k \neq 0 \end{cases}, \tag{2.3}$$

$$k_{mn} = \sqrt{\left(\frac{m\pi}{2(a+h)\theta_0}\right)^2 + \left(\frac{n\pi}{2b}\right)^2}, \tag{2.4}$$

$$k_{eff} = k_0\sqrt{\varepsilon_r(1 - j\delta_{eff})}, \tag{2.5}$$

$$\text{sinc}(x) = \sin(x)/x, \tag{2.6}$$

and

$$k_0 = \omega\sqrt{\mu_0\varepsilon_0}. \tag{2.7}$$

μ_0 and ε_0 are the permeability and permittivity of free space, respectively. The radial frequency and relative permittivity of the substrate are presented by ω and ε_r, respectively. The effective loss tangent δ_{eff} represents all the losses in the cavity. The radiation losses, the losses due to the finite conductivity of the conductor and the losses in the substrate and through surface waves can be estimated using the method described in [6]. The modal resonant frequency is given by:

$$f_{mn} = \frac{c}{2\sqrt{\varepsilon_r}}\sqrt{\left(\frac{m\pi}{2(a+h)\theta_0}\right)^2 + \left(\frac{n\pi}{2b}\right)^2}. \tag{2.8}$$

When the dimensions $2(a+h)\theta_0$ and $2b$ of the patch are fixed, Equation 2.8 indicates that the resonant frequency f_{mn} is independent of the curvature. This assumption is only valid for thin substrates with $h \ll a$ [7].

2.1.2 Radiated fields

The four walls of the lossy cavity in the cavity model are considered as the radiating apertures. Along each wall an equivalent magnetic current can be found from:

$$\bar{M} = E_\rho\hat{\rho} \times \hat{n}, \tag{2.9}$$

where E_ρ is given by Equation 2.1. These radiating walls are also referred to as radiating slots. For these magnetic currents radiating in the vicinity of an infinitely long cylindrical surface, the far zone radiation field may be obtained using the expressions

presented in [98]. The resulting components of the far zone electric fields for each cavity mode are given by [13]:

$$E_{\theta,mn}(r,\phi,\theta) = \frac{E_0 h}{2\pi^2 \sin\theta}\frac{e^{-jk_0 r}}{r}\left[1-(-1)^n e^{-j2k_0 b\cos\theta}\right] \cdot \sum_{p=-\infty}^{\infty}\frac{j^{p+1}e^{jp(\phi-\phi_0)}I(\theta_0,m,-p)}{H_p^{(2)}(k_0 a\sin\theta)}, \tag{2.10}$$

and

$$\begin{aligned} E_{\phi,mn}(r,\phi,\theta) = &-j\frac{E_0 h}{2\pi^2 a}\frac{e^{-jk_0 r}}{r}I(b,n,-k_0\cos\theta) \\ &\cdot\sum_{p=-\infty}^{\infty}\frac{j^{p+1}e^{jp(\phi-\phi_0)}}{H_p^{(2)\prime}(k_0 a\sin\theta)}\left[1-(-1)^m e^{-j2p\theta_0}\right] \\ &-j\frac{E_0 h}{2\pi^2 a}\frac{e^{-jk_0 r}}{r}\frac{\cos\theta}{k_0\sin^2\theta}\left[1-(-1)^n e^{-j2k_0 b\cos\theta}\right] \\ &\cdot\sum_{p=-\infty}^{\infty}\frac{j^{p+1}pe^{jp(\phi-\phi_0)}I(\theta_0,m,-p)}{H_p^{(2)\prime}(k_0 a\sin\theta)}, \end{aligned} \tag{2.11}$$

where

$$I(b,n,u) = \int_{-2b}^{0}\cos\left(\frac{n\pi z}{2b}\right)e^{-juz}dz, \tag{2.12}$$

and

$$I(\theta_0,m,-p) = \int_{0}^{2\theta_0}\cos\left(\frac{m\pi\phi}{2\theta_0}\right)e^{-jp\phi}d\phi. \tag{2.13}$$

The total radiated field is obtained by a summation over all the cavity modes m,n. The infinite summations in Equations 2.10 and 2.11 are summations over the cylindrical modes in which the fields have been expanded. The number of cylindrical modes needed for convergence depends on the radius of the cylinder and the angle θ, but is usually less than $2ka$ [11]. For θ-angles close to the cylinder axis, only a small number of terms are required.

2.1.3 Axial polarisation

The two slots of the cavity, oriented along the axis of the cylinder, are referred to as axial slots, while the other two slots, oriented along the circumference of the cylinder, are called circumferential slots. The patch antenna is axially polarised when fed symmetrically in ϕ, as shown in Figure 2.2. The dominant mode in the cavity will be the mode m=0, n=1 (TM_{01}). The two circumferential slots are excited equally in phase and amplitude, while the two axial slots are excited 180° out of phase. The next two higher order modes will be the TM_{20} and TM_{21} modes, with the TM_{20} mode mainly contributing to the cross-polar radiation. The TM_{21} mode contributes weakly to both the co-polar and cross-polar radiation. The TM_{01} mode itself gives rise to the E_θ co-polar radiation with no cross-polar radiation in the symmetry planes. Since the other higher modes are excited much weaker, most cross-polar radiation originate from the TM_{20} mode. A small displacement in ϕ_f will cause the TM_{10} to be excited, which will result in a higher cross-polarisation level [11]. Special care must be taken when feeding square patches, since the TM_{01} and TM_{10} will have the same resonant frequency.

2.1.4 Circumferential polarisation

The TM_{10} mode is the dominant mode for a circumferentially polarised patch, since it is fed symmetrically in z, as shown in Figure 2.3. The E_ϕ co-polar radiation is given by the two axial slots excited in phase. The two higher order modes contributing the most to the radiation are the TM_{02} and TM_{12} modes, with the cross-polarisation level mainly determined by the radiation from the TM_{02} mode.

2.1.5 Characteristics of the radiation patterns

The radiation pattern of a cylindrical patch depends on the geometries of the cylinder (a) and the patch (θ_0,b), as well as the characteristics of the substrate (h,ε_r). A comparison of the radiation patterns for patches with different substrates is shown in Figures 2.4 to 2.7. The radiation patterns were determined using the cavity model (Equations 2.10 and 2.11) at 1.8 GHz.

An air substrate was used for the first patch, with dimensions L=73.6 mm and W=76 mm.

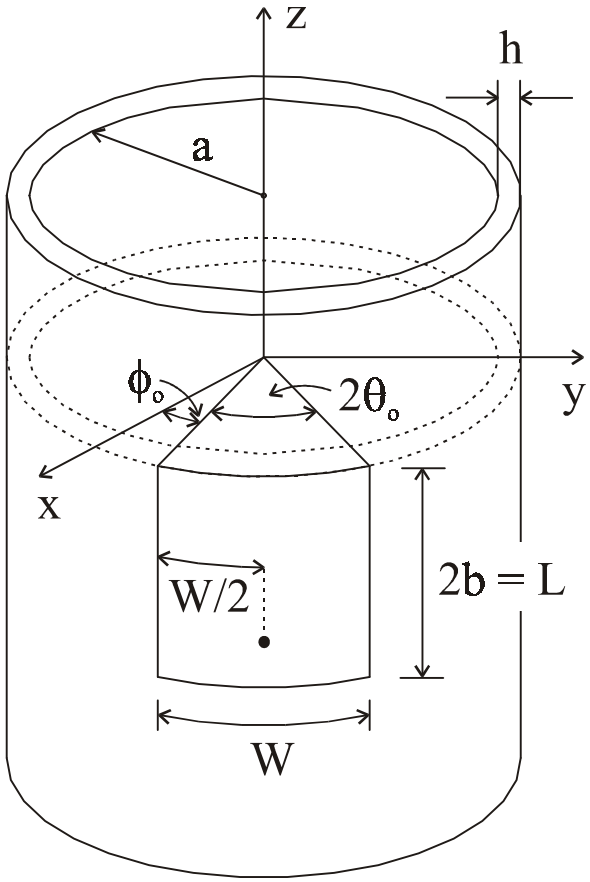

Figure 2.2: Geometry of an axial polarised patch antenna

The dimensions for the second patch were L=38.3 mm and W=42 mm and the substrate had an ε_r of 4.4. For both patches, h was 1.6 mm and $\phi_0 = 90° - \theta_0$. A cylinder, with a=131 mm, was used and the radiation patterns of the two patches were compared for both polarisations. The radiated relative power density in the E-plane and H-plane, for the patches used in the circumferential polarisation, is shown Figures 2.4 and 2.5, respectively. The patch, with an air substrate, radiates a co-polar component (P_ϕ) with a higher directivity and a lower back lobe level in both the E-plane and H-plane. The cross-polarisation level in the H-plane is also higher when using the air substrate.

For the two patches used in the axial polarisation, Figures 2.6 and 2.7 show the radiated relative power density in the H-plane and E-plane, respectively. The co-polar component (P_θ) of the air substrate patch show again a higher directivity and lower back lobe level in both principal planes. The cross-polar component in the H-plane is also higher for this patch.

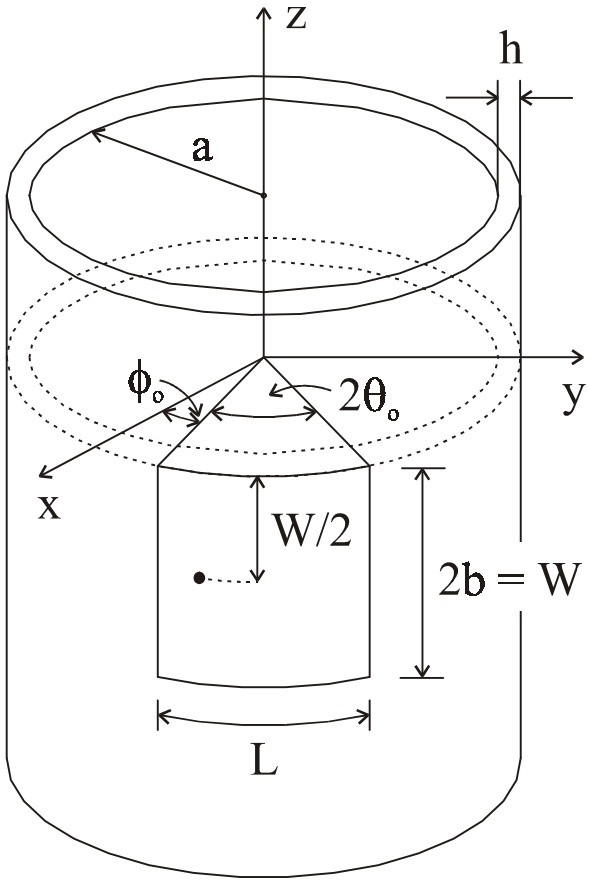

Figure 2.3: Geometry of a circumferentially polarised patch antenna

When comparing Figures 2.4 and 2.6, it is seen that the back lobe level of the axially polarised patches is much less (below -40 dB) than the back lobe level of the circumferentially polarised patches. Depending on the permittivity of the substrate, the main lobe of an axial polarised patch is either broader or narrower than the main lobe of a circumferentially polarised patch. With $\varepsilon_r = 1$, the main lobe is broader for the circumferentially polarised patch, and for the case where $\varepsilon_r = 4.4$, the axial polarised patch has the broader main beam.

In Figure 2.7 it is observed that the level of radiation increases near the axis of the cylinder. In the cavity model, the axial slots are not radiating in this cut ($\phi = 90°$) of the radiation pattern and therefore these high levels of radiation are not suppressed. In reality, the axial slots do radiate close to the cylinder axis to give the radiation pattern a finite value. In the cavity model, it is also assumed that the cylinder has an infinite length. For the radiation measurements to be comparable to the simulations using this model, the cylinder has to be at least a few wavelengths long.

The cylindrical patch with the air substrate was also simulated on a cylinder with a different radius (a=265 mm) to show the effect of curvature. Figures 2.8 and 2.9 compare the relative power density patterns of the circumferential polarisation for the two different radii in the E-plane and H-plane, respectively. The back lobe level decreases when using the larger radius, while the main lobe is only slightly effected in both principle planes. The influence of the curvature is less when using the cylindrical patch in the axial polarisation. The H-plane and E-plane relative power density patterns for the axial polarisation are compared for the two radii in Figures 2.10 and 2.11, respectively. A small decrease in the back lobe level in the H-plane is observed, while the effect of the decreased curvature on the main lobe is insignificant in both principle planes. The cross-polarisation levels for both polarisations appear to be almost unaffected by the decrease in curvature.

2.2 Cylindrical array pattern

The geometry of a typical cylindrical array can be seen in Figure 2.12. Each array element is placed on the circumference of the array at (x_n, y_n), where $n = 1 \ldots N$. The contribution of the n-th element to the far-field in direction (ϕ, θ) can be written as:

$$e\left(r, \phi, \theta\right) = E_n(r, \phi, \theta) e^{jk_0(x_n \sin\theta\cos\phi + y_n \sin\theta\sin\phi)}, \tag{2.14}$$

using the origin of the coordinate system as the reference point. $E_n(r, \phi, \theta)$ represent the co-polarised far-zone electric field of the n-th element with respect to its phase reference. The radiated electric field of the elements is influenced by the structure on which it is mounted, e.g. a conducting cylinder or mast, and must therefore be included when computing element electric fields. The total co-polarised far-zone electric field $E_{TOT}(r, \phi, \theta)$ of the array is found by superposition of the element electric fields:

$$E_{TOT}\left(r, \phi, \theta\right) = \sum_{n=1}^{N} a_n E_n(r, \phi, \theta) e^{jk_0(x_n \sin\theta\cos\phi + y_n \sin\theta\sin\phi)}, \tag{2.15}$$

where a_n denotes the relative complex excitation (amplitude as well as phase) of the n-th element.

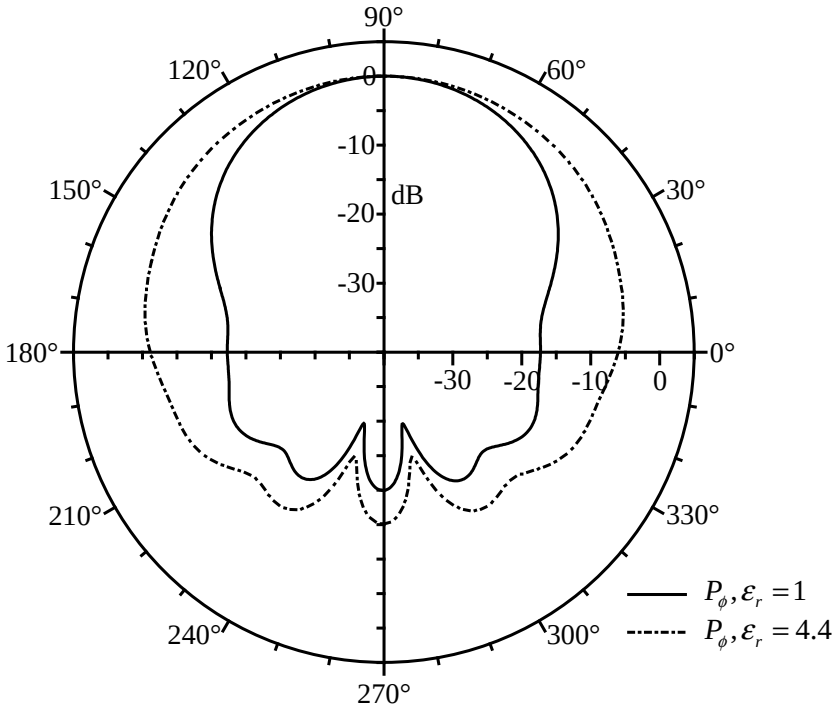

Figure 2.4: Radiated relative power density at $\theta = 90°$ (E-plane) for circumferentially polarised patches with $\varepsilon_r = 1$ and $\varepsilon_r = 4.4$

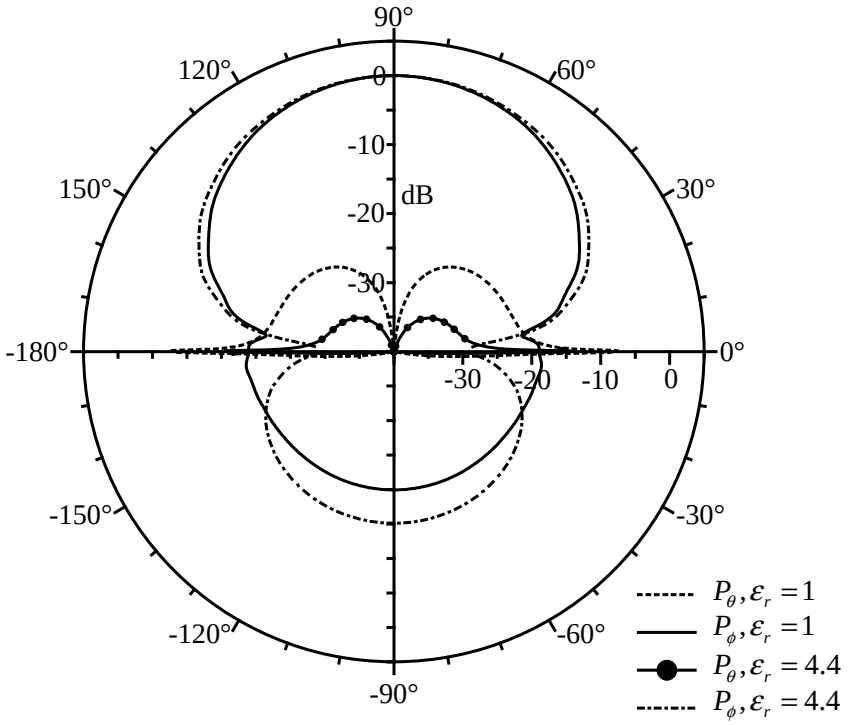

Figure 2.5: Radiated relative power density at $\phi = 90°$ (H-plane) for circumferentially polarised patches with $\varepsilon_r = 1$ and $\varepsilon_r = 4.4$

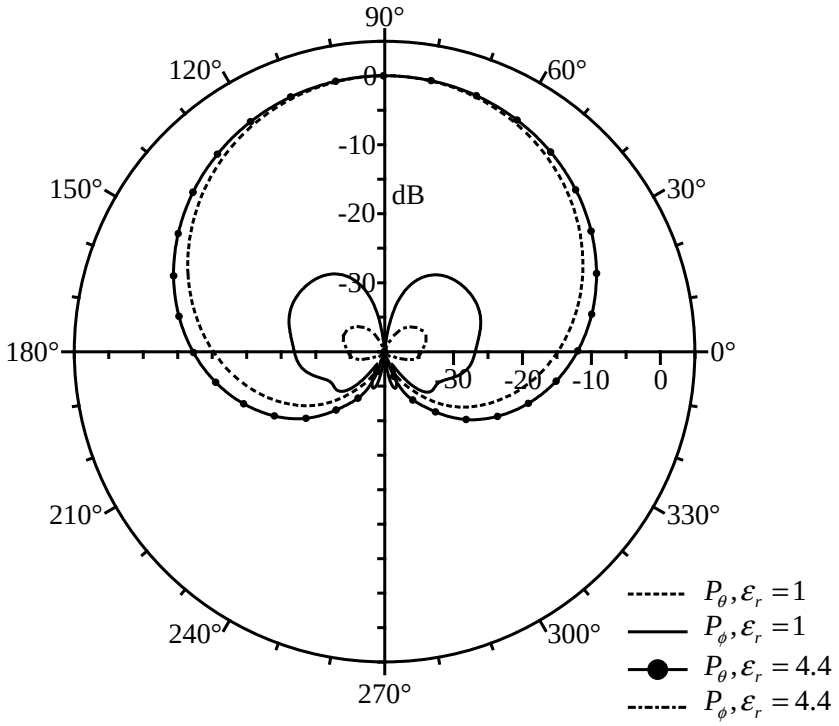

Figure 2.6: Radiated relative power density at $\theta = 90°$ (H-plane) for axial polarised patches with $\varepsilon_r = 1$ and $\varepsilon_r = 4.4$

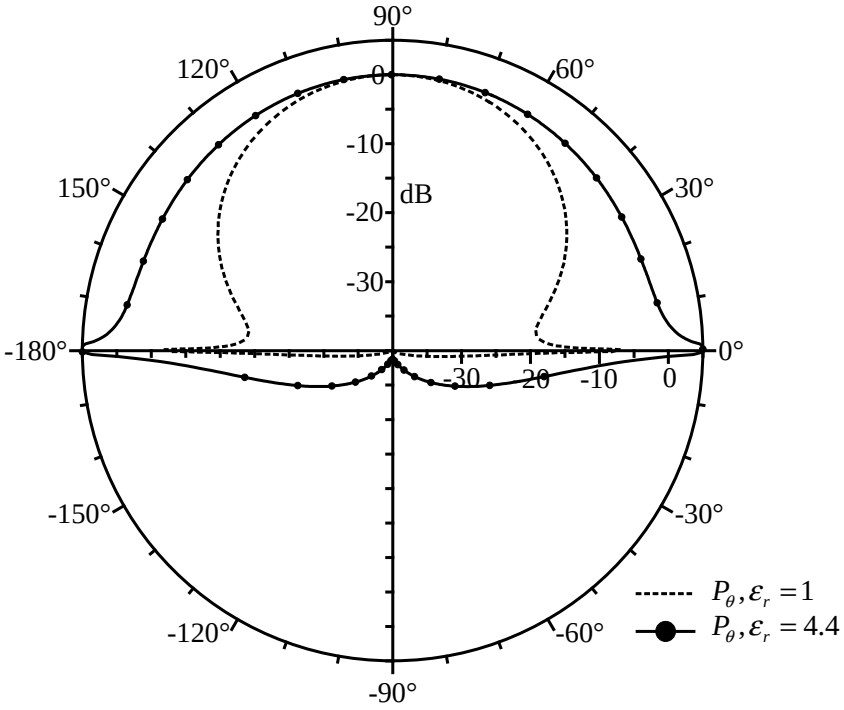

Figure 2.7: Radiated relative power density at $\phi = 90°$ (E-plane) for axial polarised patches with $\varepsilon_r = 1$ and $\varepsilon_r = 4.4$

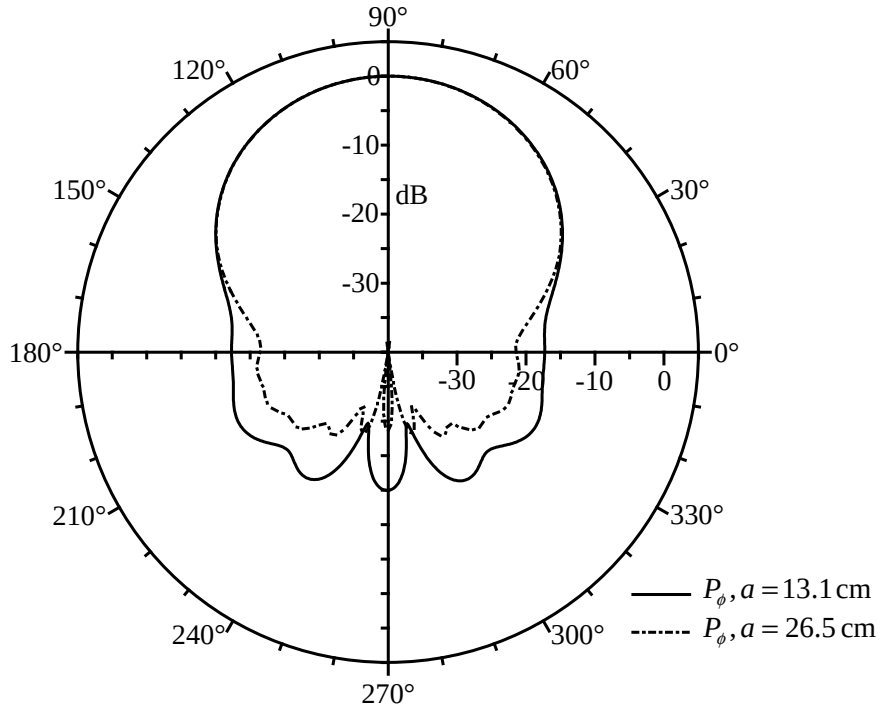

Figure 2.8: Radiated relative power density at $\theta = 90°$ (E-plane) for circumferentially polarised patches mounted on cylinders with a=13.1 cm and a=26.5 cm, respectively.

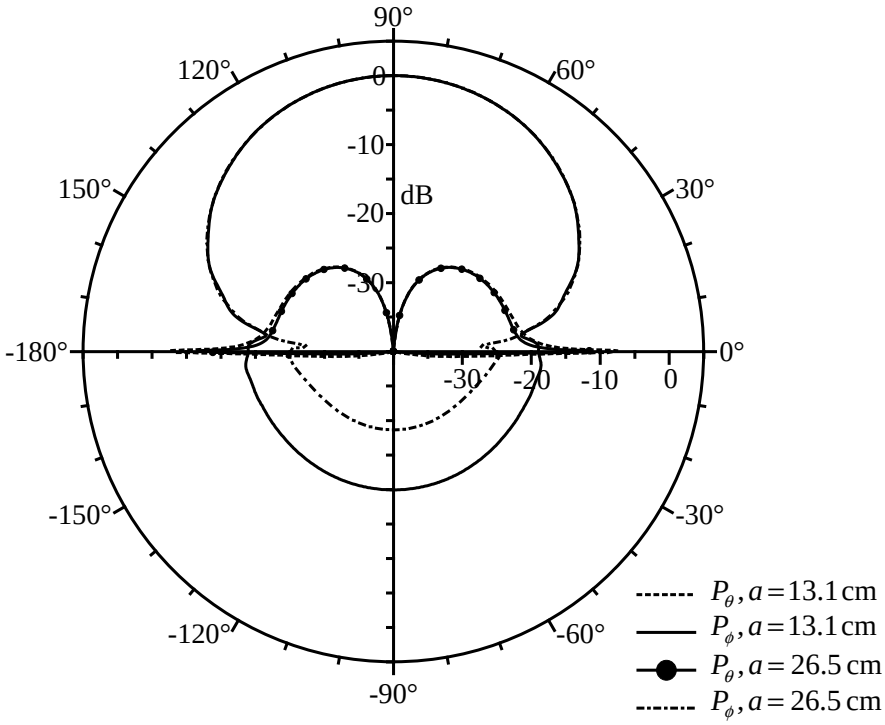

Figure 2.9: Radiated relative power density at $\phi = 90°$ (H-plane) for circumferentially polarised patches mounted on cylinders with a=13.1 cm and a=26.5 cm, respectively.

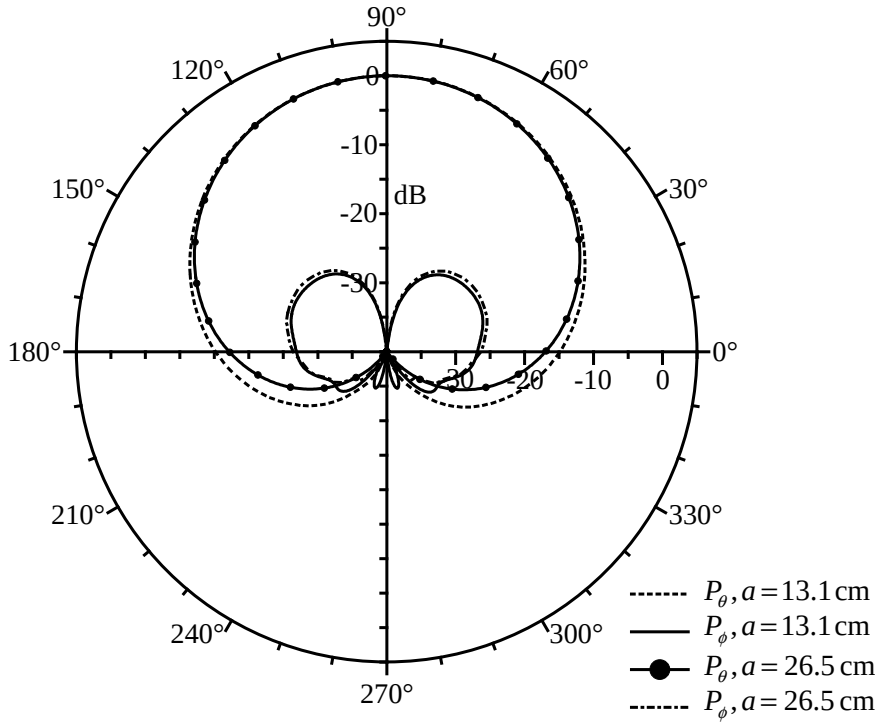

Figure 2.10: Radiated relative power density at $\theta = 90°$ (H-plane) for axial polarised patches mounted on cylinders with a=13.1 cm and a=26.5 cm, respectively.

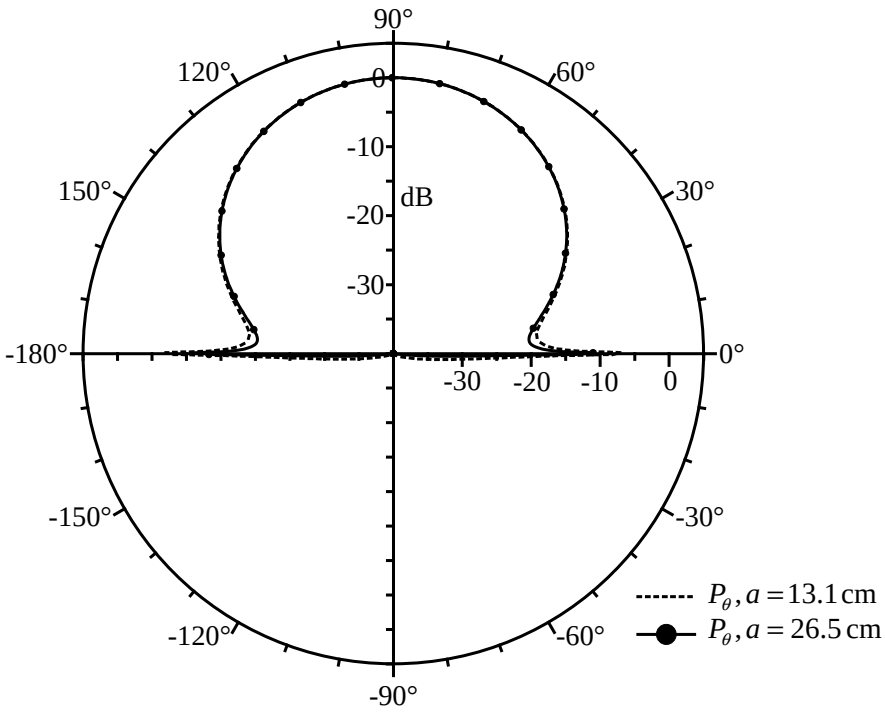

Figure 2.11: Radiated relative power density at $\phi = 90°$ (E-plane) for axial polarised patches mounted on cylinders with a=13.1 cm and a=26.5 cm, respectively.

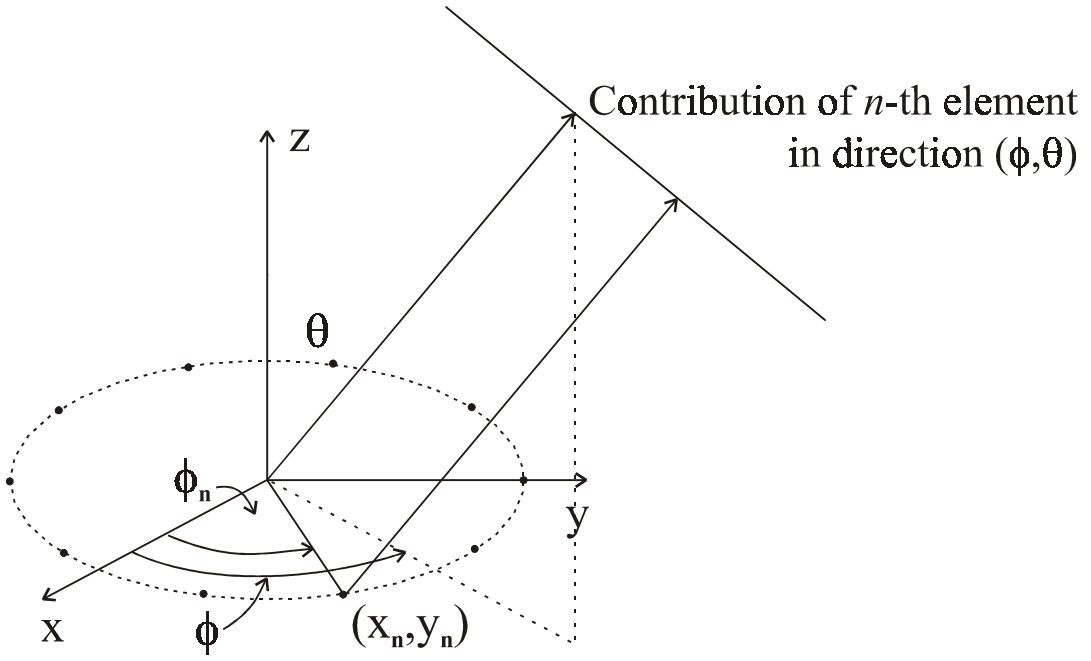

Figure 2.12: Geometry of a cylindrical array

The far-field radiation pattern of the array may then be written as:

$$F(\phi,\theta) = \sum_{n=1}^{N} a_n E_n(\phi,\theta) e^{jk_0(x_n \sin\theta\cos\phi + y_n \sin\theta\sin\phi)}, \tag{2.16}$$

with $E_n(\phi,\theta)$ being the far-field radiation pattern of the n-th element.

When only the cross-section of the radiation pattern in the plane of the cylindrical array ($\theta = 90°$) is considered, Equation 2.16 reduces to:

$$F(\phi) = \sum_{n=1}^{N} a_n E_n(\phi) e^{jk_0(x_n \cos\phi + y_n \sin\phi)}, \tag{2.17}$$

where $E_n(\phi)$ is the n-th element's radiation pattern in the $\theta = 90°$ plane. The array radiation pattern may be evaluated in vector form [57] :

$$\mathbf{F} = \mathbf{BA}. \tag{2.18}$$

The radiation pattern vector $\mathbf{F}$ is given as:

$$\mathbf{F} = [f_1, f_2, \ldots, f_q, \ldots, f_Q]^T, \tag{2.19}$$

where f_q is the value of the radiation pattern in the ϕ_q-direction for a total number of Q field points. $\mathbf{A}$ is the excitation vector:

$$\mathbf{A} = [a_1, a_2, \ldots, a_n, \ldots, a_N]^T, \tag{2.20}$$

while $\mathbf{B}$ is defined as the radiation matrix. The b_{nq}-th element of $\mathbf{B}$ is the contribution of the n-th antenna element to the radiation pattern in the q-th direction:

$$b_{nq} = a_n E_n(\phi_q) e^{jk_0(x_n \cos\phi_q + y_n \sin\phi_q)}. \tag{2.21}$$

When all the antenna elements have the same radiation pattern $E(\phi)$, polarisation properties and pointing direction, the array radiation pattern may be written as:

$$F(\phi) = E(\phi) \cdot \left[\sum_{n=1}^{N} a_n e^{jk_0(x_n \cos\phi + y_n \sin\phi)} \right]. \tag{2.22}$$

From this radiation pattern an array factor can be extracted:

$$AF(\phi) = \sum_{n=1}^{N} a_n e^{jk_0(x_n \cos\phi + y_n \sin\phi)}, \tag{2.23}$$

which is the radiation pattern of an array of isotropic point sources located at the phase centres of the original elements and with excitations equal to the original element excitations. Isotropic point sources are fictitious antenna elements that radiate an equal amount of energy in all directions.

2.2.1 Equally spaced cylindrical arrays

The geometry of an equally spaced cylindrical array in the xy-plane ($\theta = 90°$) is shown in Figure 2.13. The n-th is located at the angle:

$$\phi_n = \frac{2\pi n}{N}. \tag{2.24}$$

The far-field array factor for an equally spaced array with elements identical in radiation pattern, is given by [41]:

$$\begin{aligned} AF(\phi) &= \sum_{n=1}^{N} a_n e^{jk_0 R\cos(\phi - \phi_n)} \\ &= \sum_{n=1}^{N} a_n e^{jk_0 R\cos\left(\phi - \frac{2\pi n}{N}\right)}, \end{aligned} \tag{2.25}$$

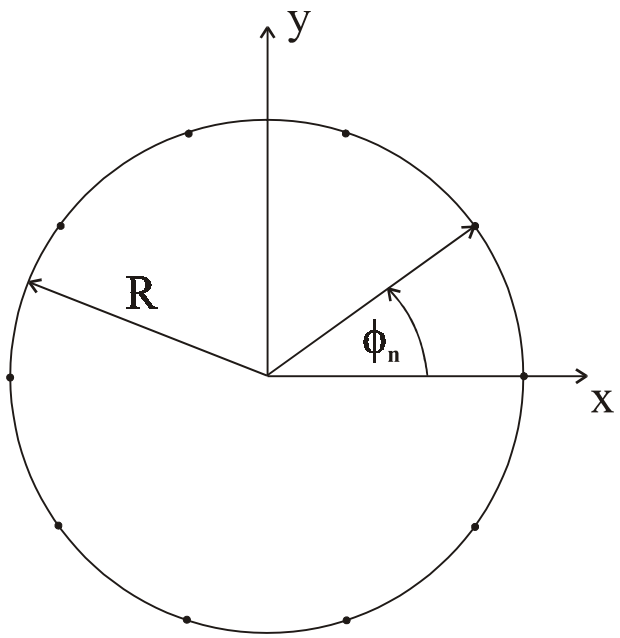

Figure 2.13: Geometry of an equally spaced cylindrical array in the xy-plane

where the radius of the cylindrical array is equal to R.

These equally spaced arrays are very suitable to form omnidirectional radiation patterns. It is evident from symmetry that any constant-amplitude excitation with an integral number of closed cycles of phase variations around the array will produce an omnidirectional pattern. Such an excitation is called a phase-sequence excitation [41]. There will, however, always be a ripple in the array radiation pattern which will depend on the distances between the antenna elements and on the element radiation patterns [42] . The m-th sequence excitation is one in which the total phase change around the array is $m2\pi$, with m an integer. For $m = 0$, all the elements are fed in phase, which also gives an omnidirectional array pattern. Consequently, the excitation of the n-th element for the m-th sequence excitation is:

$$a_{nm} = e^{j\frac{2\pi mn}{N}}. \tag{2.26}$$

The element excitations for a sequence excitation of order $m + N$ will be the same as for the m-th sequence excitation, since sine and cosine functions are periodical with 2π. Using Equation 2.26 it can also be shown that the element excitations of the $(m + p)$-th sequence excitation are orthogonal to those of the m-th sequence excitation, with $p \neq N$. The sequence excitations of orders 0 to $N-1$ thus form a complete orthogonal base for the space of element excitations. Every possible array pattern can therefore be

realised by the superposition of N sequence excitations. The transformations between the vectors of element excitations and sequence excitations are given by:

$$a_n = \sum_{m=0}^{N-1} s_m e^{j\frac{2\pi mn}{N}}, \tag{2.27}$$

and

$$s_m = \frac{1}{N}\sum_{n=0}^{N-1} a_n e^{-j\frac{2\pi mn}{N}}. \tag{2.28}$$

Equation 2.27 and Equation 2.28 can be seen as a discrete Fourier transform (DFT) and an inverse discrete Fourier transform (IDFT), respectively. Subsequently, the far-field array factor of the m-th sequence excitation can be expressed as:

$$AF_m(\phi) = \sum_{n=0}^{N-1} s_m e^{j\frac{2\pi mn}{N}} e^{jk_0 R\cos\left(\phi-\frac{2\pi n}{N}\right)}. \tag{2.29}$$

Since the element excitations are superpositions of N sequence excitations, the array factor becomes:

$$AF(\phi) = \sum_{m=0}^{N-1}\sum_{n=0}^{N-1} s_m e^{j\frac{2\pi mn}{N}} e^{jk_0 R\cos\left(\phi-\frac{2\pi n}{N}\right)}. \tag{2.30}$$

When the resulting array pattern has a constant amplitude and linear phase, it is called a phase mode [44]. The order of the phase mode is determined by the number of phase variations over 2π. A phase mode of order m is:

$$p_m(\phi) = e^{jm\phi}. \tag{2.31}$$

The zero order phase mode has constant amplitude and phase, while the negative order phase modes indicate a reverse variation of phase change with angle. For small inter-element spacings, the array can be approximated by a continuous source of radiation and the array factor can then be expressed as [43]:

$$AF(\phi) = N\sum_{m=-m_{max}}^{m=m_{max}} j^m s_m J_m(k_0 R) e^{jm\phi}, \tag{2.32}$$

where $J_m(x)$ is the Bessel function of the first kind of order m and $m_{max} < N/2$. This array factor is a superposition of N scaled phase modes with $-N/2 < m < N/2$. Consequently, a pattern caused by a sequence excitation of order m is a good approximation for a phase mode of the same order if the array radius is small.

2.3 Null synthesis techniques

Various null synthesis techniques for omnidirectional patterns have been presented [41, 43–55]. These techniques utilise different characteristics of a cylindrical array to obtain a null at the desired angle location. Some use the sequence excitations, phase modes or the orthogonal base of realisable array patterns, while others utilise pattern search techniques. A short overview of these techniques will be given after defining some null synthesis parameters.

2.3.1 Definitions of parameters in null synthesis

The definitions describing the omnidirectional radiation pattern with a null, differ from conventional beam forming parameters such as beam width and side lobe levels. Illustrations of the definitions used to characterise the null pattern, are given in Figure 2.14. The gain ripple (in dB) is defined as the ratio between the maximum and minimum level in the omniregion. The angular distance between the two points, 10 dB below the maximum, is defined as the null width. The null depth is given by the ratio of the radiation intensity in the direction of the null and the maximum, which is also an indication of the suppression level of the interference. For null depths smaller than 10 dB, another appropriate level may be defined at which the null width is measured. The definition of gain ripple is only valid if the value of the ripple is below this null width definition level.

2.3.2 Superposition of sequence excitations

The superposition of two sequence excitations to produce a null in an omnidirectional radiation pattern, was presented by Davies and Rizk [44]. A zero crossing null, where the radiation pattern show an abrupt phase reversal across the angle position of the null, was produced. The two phase modes, which had the same amplitude, but were 180° out of phase in the direction of the null, were utilised. The difference in the orders of the two modes had to be exactly one to avoid any other abrupt phase reversals. The authors consequently employed the zero and first order sequence excitations. The

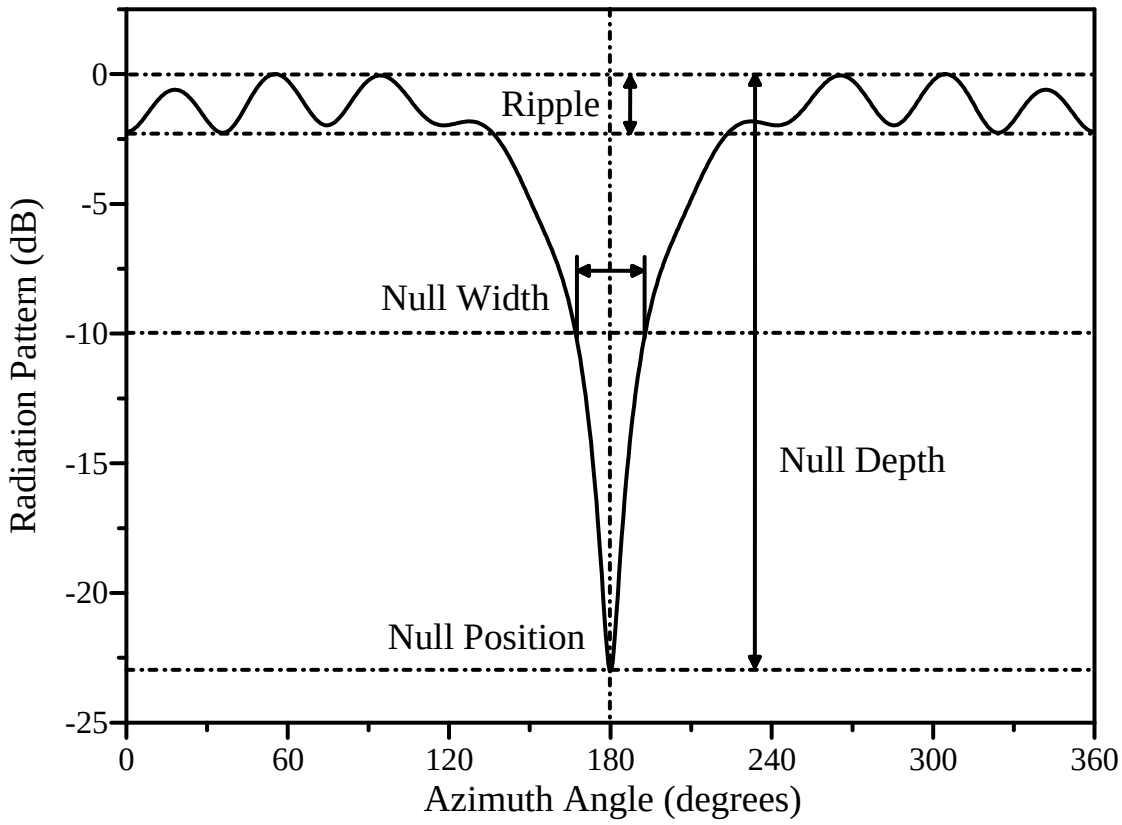

Figure 2.14: Definitions of parameters used to characterise null forming

excitations of the n-th element was:

$$a_n = e^{j2\pi\frac{n}{N}} + Ae^{j\phi_p}. \tag{2.33}$$

The levels of excitation of the two modes were made equal by means of an attenuator A, and the direction of the null was controlled by a phase shifter ϕ_p. Acceptable null depths are obtainable if the number of elements and the radius of the array is kept small. If the inter-element spacing is not kept small, the two modes do not exactly cancel each other. This will lead to finite null depths and errors in the direction of the null. This technique produced very wide nulls as the amplitude of the radiation pattern falls monotonically from the maximum towards the null.

As an extension of this technique, the above authors also proposed the superposition of a third sequence excitation to reduce the null width. A dipole type or figure-of-eight pattern was superposed to the original pattern. This type of pattern was produced by the sequence excitations of orders 1 and -1 and has two zero crossing nulls. One of the two nulls was made to coincide with the original null. The complete excitation vector

was given by:

$$a_n = Ae^{j\phi_p} + (B+1)e^{j2\pi\frac{n}{N}} + Be^{\left(j2\phi_p - j2\pi\frac{n}{N}\right)}. \tag{2.34}$$

The decrease in null width is obtained at the expense of higher gain ripple. The attenuator B controls the null width, but also has to be fixed at a suitable value to achieve an acceptable compromise between the null width and gain ripple.

Lim and Davies [41] proposed the use of two phase modes with a higher difference in order. This would have decreased the null width, but also would have lead to additional nulls in the radiation pattern. To avoid the additional nulls, the zero order mode was replaced with a beam pattern, which had a main beam of constant phase in the direction of the null. The beam pattern with a constant phase beam in the direction ϕ_p was obtained for a cylindrical array of omnidirectional elements by using the element excitations:

$$a_{n,beam} = e^{-jk_0R\cos\left(\phi_p - 2\pi\frac{n}{N}\right)}. \tag{2.35}$$

A sequence excitation, which was multiplied with a complex factor A, was added to the excitation of the constant phase beam to obtain a null in the direction ϕ_p. The factor A had to satisfy the following condition:

$$A \cdot F_m(\phi_p) + F_{beam}(\phi_p) = 0, \tag{2.36}$$

where $F_m(\phi_p)$ was the far-field radiation pattern of the sequence excitation of order m. The complex factor was found to be:

$$A = -\frac{N}{F_m(\phi_p)}, \tag{2.37}$$

and the resulting element excitations were:

$$a_n = e^{-jk_0R\cos\left(\phi_p - 2\pi\frac{n}{N}\right)} - \frac{N}{F_m(\phi_p)}e^{j\frac{2\pi mn}{N}}. \tag{2.38}$$

The sequence excitation in Equation 2.38 approximates a phase mode of the same order (m). Theoretically, an infinitely deep null with low gain ripple can be achieved. The gain ripple is determined by the interference of the phase mode with the sidelobes of the phase constant beam. The amount of interference is influenced by the number of elements, the array radius and the order of the phase mode. For a small number of

elements in the array, the order of the phase mode is usually low (zero or one). Larger arrays require a higher order phase mode to decrease the null width, which may result in an increased gain ripple. Therefore, the optimal order of the phase mode to be used, is determined by the radius of the array, the number of elements and the required ripple and null width.

2.3.3 Fourier approximation of an ideal pattern

The phase modes, which can be approximated by sequence excitations, form an orthogonal base for the array factor. A pattern can thus be synthesised by transforming the desired pattern into a number of phase modes with a Fourier transformation and then synthesising the phase modes with the sequence excitations. A Fourier transformation will however result in an infinite number of phase modes, but only the realisable orders of phase modes may be used to synthesise the pattern ($m \leq N/2$).

Lim [43] proposed the approximation of an ideal zero pattern using this method of approximation. For a minimum null width, an abrupt phase reversal in the pattern was needed in the direction of the null. To avoid the occurrence of a second null, the phase in the omniregion also had to change progressively at half the rate of the change in azimuth angle. An idealised pattern that satisfied these requirements was:

$$\begin{aligned} F_0(\phi) &= e^{j\frac{2\pi-\phi+\phi_p}{2}}, \\ \phi_p &\leq \phi \leq \phi_p + 2\pi. \end{aligned} \tag{2.39}$$

The phase of the pattern changes linearly from 0 (at $\phi = \phi_p$) to π (at $\phi = \phi_p + 2\pi$) and has an abrupt phase reversal at ϕ_p, as shown in Figure 2.15 for $phi_p = 180°$.

The approximation of the amplitude pattern of $F_0(\phi)$ will result in a null of finite depth, because the realisable pattern is limited in bandwidth and the derivations, with respect to ϕ, also have to be smooth. Using the standard method for calculating Fourier coefficients, the set of phase modes can be determined as:

$$\begin{aligned} p_m &= \frac{1}{2\pi} \int_{\phi_p}^{\phi_p+2\pi} F_0(\phi)\, e^{-jm\phi} d\phi \\ &= \frac{e^{-jm\phi_p}}{\pi\left(m - \frac{1}{2}\right)}. \end{aligned} \tag{2.40}$$

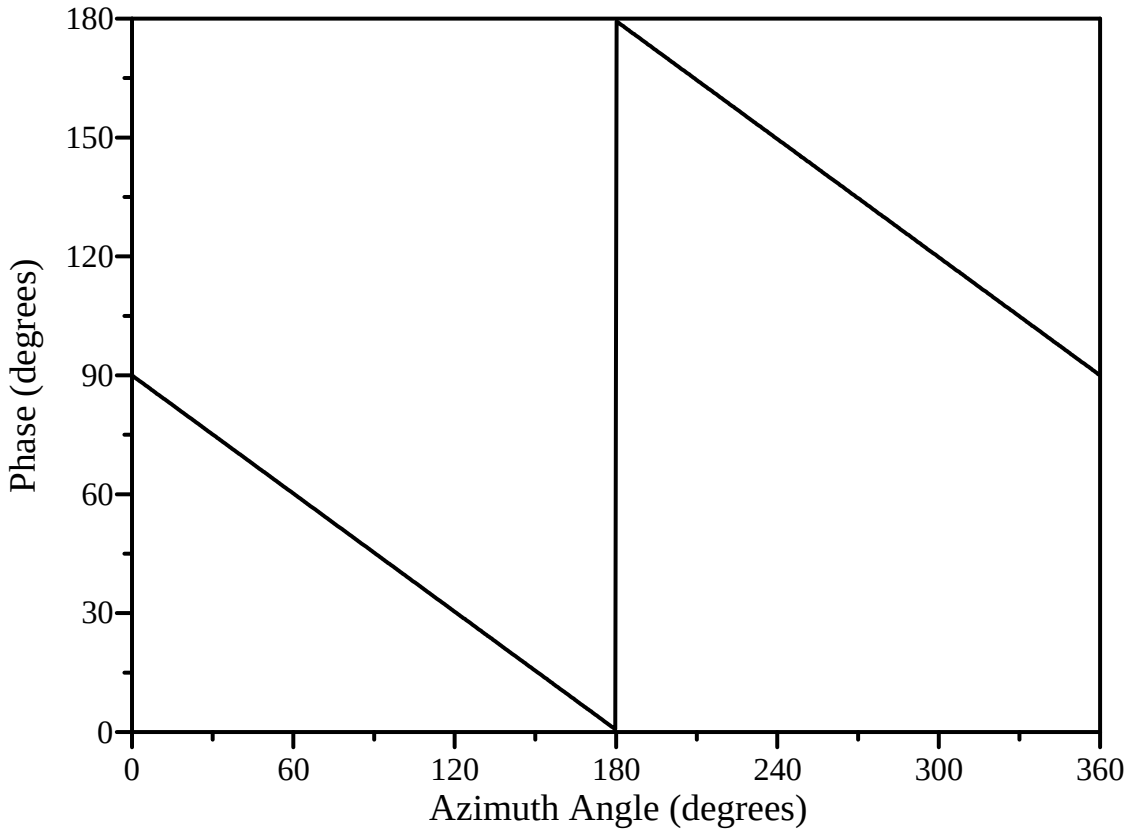

Figure 2.15: Phase of the idealised null pattern

For cylindrical arrays with identical elements and small inter-element spacings, the resulting sequence excitations will be:

$$s_m = \frac{e^{-jm\left(\frac{\pi}{2}+\phi_p\right)}}{\pi N \left(m-\frac{1}{2}\right) J_m(k_0 R)}, \tag{2.41}$$

where $J_m(x)$ is the Bessel function of the first kind of order m. The element excitations are obtained from the DFT relation in Equation 2.27.

The Fourier approximation will yield a pattern with a relatively narrow null, but with a gain ripple of about 2 dB. The realisable null depths are also low when a small number of elements are used. For small inter-element spacings ($< \lambda_0/4$) and radii, where the Bessel function $J_m(k_0 R)$ is not close to zero, the results appear to be insensitive to the array radius. For certain array radii, it will not be possible to create all the phase modes in the far field, if one or more Bessel functions $J_m(k_0 R)$ are very small or zero [43]. For the sequence excitations, where $J_m(k_0 R)$ is very small, the phase mode distortions in the far field pattern of these excitations will be much larger in amplitude than the wanted phase modes. The corresponding sequence excitations will be very large and

the distortion will dominate the far field, resulting in a large error of the approximation. Since the approximation is a superposition of phase modes, it will also lead to errors when the far field patterns, caused by the sequence excitations, are not exactly phase modes.

2.3.4 Orthogonal projection method

Instead of using the phase modes, the patterns g_m, caused by the sequence excitations, can be used as basis functions. These patterns are also mutually orthogonal and span the whole space of possible array patterns. Unlike the phase modes in the Fourier approximation, they can be synthesised exactly. The approximation will thus be better, especially when using larger inter-element spacings. Vescovo [50] applied this synthesis procedure to cylindrical arrays to synthesise beam patterns.

Every realisable array pattern, $F(\phi)$, of a cylindrical array with equally spaced antenna elements, can be written as the result of the sequence excitations s_m:

$$F(\phi) = \sum_{m=0}^{N-1} s_m g_m(\phi), \tag{2.42}$$

where

$$g_m(\phi) = \sum_{n=0}^{N-1} e^{j2\pi \frac{mn}{N}} E_n(\phi). \tag{2.43}$$

For a cylindrical array of equally spaced elements, the $g_m(\phi)$ of two different values of m are orthogonal to each other. A complete orthogonal base for the space of realisable array patterns is thus given by $g_m(\phi)$. For a cylindrical array of omnidirectional elements $g_m(\phi)$ is given by:

$$g_m(\phi) = \sum_{n=0}^{N-1} e^{j2\pi \frac{mn}{N}} e^{jk_0 R \cos\left(\phi - \frac{2\pi n}{N}\right)}. \tag{2.44}$$

The unconstrained optimal array pattern $F_{optim}(\phi)$ is the orthogonal projection of the idealised pattern $F_0(\phi)$ onto the space of realisable array patterns, when $F_{optim}(\phi)$ gives the minimum squared distance between $F(\phi)$ and $F_0(\phi)$. The squared distance $\rho^2(\mathbf{A})$ is defined as:

$$\rho^2(\mathbf{A}) = \int_0^{2\pi} |F(\phi; \mathbf{A}) - F_0(\phi)|^2 \, d\phi, \tag{2.45}$$

where $F(\phi; \mathbf{A})$ denotes the array radiation pattern for the excitation vector $\mathbf{A}$. The unconstrained optimum sequence excitations are thus obtained through the orthogonal projection [50]:

$$s_{optim\_m} = \frac{\langle F_0(\phi), g_m(\phi) \rangle}{\|g_m(\phi)\|^2}, \tag{2.46}$$

with the scalar product given by:

$$\langle f, g \rangle = \int_0^{2\pi} f(\phi) g(\phi) d\phi, \tag{2.47}$$

and the norm obtained from:

$$\|f\| = \sqrt{\langle f, f \rangle}. \tag{2.48}$$

The idealised radiation pattern $F_0(\phi)$ of [43] in Equation 2.39, may be used in the projection method to form a null in an otherwise omnidirectional array pattern. This null synthesis technique was proposed by Abele *et al* [53, 54]. The pattern $F_0(\phi)$ is projected onto the space of realisable array patterns of a cylindrical array of omnidirectional elements, to obtain the sequence excitation. The element excitations are then obtained through the DFT relation.

When the inter-element spacing is small ($\ll \lambda_0/2$), the base functions $g_m(\phi)$ are good approximations of the phase modes of the pattern and consequently the results of the projection method and the Fourier approximation will be comparable. The projection method also takes into account the distortion of the phase modes and will therefore give better results than the Fourier approximation for larger inter-element spacings. Figures 2.16 and 2.17 respectively compare the amplitude and phase of the radiation patterns for a single null, using the Fourier approximation and orthogonal projection method. An array with 16 elements and a radius of λ_0 was used to form an infinitely deep null at 180°. Using this small inter-element spacing, the two methods yield similar results in both amplitude and phase. The amplitude and phase of the radiation patterns for the same null, using a larger inter-element spacing ($R = 1.385\lambda_0$), are shown in Figures 2.18 and 2.19, respectively. For this larger inter-element spacing, the orthogonal projection method produces a deeper null with less gain ripple. A smaller phase ripple is also observed in the phase pattern of the orthogonal projection method.

The gain ripple may be reduced by using window functions [53, 54]. The spectral components of the array pattern, which have to be multiplied with the window function,

are the phase modes. Since the sequence excitations and phase modes are related through a multiplication of a constant factor, the window function may be applied to the sequence excitations, instead of the phase modes.

Abele [54] proposed the application of a Hamming window of length N to the sequence excitations:

$$W_{HM}(k) = 0.54 + 0.46\cos\left(2\pi\frac{k}{N}\right). \tag{2.49}$$

The idealised pattern has a constant phase slope of a $\frac{1}{2}$ and therefore its Fourier components are symmetric to $k = \frac{1}{2}$. This symmetry may not be disturbed by the application of the window in order to maintain the linear phase change. The best results are thus obtained if the window is shifted and the m-th sequence excitation coefficient is multiplied by $W(m - \frac{1}{2})$. The window function may be applied to the sequence excitation coefficients of both the Fourier approximation and the orthogonal projection. The ripple is decreased using the window function, while the null width is increased. The null depth may also be significantly increased. As an example, an array with $N = 16$ and $R = \lambda_0$ was used to form a single null at 180°. The effects of the Hamming window on the amplitude and phase of the radiation patterns resulting from the orthogonal projection method, are shown in Figures 2.20 and 2.21, respectively. It is observed that although a deeper null with less ripple is formed, the null width is increased.

The idealised pattern can be extended to contain multiple phase reversals to achieve more than one null in an otherwise omnidirectional pattern. Abele proposed idealised patterns for an odd and even numbers of nulls. The phase reversals for an even number of nulls sum up to a total phase change of zero, while the phase reversals for an odd number of nulls give an overall phase change of ±180°. Hence, a linear phase change has to be introduced to a pattern with an odd number of nulls, while no phase is needed for an even number of nulls.

The null widths of the multiple nulls do not differ much from the null width of a single null if the angular spacing between the nulls are kept large enough. On the other hand, the ripple changes significantly as the ripple caused by the abrupt phase reversals are superimposed. The angular distances between the nulls determine if there will be an increase or decrease in the ripple between the nulls. The angular distance between two nulls may not be too small, otherwise one null will be formed between the nulls.

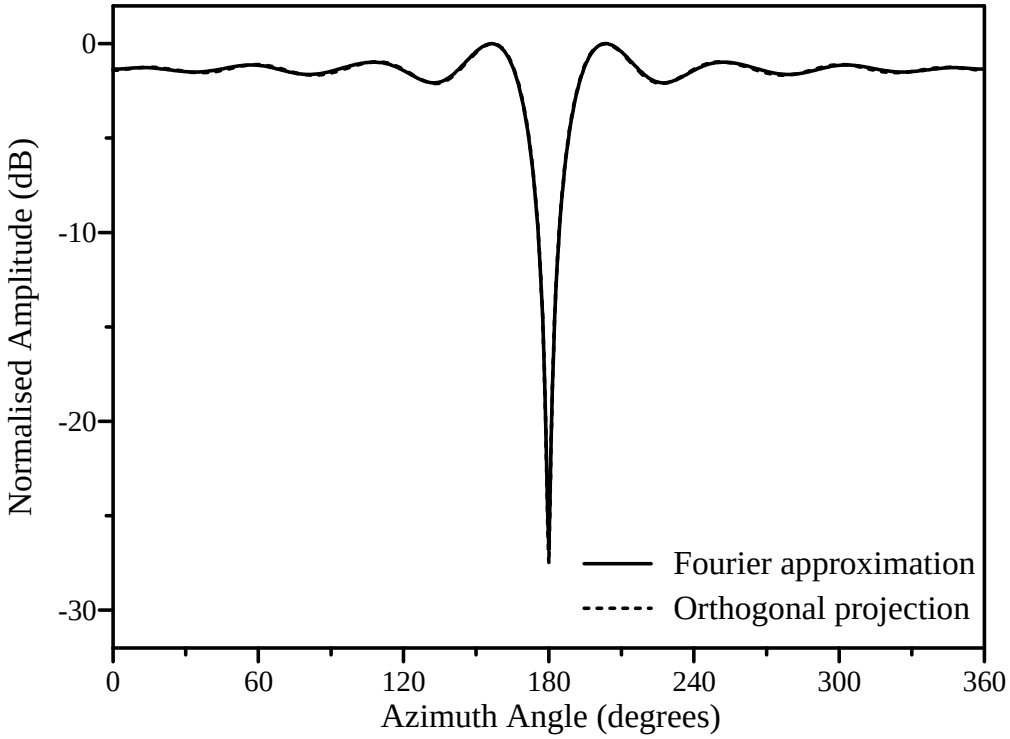

Figure 2.16: Comparison of the amplitude radiation patterns for a single null using the Fourier approximation and orthogonal projection (N=16 and $R = \lambda_0$)

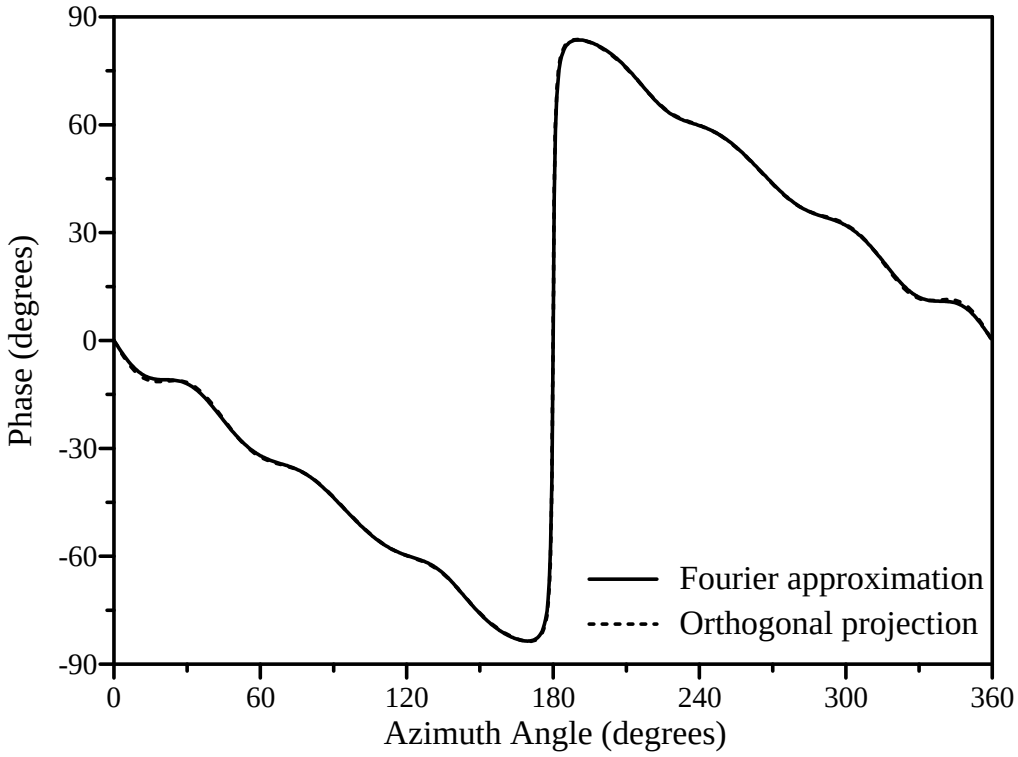

Figure 2.17: Comparison of the phase patterns for a single null using the Fourier approximation and orthogonal projection (N=16 and $R = \lambda_0$)

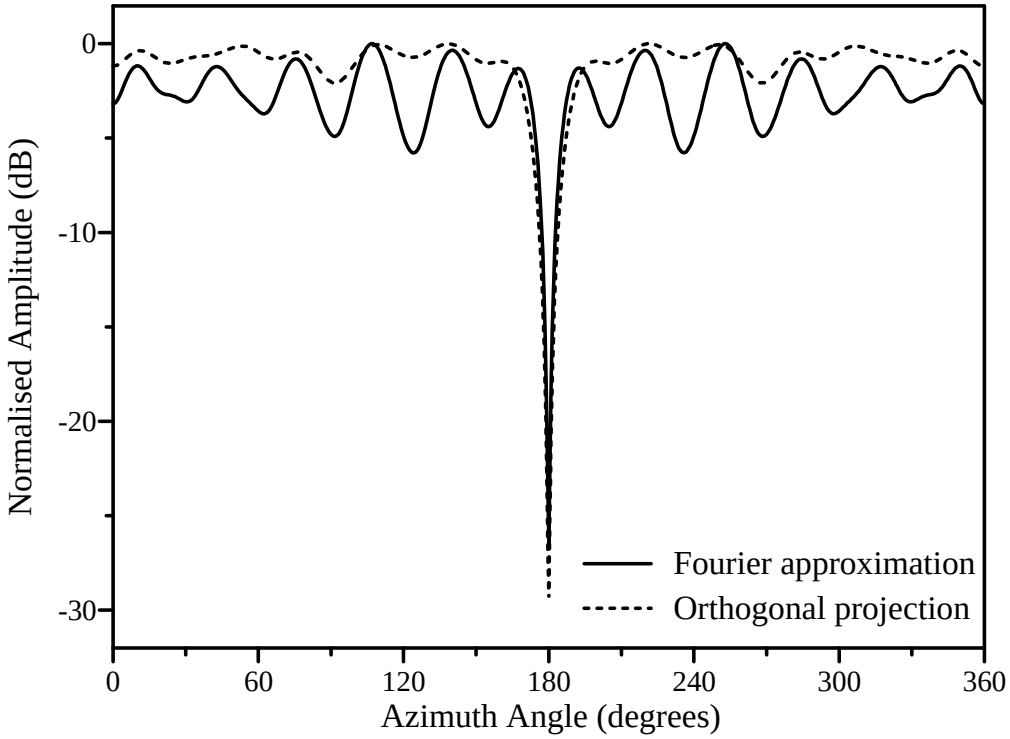

Figure 2.18: Comparison of the amplitude radiation patterns for a single null using the Fourier approximation and orthogonal projection (N=16 and $R = 1.385\lambda_0$)

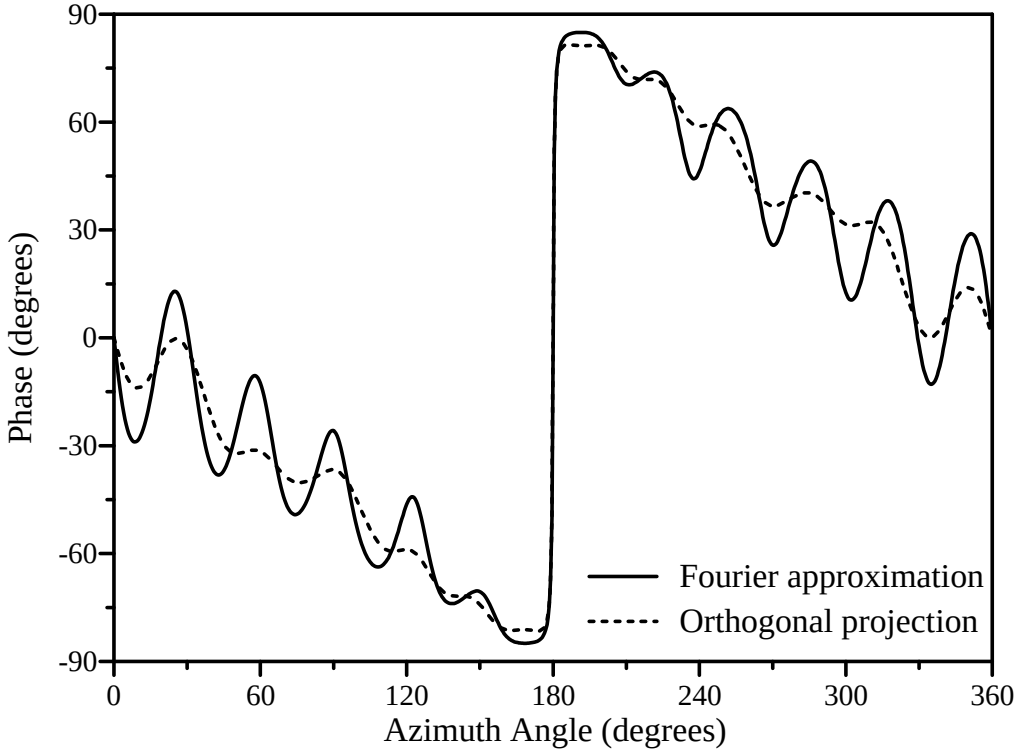

Figure 2.19: Comparison of the phase patterns for a single null using the Fourier approximation and orthogonal projection (N=16 and $R = 1.385\lambda_0$)

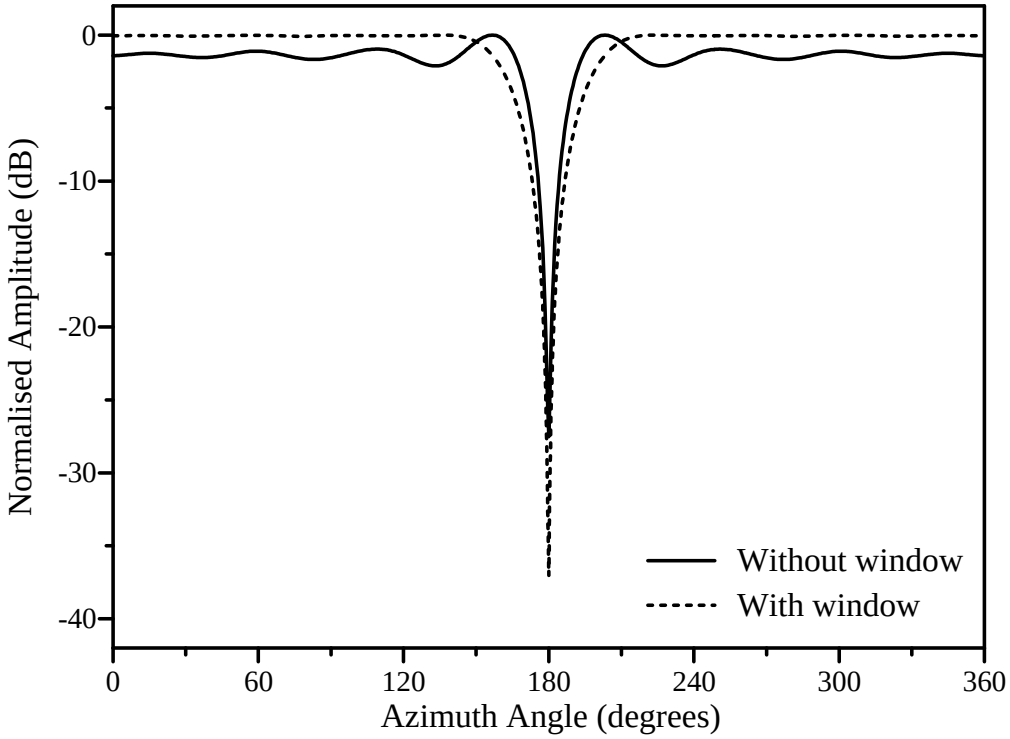

Figure 2.20: Comparison of the amplitude radiation patterns for a single null using the orthogonal projection method with and without a Hamming window (N=16 and $R = \lambda_0$)

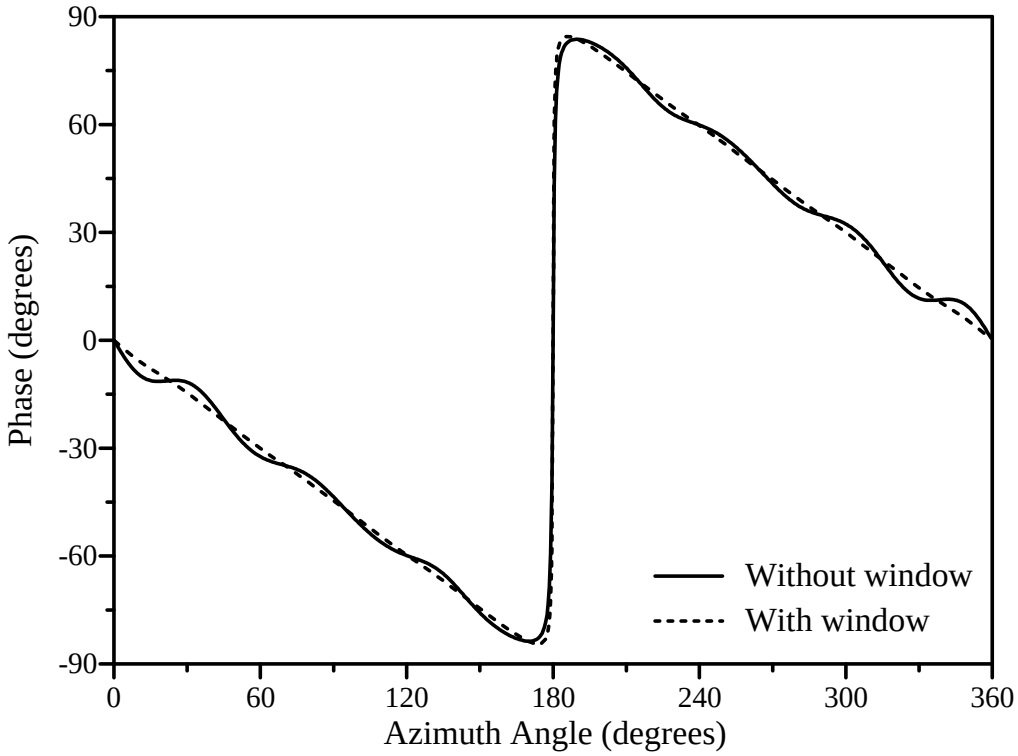

Figure 2.21: Comparison of the phase patterns for a single null using the orthogonal projection method with and without a Hamming window (N=16 and $R = \lambda_0$)

An omnidirectional pattern with two nulls at 90° and 270°, respectively, were simulated using the orthogonal projection method with a Hamming window. Figures 2.22 and 2.23 show the resulting amplitude and phase of the radiation pattern, respectively. An additional null was introduced at 180° and the amplitude and phase of the radiation pattern with three nulls are shown in Figures 2.24 and 2.25.

The difference in the phase patterns for odd and even nulls can be seen when Figures 2.23 and 2.25 are compared. A linear phase change is required for the introduction of the three nulls, whereas introduction of two nulls require no phase change. When comparing Figures 2.22 and 2.24, the effect of the spacing between the nulls on the null depths can also be seen. The null depths changed as the null spacing decreased from 180° to 90°.

Phase reversals of ±180° do not guarantee infinitely deep nulls. In general, the depths of the realised nulls depend on the array radius, the number of elements and the angular distance between the nulls. Abele [54] proposed the use of a variable phase step to provide control over the realised null depth. For a phase step of angle α, the absolute value of the average of both sides of the step will be:

$$\begin{aligned} \left|\hat{F}\right| &= \frac{|1+e^{j\alpha}|}{2} \\ &= \cos\frac{\alpha}{2}. \end{aligned} \tag{2.50}$$

If the desired null depth is expressed in dB relative to the maximum of the pattern, the required phase difference to achieve this null depth will be:

$$\alpha = 2\arccos\left(10^{\hat{F}_{dB}/20}\right). \tag{2.51}$$

The overall phase slope for a single null has to be $\alpha/2\pi$ to keep the pattern smooth in the omni-region. To introduce multiple nulls with specified null depths in the idealised pattern, the overall phase difference, after introducing the appropriate phase steps, has to be cancelled by a linear phase change. Therefore, the required phase slope of the idealised pattern for a number (L) of step angles α_l will be:

$$\nu = -\frac{1}{2\pi}\sum_{l=1}^{L}\Delta_l\alpha_l, \tag{2.52}$$

where Δ_l is the step direction of the phase step which may be equal to -1 or 1.

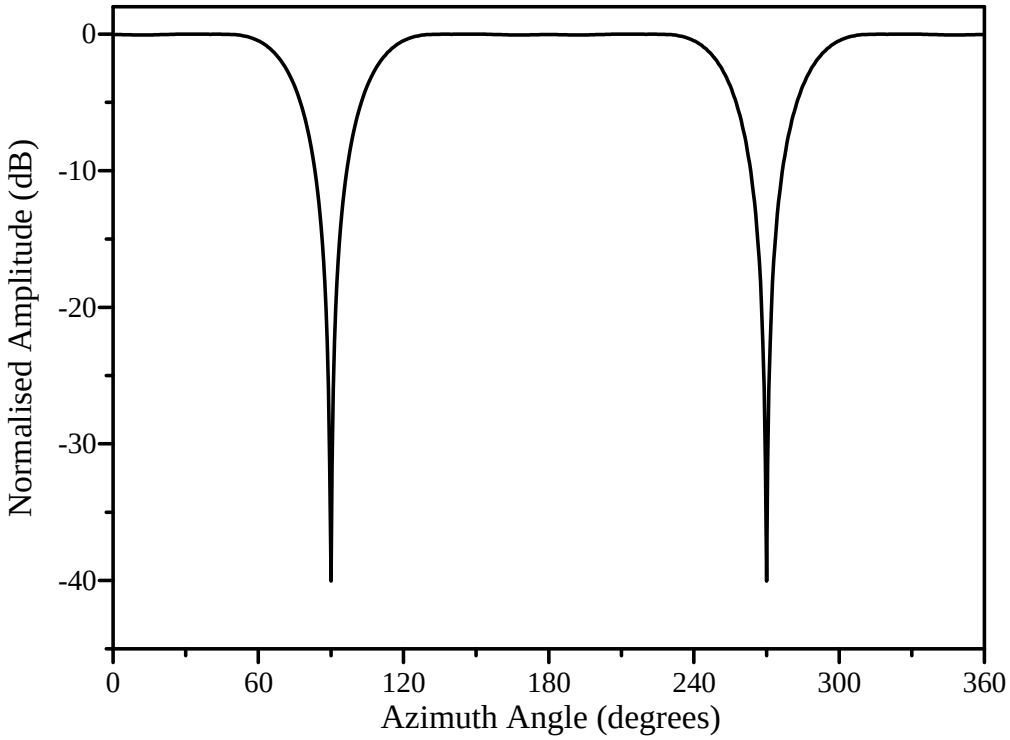

Figure 2.22: Amplitude radiation pattern for two nulls using the orthogonal projection method with a Hamming window (N=16 and $R = \lambda_0$)

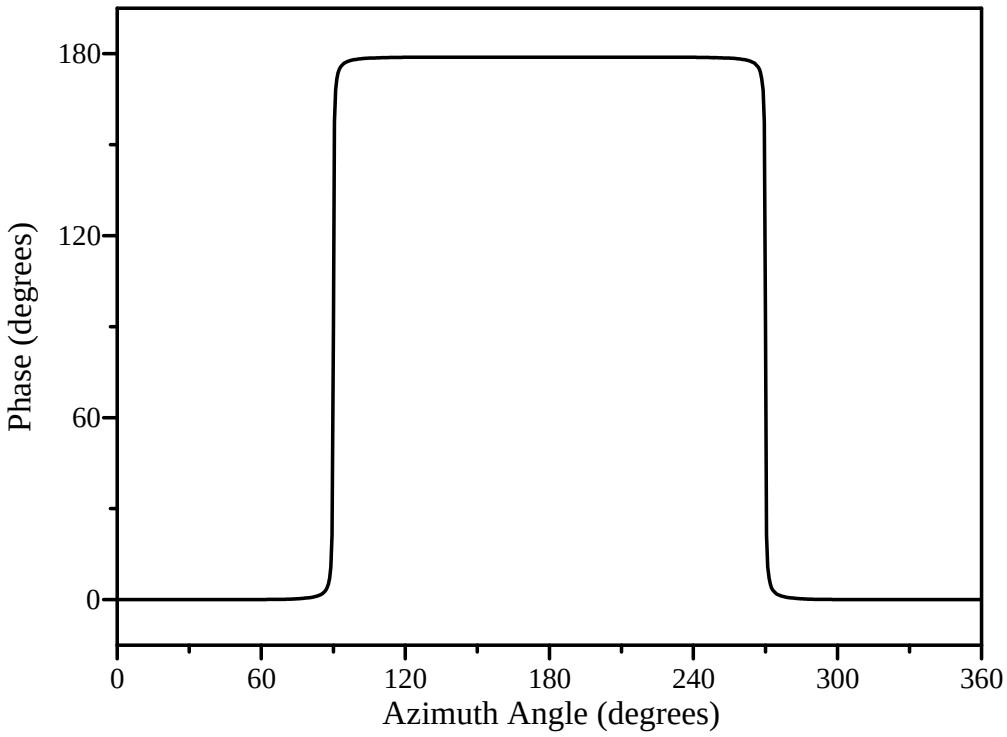

Figure 2.23: Phase pattern for two nulls using the orthogonal projection method with a Hamming window (N=16 and $R = \lambda_0$)

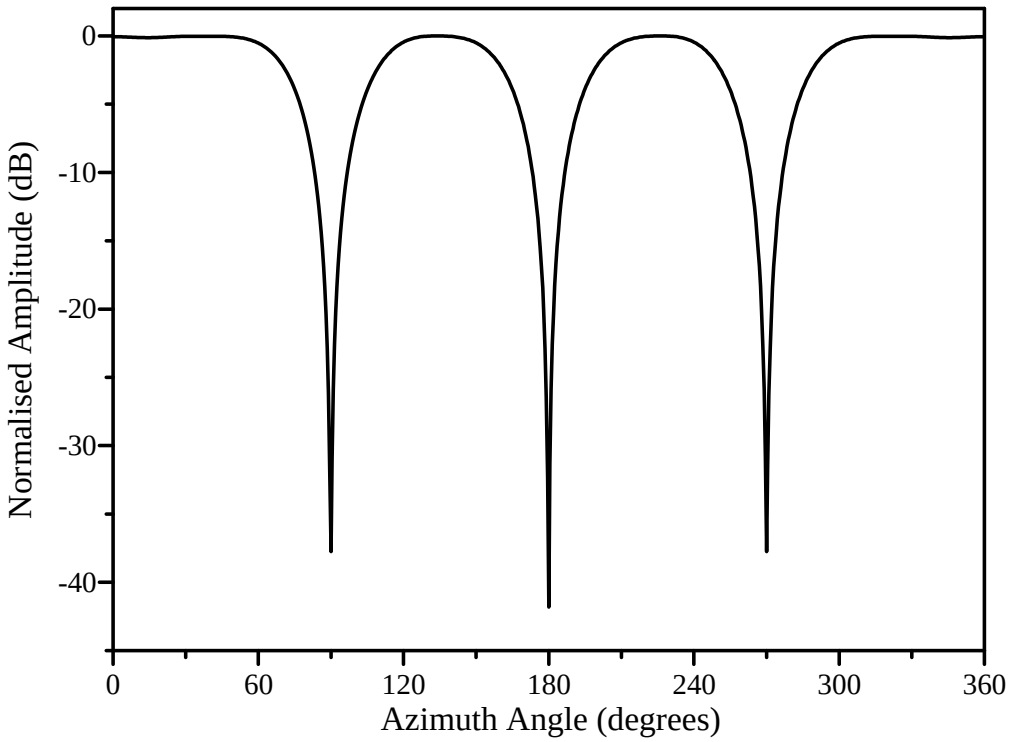

Figure 2.24: Amplitude radiation pattern for three nulls using the orthogonal projection method with a Hamming window (N=16 and $R = \lambda_0$)

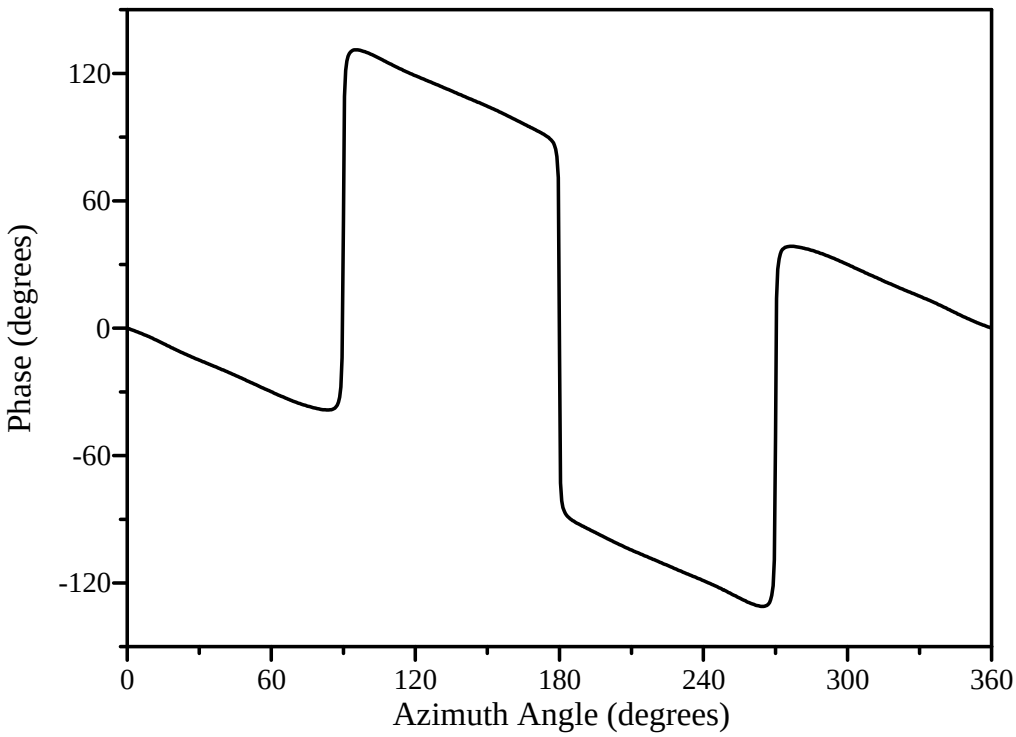

Figure 2.25: Phase pattern for three nulls using the orthogonal projection method with a Hamming window (N=16 and $R = \lambda_0$)

The directions of the phase steps are chosen in such a way as to minimise the sum of the phase differences and consequently minimise the required phase slope. If the previously mentioned windowing is required, the window displacement must be equal to ν. This method provides control over the null depths with acceptable accuracy, if the null depths are kept below 20 dB. Again the accuracy depends on the array configuration as well as the angular spacing between the nulls. The specified angular position of a null also has an influence on the null depth accuracy.

As an example, three nulls of depths 10 dB, 15 dB and 25 dB were required at 60°, 180° and 270°, respectively. The orthogonal projection, with a Hamming window, was utilised to form the desired nulls in the omnidirectional pattern of a 16 element array with a radius of λ_0. Figures 2.26 and 2.27 show the resulting amplitude and phase of the realised radiation pattern. The realised null depths are 9.9 dB, 15.1 dB and 24.1 dB at 60°, 180° and 270°, respectively. Each null depth requires a different phase step, as seen in the phase pattern in Figure 2.27. As the required null depth decreases, the null is also broadened.

2.3.5 Pattern synthesis with null constraints

When the radiation pattern is already given, Vescovo [50,51,55] proposed a method to introduce nulls into the pattern subsequently. The method was applied to reduce the sidelobe level by forming additional nulls near the main beam in a conventional beam pattern.

A radiation pattern, which does not necessarily satisfy the null constraint, is given by the N excitations a_n^0. The L null constraints, at the angles ϕ_l, are given by $F(\phi_l) = 0$ for $l = 1 \ldots L-1$.

The N excitations that minimise the Euclidean distance between the radiation pattern of a_n^0 and the pattern that satisfies the null constraint, are defined as a'_n. The squared Euclidean distance between the two patterns given by the sequence excitations s_m^0 and s'_m, is defined as:

$$\begin{aligned} \eta^2 &= \sum_{k=0}^{N-1} \left| b_m^0 - b'_m \right|^2 \\ &= \left\| \mathbf{b}^0 - \mathbf{b}' \right\|^2, \end{aligned} \tag{2.53}$$

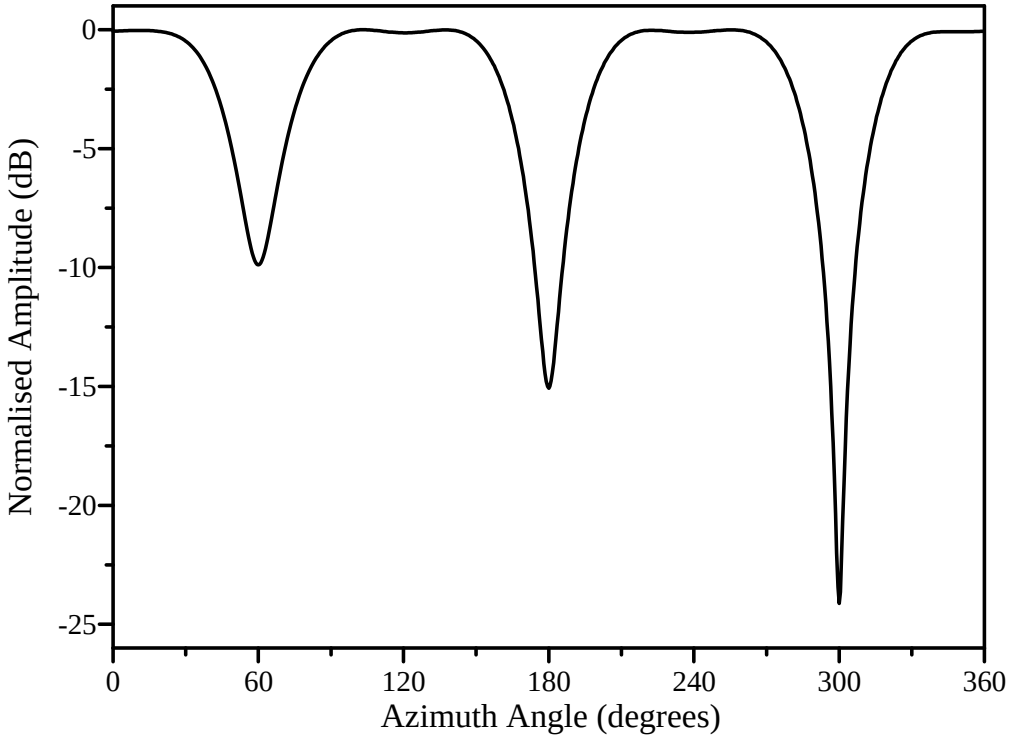

Figure 2.26: Amplitude radiation pattern of three nulls of required depths 10 dB, 15 dB and 25 dB at 60°,180° and 270°, respectively. (N=16 and $R = \lambda_0$)

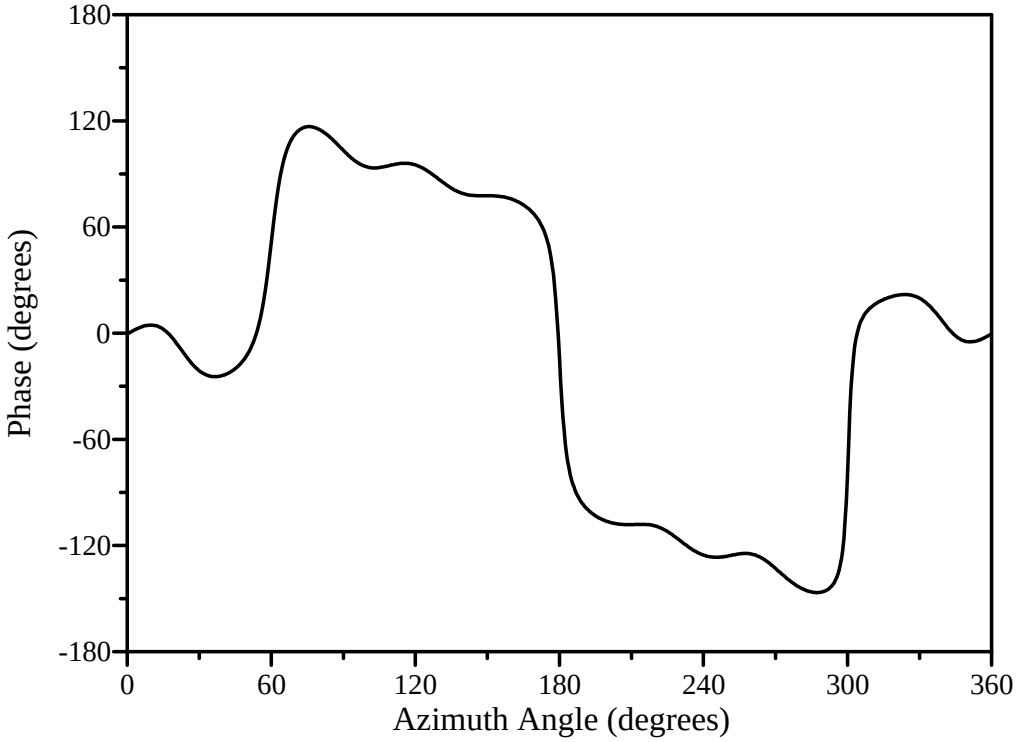

Figure 2.27: Phase pattern for three nulls of required depths 10 dB, 15 dB and 25 dB at 60°,180° and 270°, respectively. (N=16 and $R = \lambda_0$)

where

$$b_m^0 = \|g_m\| s_m^0 \tag{2.54}$$

and

$$b_m' = \|g_m\| s_m'. \tag{2.55}$$

Subsequently, the null constraints can be expressed as $\mathbf{B}\mathbf{b}' = 0$, where $\mathbf{B} = [B_{lm}]$ and $B_{lm} = g_m(\phi_l)/\|g_m\|$ for $l = 0 \ldots L-1$ and $m = 0 \ldots N-1$. The problem can therefore be described as minimising the Euclidian distance $\|\mathbf{b}^0 - \mathbf{b}'\|^2$ under the constraint $\mathbf{B}\mathbf{b}' = 0$. The optimal vector $\mathbf{b}'$ is given by [51]:

$$\mathbf{b}' = [\mathbf{I}_N - \mathbf{B}^H(\mathbf{B}\mathbf{B}^H)^{-1}\mathbf{B}]\mathbf{b}^0, \tag{2.56}$$

where $\mathbf{I}_N$ is a $N \times N$ identity matrix and $\mathbf{B}^H$ denotes the complex conjugate transpose of $\mathbf{B}$.

To obtain an omnidirectional pattern with nulls, the excitation vector $\mathbf{a}^0$ must be chosen in such a way as to yield an acceptable $\mathbf{a}'$. For the lowest possible ripple, $\mathbf{a}^0$ will be an excitation vector, which results in an omnidirectional pattern. The method produces infinitely deep nulls exactly at the desired angles, but with a gain ripple which can be as high as 20 dB.

Vescovo also proposed this technique to introduce nulls in the desired pattern of an arc array of directional elements [56]. Each directional element had a theoretical radiation pattern of:

$$E_n(\phi) = 1 + \cos(\phi - \phi_n). \tag{2.57}$$

Since the element radiation patterns point in different directions, the element pattern can not be factorised out of the array pattern to obtain an array factor [4,57]. Therefore, the orthogonal base defined in Equation 2.43 is used to obtain the desired pattern through the projection method. Additional nulls are formed afterwards by using null constraints.

2.3.6 Constrained minimisation with Lagrange multipliers

In this method, the distance between an idealised pattern and the realised pattern is also minimised [47]. As opposed to other methods, the idealised pattern has a constant phase and therefore the phase of the realised pattern will be almost constant. This

will result in an tangential null, where the phase is constant within the null and the resulting null width will consequently not be optimal. The squared error function:

$$\varepsilon^2 = \int_{-\pi}^{\pi} |AF(\phi) - 1| \, d\phi, \tag{2.58}$$

is minimised, subject to $AF(\phi_p) = 0$, where ϕ_p is the angle position of the null. The squared error is minimised using the method of Lagrange multipliers, which result in the vector of element excitations:

$$\mathbf{a} = \mathbf{Q}^{-1} \left[\mathbf{p} - \frac{\mathbf{d}^H(\phi_p)\mathbf{Q}^{-1}\mathbf{p}}{\mathbf{d}(\phi_p)\mathbf{Q}^{-1}\mathbf{d}(\phi_p)} \mathbf{d}(\phi_p) \right], \tag{2.59}$$

where $\mathbf{Q}$ is an $N \times N$ matrix with elements:

$$Q_{ij} = J_0 \left(2k_0 R \sin \left(\frac{\pi}{N} |i - j| \right) \right). \tag{2.60}$$

The N-dimensional vectors $\mathbf{d}(\phi)$ and $\mathbf{p}$ have elements:

$$d_i(\phi) = e^{jk_0 R \cos\left(\phi - \frac{2\pi}{N}\right)}, \tag{2.61}$$

and

$$p_i(\phi) = J_0(k_0 R), \tag{2.62}$$

respectively.

The realised pattern of this method has an infinitely deep null exactly at the desired location of the null. The tangential null is wider than the zero-crossing null and show a gain ripple between 2.5 and 3.5 dB. The constant idealised phase appears not to be suitable for the synthesis of an omnidirectional pattern with a narrow null and low gain ripple.

2.3.7 Constrained optimisation techniques

The methods, which have been discussed in the previous sections, all provide an omnidirectional pattern with nulls, but with different null depths, null widths and gain ripples. These methods do not have the ability to constrain a certain property of the array pattern.

Constrained optimisation allows the prescription of some of the characteristics of the array pattern, while optimising the others. The null width, for example, may be optimised for a given gain ripple and null depth, or the gain ripple may be minimised, while specifying the null width and null depth values. An optimisation technique may also allow the definition of any criteria relevant to the specified application e.g. allowable excitation amplitudes and phases.

These optimisation techniques may utilise methods such as the least squares optimisation method [45], the minimax and linear programming methods [48], the Hooke and Jeeves algorithm [45] and the simulated annealing method [52]. Prasad [45] applied the least squares optimisation method to circular and arc arrays to form a beam pattern with a specified beamwidth. Additional nulls were also placed in the sidelobe region by using null constraints while minimising the mean square difference between the desired pattern and the optimum pattern. The Hook and Jeeves algorithm was also used to perform an iterative search to find the optimum excitation vector while satisfying the null constraints. During the search, the sidelobe level was minimised.

For linear arrays, Mismar [48] introduced a method to locate nulls in the prescribed directions while keeping the main beam towards the desired signal. A minimax approximation technique is used to search for the maximum point in the constraint region to control the sidelobe level directly, while at the same time control the main beam characteristics as required. Ares *et al.* [52] used a simulated annealing technique to produce beam patterns for a circular arc array on a cylinder. A cost function, which could include terms to control the radiation pattern, was minimised. Terms which placed constraints on the excitations, could also be included in the cost function.

Since the desired pattern is a function of the excitation vector, the search is executed in a $2N$-dimensional space. A high computational expense is thus encountered. The choice of the starting values also plays a very important roll in the success of these pattern search techniques. Choosing the starting values carefully can limit the computational time and avoid local minima. The use of an excitation vector, with a resulting pattern error close to the global minimum, is encouraged.

2.4 Mutual coupling compensation

If the element excitations, obtained from the null synthesis technique, are applied to the antenna elements, distortion of these excitations may occur due to the mutual coupling between the antenna elements in the array. The consequent errors in the element excitations deteriorate the desired radiation pattern [72, 73]. Therefore, the mutual coupling must be compensated for to avoid errors in the desired characteristics of the null.

Lo [74] investigated the effect of the mutual coupling on the beam scanning and null steering performance of a linear monopole array. It was found that null filling and/or null steering errors occurred when the mutual coupling was not compensated for during the computation of the element excitations. The effect of the mutual coupling on the null pattern of a cylindrical dipole array was studied by Abele *et al.* [54]. The mutual coupling between the dipoles had a deforming effect on the the null pattern. Null filling and null position errors also occurred and the gain ripple was increased.

One direct way of minimising the effect of the mutual coupling, is by reducing the mutual coupling itself. The antenna elements in the array, for example, can be designed in such a way as to exhibit small coupling values. Absorbing material can be placed between the elements to reduce the coupling or the spacing between the elements can be chosen in such a way, that the coupling has an insignificant effect on the desired radiation pattern.

Another way of dealing with the coupling, is to compensate for it in the pattern synthesis technique. Impedance and coupling matrixes are used in the pattern synthesis technique to compute corrected element excitations, which compensate for the mutual coupling. According to Ghorbani [87], the mutual coupling also causes a mismatch between the driving impedances of the antenna elements and the feeding system of the array. This effect may significantly degrade the performance of narrowband arrays. These driving impedances can be corrected by altering the physical properties of the antenna elements to obtain the desired driving impedances for a required set of element excitations. A short overview of these techniques is given in the following sections.

2.4.1 Minimising the mutual coupling effects

Lo and Vu [74] investigated the use of guard elements in a linear monopole array to reduce the effect of the mutual coupling on null steering. Due to mutual coupling, the active element patterns are not comparable, which result in null filling and null steering errors. It was found that by placing guard elements at both ends of the linear array, the active element patterns resemble each other more closely. The perturbation of the zeros is reduced and consequently the null filling and null steering error are minimised. The method does not completely compensate for the mutual coupling, but is able to minimise the coupling effect without changing the element excitations.

When computing the coupling between array elements, the coupling of the electromagnetic fields in the free space immediately above the elements, is usually considered in the calculation. For microstrip array elements constructed on the same common substrate, additional coupling occurs due to the surface wave in the substrate. When using thick substrates, this surface wave coupling can be very strong due to a larger surface wave being generated. Bamford *et al* [81] examined the direct radiation and surface wave coupling separately through a method based on the reaction theorem. The behaviour of the total coupling was also studied for various element separation distances and substrate thicknesses. It was found that when the two coupling parameters are in phase, they add to form an upper limit curve for the coupling, but also form a lower limit curve when they are opposite in phase. A reduction in mutual coupling is thus possible through an appropriate choice of substrate thickness and separation distance between the array elements. The possible heights for the substrate are usually determined by the required bandwidth and the available substrate thicknesses as supplied by the manufacturers. Similarly, the possible separation distances are limited by the desired radiation pattern characteristics. Therefore, the reduction of the mutual coupling using this method may be limited by the requirements on the impedance and radiation behaviour of the array.

2.4.2 Compensation using coupling and impedance matrixes

Steyskal and Herd [76] showed that the element excitations a_n can always be chosen in such a way as to compensate for the pattern error due to mutual coupling. The technique uses the formulation that any composite array pattern is a weighted sum

of the isolated element patterns and that the mutual coupling parasitically excites all the elements. The mutual coupling can thus be compensated for by driving the array with modified element excitations in such a way that the desired radiation pattern is obtained in the presence of these parasitics. The coupling perturbed signals and the unperturbed desired signals, can be related through a coupling matrix $\mathbf{C}$:

$$\mathbf{v} = \mathbf{C}\mathbf{v^d}, \tag{2.63}$$

where the vectors $\mathbf{v}$ and $\mathbf{v_d}$ represent the coupling perturbed signals v_n and the desired signals v_n^d, respectively. The compensation for the mutual coupling can thus be accomplished by simply multiplying the received signals $\mathbf{v}$ with the inverse of the coupling matrix:

$$\mathbf{v^d} = \mathbf{C^{-1}}\mathbf{v}. \tag{2.64}$$

This method restores the signals as being received by the isolated antenna elements in the absence of coupling. The coupling coefficients can be obtained from two different methods: a Fourier decomposition of the measured element patterns or coupling measurements between the array ports. The matrix $\mathbf{C^{-1}}$ may be very difficult or impractical to realise with an analog network, but can be easily realised in a digital beam forming antenna system. Darwood *et al* also extended this technique for planar arrays [82]. The method assumes that the current distribution over the array elements is not affected by the coupling and remains unchanged from one element to the other in the array. It is furthermore assumed that only the input impedance of the element is affected by the mutual coupling. This approach may fail when electrically large elements and arrays of dissimilar elements are considered.

Any errors in the coupling matrix, due to these assumptions, will contribute to the degradation of difference beam patterns. Fletcher *et al* [80] derived a covariance matrix for any signal direction of arrival that includes the effects of the mutual coupling. By multiplying the inverse of this covariance matrix with the coupling corrected difference beam excitation vector, an optimum excitation vector is found which restores the difference beam pattern.

Derneryd [79] proposed an alternative way of viewing the matrix multiplication technique. An array antenna can be represented by a multiport network that is characterised by a $N \times N$ scattering matrix, $\mathbf{S}$ [75]. This scattering matrix relates the forward

and backward travelling waves, $\mathbf{v}^+$ and $\mathbf{v}^-$, respectively, on the feed lines:

$$\mathbf{v}^- = \mathbf{S}\mathbf{v}^+. \tag{2.65}$$

The array excitation vector $\mathbf{A}$ is given by the sum of the incident and reflected signals and in the transmitting mode it becomes:

$$\begin{aligned} \mathbf{A} &= \mathbf{v}^+ + \mathbf{v}^- \\ &= (\mathbf{I} + \mathbf{S})\mathbf{v}^+ \\ &= \mathbf{C}\mathbf{v}^+, \end{aligned} \tag{2.66}$$

where I is the unit matrix. The modified incident signals to produce the desired radiation pattern in the mutually coupled environment, is thus given by:

$$\mathbf{v}^+ = \mathbf{C}^{-\mathbf{1}}\mathbf{v}^{\mathbf{d}}. \tag{2.67}$$

These modified signals can be controlled by amplifiers and phase shifters.

The inclusion of the mutual coupling in the relation of the incident and reflected waves is also applied by Eclercy *et al* [72, 77], though in this method the effect of the mutual coupling is taken into account in the radiated field of the array. The reflection coefficient at the feed line of the n-th antenna element is defined as:

$$\Gamma_n = \frac{v_n^-}{v_n^+}, \tag{2.68}$$

where

$$v_n^- = \sum_{p=1}^{N} S_{np} v_p^+. \tag{2.69}$$

Keeping the mutual coupling in mind, the radiation pattern can be written as:

$$\begin{aligned} F(\phi) &= \sum_{n=1}^{N} E_n(\phi)(v_n^+ + v_n^-)e^{jk_0(x_n\cos\phi + y_n\sin\phi)} \\ &= \sum_{n=1}^{N} E_n(\phi)v_n^+(1+\Gamma_n)e^{jk_0(x_n\cos\phi + y_n\sin\phi)}. \end{aligned} \tag{2.70}$$

This radiation pattern is then used in the pattern synthesis method to obtain the modified element excitations, which compensate for the mutual coupling.

Using the vector notation of Equation 2.18, the array radiation pattern can be written as [83]:

$$\begin{aligned} \mathbf{F} &= \mathbf{B}(\mathbf{I} + \mathbf{S})\mathbf{v}^{+} \\ &= \mathbf{B}'\mathbf{v}^{+}, \end{aligned} \tag{2.71}$$

where $\mathbf{A}$ is replaced using Equation 2.66. The matrix $\mathbf{B}'$ and the pattern $\mathbf{F}$ are computed at more angles than there are elements in the array. The solution for $\mathbf{v}^{+}$ is thus obtained in a least squares sense. This method assumes that the element patterns are all equal to the element pattern of an isolated element. Where antenna elements are closely spaced, the current distributions of the elements are changed by the coupling, resulting in active element patterns. Taking this into consideration, Caccavale *et al* [85] proposed an active element convex programming method (ACE-COP), in which the array radiation pattern is expressed as the superposition of active element patterns. The method is mostly applicable to small arrays, due to the additional computational burden required by the evaluation of the active element patterns. In large arrays, where most of the elements experience similar electromagnetic environments, it can be assumed that all the elements radiate the same active element pattern. This approach is referred to as the modified element pattern (m.e.p.) technique [85].

The correction for the mutual coupling may also be done through the impedance [54, 78,85] or admittance [84] relations between the antenna element currents and voltages. If the currents of the antenna elements are set proportional to the computed excitation coefficients, the driving voltages of the elements can be expressed as:

$$\mathbf{V} = \mathbf{Z}\mathbf{I}, \tag{2.72}$$

with $\mathbf{V}$ and $\mathbf{I}$ being $1 \times N$ the driving voltage and current vectors, respectively, and $\mathbf{Z}$ being a $N \times N$ impedance matrix. The driving voltage of the m-th element, that compensates for the mutual coupling with the other antenna elements, can thus be

written as:

$$\begin{aligned} V_m &= \sum_{n=1}^{N} Z_{mn} I_n \\ &= Z^s_{mm} I_m + \sum_{\substack{n=1 \\ n \neq m}}^{N} Z_{mn} I_n, \end{aligned} \tag{2.73}$$

where Z^s_{mm} is the self impedance of the m-th antenna element and Z_{mn} is the mutual impedance between the m-th and n-th antenna elements. The self and mutual impedances depend on the type of antenna elements as well as the mounting structure used to construct the array. Abele *et al* [54] introduced a variable:

$$Z_n = \begin{cases} Z^s_{nn} & \text{for } n \bmod N = 0, \\ Z_{1,n \bmod N} & \text{for } n \bmod N \neq 0, \end{cases} \tag{2.74}$$

for $n = 1 \ldots N$. Equation 2.73 can then be written as:

$$\begin{aligned} V_m &= \sum_{n=1}^{N} Z_{m-n} I_n \\ &= \{Z_n; n = 1 \ldots N\} * \{I_n; n = 1 \ldots N\}, \end{aligned} \tag{2.75}$$

where the asterisk denotes a circular convolution.

The correction for the mutual coupling can be included in the design procedure by multiplying the desired sequence excitation coefficients with the DFT of the impedances Z_n, before computing the element excitations a_n. The element currents and driving voltages are then defined as:

$$I_n = I_0 \cdot \text{IDFT}\{s_m; m = 1 \ldots N\}, \tag{2.76}$$

and

$$V_n = I_0 \cdot \text{IDFT}(\text{DFT}\{Z_n; n = 1 \ldots N\} \cdot \{s_m; m = 1 \ldots N\}). \tag{2.77}$$

When setting the element voltages proportional to the excitation coefficient, similar expressions can be found for the necessary driving currents, using the admittance relation:

$$\mathbf{I} = \mathbf{Y}\mathbf{V}. \tag{2.78}$$

The driving current of the m-th element may also be written as:

$$\begin{aligned} I_m &= \sum_{n=1}^{N} Y_{mn} V_n \\ &= Y^s_{mm} V_m + \sum_{\substack{n=1 \\ n \neq m}}^{N} Y_{mn} V_n, \end{aligned} \tag{2.79}$$

with Y^s_{mm} and Y_{mn} respectively denoting the self admittance of the m-th element and mutual admittance between the m-th and n-th elements.

2.4.3 Modification of the driving impedances

From Equation 2.73, the driving impedance of the m-th element can be expressed as:

$$Z^a_m = Z^s_{mm} + \sum_{\substack{n=1 \\ n \neq m}}^{N} Z_{mn} \frac{I_n}{I_m}. \tag{2.80}$$

It is observed that the driving impedances do not only depend on the configurations of the array and the antenna elements, but also on the currents of the elements. When designing the feed network of the array, it is these driving impedances which have to be matched. If the mismatches at the feed ports are not taken into account, it may significantly degrade the performance of narrowband arrays. The resulting driving impedances obtained from the radiation pattern correction methods remain unmatched and unequal. Consequently, the design of a feeding and matching network can be complicated.

Another possibility is to alter the individual element geometries physically in order to have equal driving impedances for the required element excitations [86, 88, 89]. Yang *et al* [86] proposed this technique for an electromagnetically coupled (EMC) dipole antenna array. From Equation 2.79, the driving admittance of each element in the array can be obtained as:

$$Y^a_m = Y^s_{mm} + \sum_{\substack{n=1 \\ n \neq m}}^{N} Y_{mn} \frac{V_n}{V_m}. \tag{2.81}$$

In a linear system, a second design equation can be derived from the current in each dipole:

$$\frac{I_m^a}{V_m} = \frac{I_{mm}}{V_m} + \sum_{\substack{n=1 \\ n \neq m}}^{N} \frac{I_{mn}}{V_n}, \tag{2.82}$$

where I_{mm} is the current of the m-th dipole in the absence of other dipole and I_{mn} is the current of the m-th dipole due to the current on the n-th dipole. The admittances and currents are functions of the voltages, dipole lengths and dipole offsets from the microstrip feed line. For a given design goal, e.g. the active currents on the dipoles, a set of dipole lengths and offsets is found, which not only satisfies Equation 2.82, but also provides the prescribed driving admittances seen by the feed lines. Design curves for the mutual admittances and self admittances are obtained from a method of moments solution. A desired bandwidth and voltage standing wave ratio (VSWR) at the resonant frequency are obtainable, while finding good agreement between the desired and measured radiation patterns.

Chen *et al* proposed a similar technique for a linear array of parallel dipoles [88]. In this case, the lengths and the radii of the dipoles were changed to obtain the desired radiation pattern as well as equal driving impedances for the dipoles. This resulted in a feed network that was much simpler than usual. The technique was also extended to planar dipole arrays [89]. Input impedances of 75Ω for the dipoles, as well as the required radiation pattern, were obtained.

2.5 Summary

Different characteristics of the cylindrical microstrip patch antenna have been discussed. The cavity model was used to illustrate the influence of some of the design parameters of the cylinder and the patch antenna on the radiated element pattern. Therefore the design of the antenna element, has an influence on the characteristics of the total radiated array pattern. Since the radiation characteristics of the cylindrical patch antenna also depend on the polarisation, the choice of polarisation must be included in the design procedure of the array pattern.

The radiated array pattern of a cylindrical array has also been discussed. Equally spaced cylindrical arrays have the unique characteristic that they can produce omni-

directional patterns by being excited with phase-sequence excitations. A combination of these sequence excitations can be used to form a desired array radiation pattern. The element excitations are obtained from the resulting coefficients of the sequence excitations through a discrete Fourier transform.

An omnidirectional radiation pattern, with nulls at the specified angle directions, is defined as the desired radiation pattern. An overview of null synthesis techniques was given to obtain this desired radiation pattern with cylindrical arrays. The superposition of sequence excitations is only suitable for arrays with a small number of elements, while the Fourier approximation perform well only for small inter-element spacings. When null constraints are used to form the nulls, the resulting ripple is very high. The increased null width is the main drawback of constraint minimisation with Lagrange multipliers. The orthogonal projection method and its extensions are well suited to form the desired radiation pattern for most cylindrical array configurations. Some control over the null depths and ripple are provided through variable phase steps and a window function. Pattern optimisation techniques can be used to obtain the desired pattern, while optimising certain array pattern characteristics. In Chapter 3, the orthogonal projection method is extended for a cylindrical microstrip patch array to provide an omnidirectional pattern with one or more nulls. The resulting excitation vector is also used as the starting value for two optimisation algorithm, which allows the specification and/or optimisation of certain pattern characteristics, e.g. null depth, null width and gain ripple.

The synthesis of the radiation pattern is influenced by the mutual coupling between the antenna elements. If the mutual coupling is not compensated for in the design procedure, the consequent errors in the element excitations may deteriorate the radiation pattern. Minimisation of the coupling reduces the effect of the coupling on the radiation pattern, but does not totally compensate for the coupling. By using a coupling or impedance matrix to include the mutual coupling in the design procedure, the coupling is completely compensated for. However, the driving impedances remain unmatched and may result in complicated feed networks. As an alternative, the geometries of the elements may be varied to provide matched and equal driving impedances for all the antenna elements, given a required set of element excitations. This compensation technique is applied to the cylindrical patch array in Chapter 4 by altering the geometries of the patch antenna elements. This technique provides the desired pattern by correcting the driving impedances.

CHAPTER 3

NULL SYNTHESIS

The desired omnidirectional radiation pattern with nulls can be obtained by using a null synthesis technique, which incorporates the characteristics of the conformal microstrip patches. In this chapter, three pattern synthesis techniques are used to form the desired null pattern.

Abele et al. [53] introduced a null synthesis technique for a cylindrical dipole array. The technique utilised the orthogonal projection method and projected an idealised null pattern onto the orthogonal base of realisable array patterns. The orthogonal projection method of Abele [53] is extended to include the radiation characteristics of microstrip patches mounted on a conducting cylinder. An idealised null pattern is then projected onto the space of realisable array patterns to obtain the element excitations.

The orthogonal projection method provides an optimal array pattern with the minimum pattern error (in a mean square sense). This implies that the amplitude and phase of the radiation pattern are optimised simultaneously, which may not provide the desired amplitude pattern characteristics. The Objective Weighting method, previously applied in other fields of computational electromagnetic problems [96, 97], is therefore used to improve the amplitude pattern characteristics. A global performance function is defined by utilising both the amplitude pattern error and the phase pattern error. This global performance function is then minimised by using the element excitations obtained from the orthogonal projection method as the starting values.

A constrained optimisation algorithm is also utilised to provide control over the individual amplitude pattern characteristics. The squared distance between the desired

pattern and the resulting pattern is minimised while constraining the characteristics of the amplitude pattern. The optimal element excitations provided by the orthogonal projection method are also used as starting values for the optimisation technique.

The null forming performance of the three techniques will be compared in this chapter. The resulting null patterns of the cylindrical microstrip patch array and an array of omnidirectional dipole elements are also compared. Furthermore, the influence of the array geometry (e.g. inter-element spacing and number of elements) and element radiation pattern on the amplitude pattern characteristics, are investigated.

3.1 Orthogonal projection method

3.1.1 Modification of the orthogonal base

The orthogonal projection method for equally spaced antenna elements, may be extended to include the radiation pattern of a conformal microstrip patch antenna. The extension is done by modifying the orthogonal base for the space of realisable array patterns given by $g_m(\phi)$, which is defined in Equation 2.43. The omnidirectional radiation pattern of the n-th antenna element is replaced with the directional radiation pattern of a cylindrical microstrip patch antenna. A similar technique was proposed by Vescovo [56] for an arc array of theoretical directional antenna elements. An element pattern can not be factorised out of the array pattern to obtain an array factor, since all the element patterns point in different directions. Once the orthogonal base has been extended, the unconstrained optimum sequence excitations are obtained from the projection of the ideal null pattern, $F_0(\phi)$, in Equation 2.39 onto the orthogonal base using Equation 2.46.

The element pattern may be obtained from either simulation or measurement. The projection method does not consider the mutual coupling between the antenna elements and it is also assumed that the antenna elements do not disturb each other's current distributions. Each element radiation pattern is thus identical to the radiation pattern of an isolated antenna in both shape and strength. The input impedance of each antenna element is furthermore assumed to be matched to the impedance of its port in the feeding network.

For electrically thin patch antennas, the cavity model have been shown to be sufficient to compute the characteristics of the patch antenna [23, 24, 29]. The two components of the radiation pattern, using the cavity model, are defined in Equations 2.10 and 2.11. To improve the bandwidth and gain performance, electrically thick patches are usually considered. For these electrically thick patches, hybrid modes are excited, which are neither pure TE nor TM polarized waves and require more accurate analysis methods [14]. The characteristics of these patches are therefore obtained from a finite difference time domain (FDTD) analysis program [30]. An infinitely long cylinder is considered in the cavity model and the effect of the edges of the cylinder on the radiation pattern are thus neglected [13]. The FDTD software may also be used to incorporate the effects of finite cylinders. Since the co-polar component will be used to form the desired radiation pattern, the element radiation pattern will refer only to the co-polar component of the radiation pattern of the patch antenna element.

3.1.2 Results of the projection method

The geometries of probe-fed axially and circumferentially polarised patch antenna arrays are used to illustrate the performance of the null synthesis method. The results are also compared with the results obtained with the null synthesis algorithm for omnidirectional element arrays. A cylindrical dipole array is used as a representative example.

Figure 3.1 illustrates the configuration of a typical cylindrical patch array, with d_ϕ and s_ϕ being the inter-element and edge spacing, respectively. Electrically thin conformal microstrip patches were designed for a resonant frequency of 1.8 GHz for the dominant mode, using $h = 0.159$ cm and $\varepsilon_r = 2.3$. $L = 2b = 5.44$ cm and $W = 2\theta_0 = 6$ cm for the axially polarised patches and $W = 2b = 6$ cm and $L = 2\theta_0 = 5.44$ cm for the circumferentially polarised patches. For the first example, six elements and an inter-element spacing of $d_\phi = 0.5\lambda_0$ was used. A null of infinite depth at 180° was desired. Therefore, an ideal null pattern with an abrupt phase reversal at 180° was projected onto the orthogonal base formed by the six element patterns. The unconstrained optimum sequence excitations obtained from the projection method, are then multiplied with a Hamming window to reduce the ripple in the omniregion, as proposed by Abele *et al* [53, 54]. The resulting sequence excitations are used to calculate the element excitations through the DFT relation in Equation 2.28.

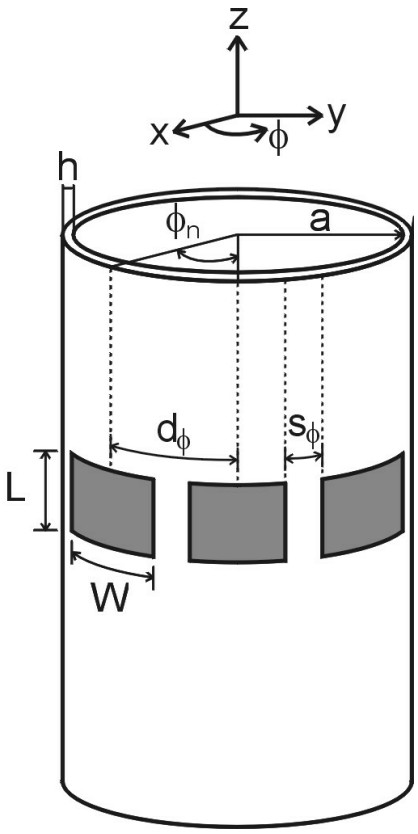

Figure 3.1: Configuration of a typical cylindrical microstrip patch antenna array

The array radiation patterns in Figure 3.2 were formed using the resulting element excitations for the axially and circumferentially polarised patch arrays. The radiation pattern obtained for a dipole array with the same number of elements and inter-element spacing is also shown for comparison. When comparing the nulls formed at 180° by the three cylindrical array configurations, it is seen that the resulting null characteristics are different. The circumferentially polarised patch array forms the deepest null with the least ripple, while the smallest null width is given by the axially polarised patch array. The differences in the resulting ripple and null widths are mainly due to the different antenna element patterns. The arrays with directional patch elements yielded better results than the array with omnidirectional dipole elements. Figure 3.3 also compares the phase of the resulting radiation patterns. All three phase patterns have an abrupt phase reversal at 180°, with the circumferentially polarised patch array having the least ripple in its phase pattern.

The number of elements of the arrays were increased to $N = 10$, while keeping the $0.5\lambda_0$ inter-element spacing. The same null with an infinite depth at 180° was required.

Figures 3.4 and 3.5 respectively compare the resulting amplitude and phase patterns of the projection method for the three arrays. Due to the increase in the degrees of freedom, the differences in the characteristics of the resulting null patterns of the arrays are less. A higher slope in the phase reversal and a decrease in ripple and null width are also observed for the increase in the number of array elements. The deepest null with the least ripple is formed by the circumferentially polarised patch array, while the smallest null width is obtained with the dipole array.

To study the influence of the number of array elements on the characteristics of the nulls, obtained with the projection method, the inter-element spacing was kept constant at $0.5\lambda_0$, while varying the number of elements ($6 \leq N \leq 20$). A null of infinite depth in the direction of the first element ($\phi_n = 2\pi/N$) was required. For each of the three array configurations, the gain ripple, null width and null depth are compared in Figures 3.6, 3.7 and 3.8, respectively. A gradual decrease in the ripple and null width is observed for the circumferentially and axially polarised patch arrays as the number of elements is increased. The null width of the resulting null patterns of the three arrays also become similar for a large number of elements ($N \geq 15$). When using the dipole array, a high gain ripple is observed for certain numbers of elements (e.g. $N = 11$ and $N = 14$). The high level of the ripple is due to the interference between dipole elements opposite each other in the cylindrical array. For a given array radius and a number of array elements, two dipole elements opposite each other can interfere strongly because of their omnidirectional radiation patterns. Consequently, the distortion in the dipole array patterns inhibits a smooth decrease in the gain ripple and null width as the number of elements is increased. On the other hand, the microstrip patches have directive radiation patterns and the ripple in the omnidirectional pattern is thus less. Figure 3.8 shows that maximum null depths are obtained with $N = 9$ and $N = 11$ for the axially and circumferentially polarised patch arrays, respectively. When a cylindrical dipole array is used, a maximum null depth may be obtained with $N = 19$.

While keeping the number of array elements constant at $N = 10$, the inter-element spacing was varied, yielding the results for the ripple, null width and null depth in Figures 3.9, 3.10 and 3.11, respectively. An omnidirectional array pattern with a single infinitely deep null at 180° was desired for all three array configurations. Using the circumferentially polarised patch array, a smooth increase in gain ripple is observed as the inter-element spacing is increased. Except for the abrupt increase in the ripple at $d_\phi = 0.625\lambda_0$, the ripple also increases smoothly as the inter-element spacing is

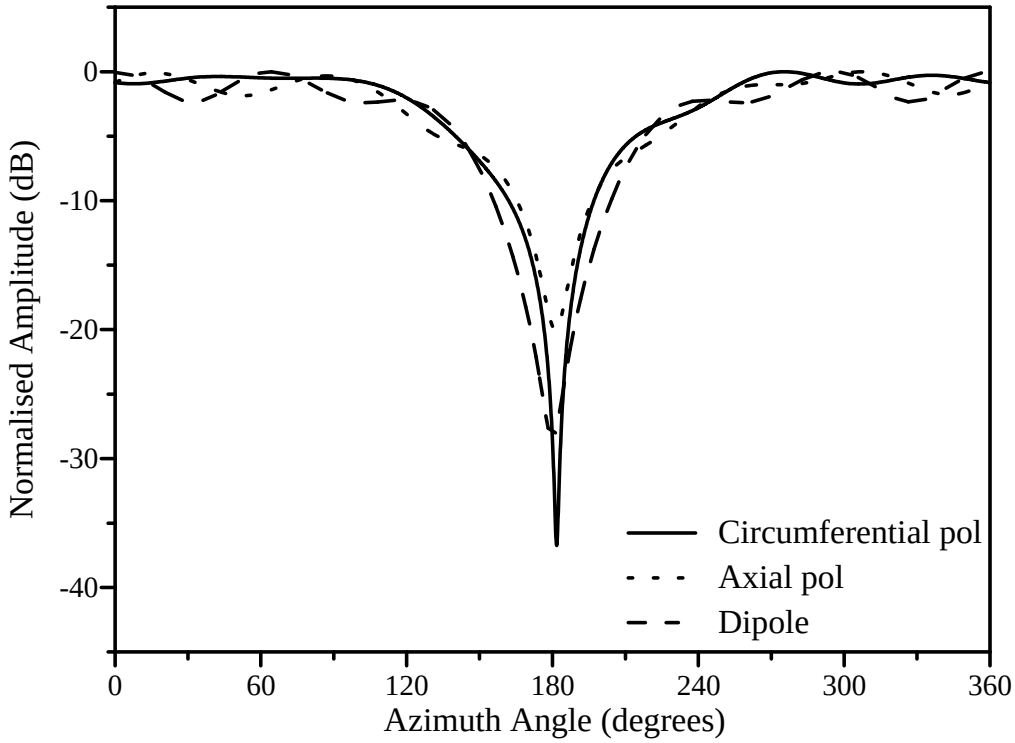

Figure 3.2: Radiation pattern of a cylindrical array (N=6 and $d_\phi = 0.5\lambda_0$) with a single null

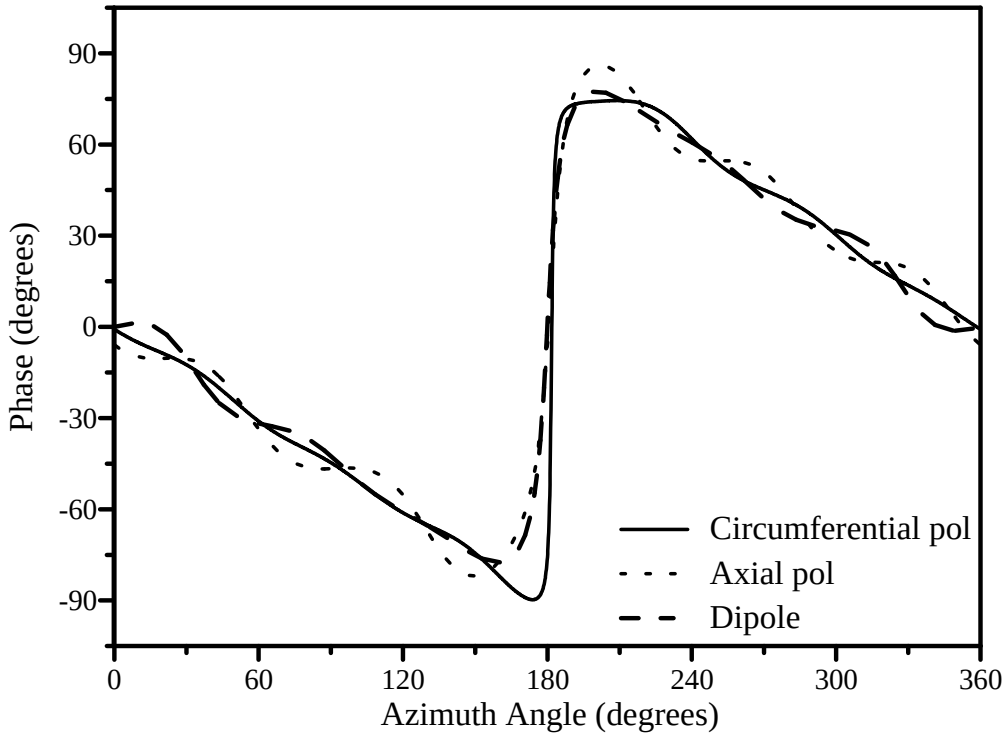

Figure 3.3: Phase of the radiation pattern for a cylindrical array (N=6 and $d_\phi = 0.5\lambda_0$) with a single null

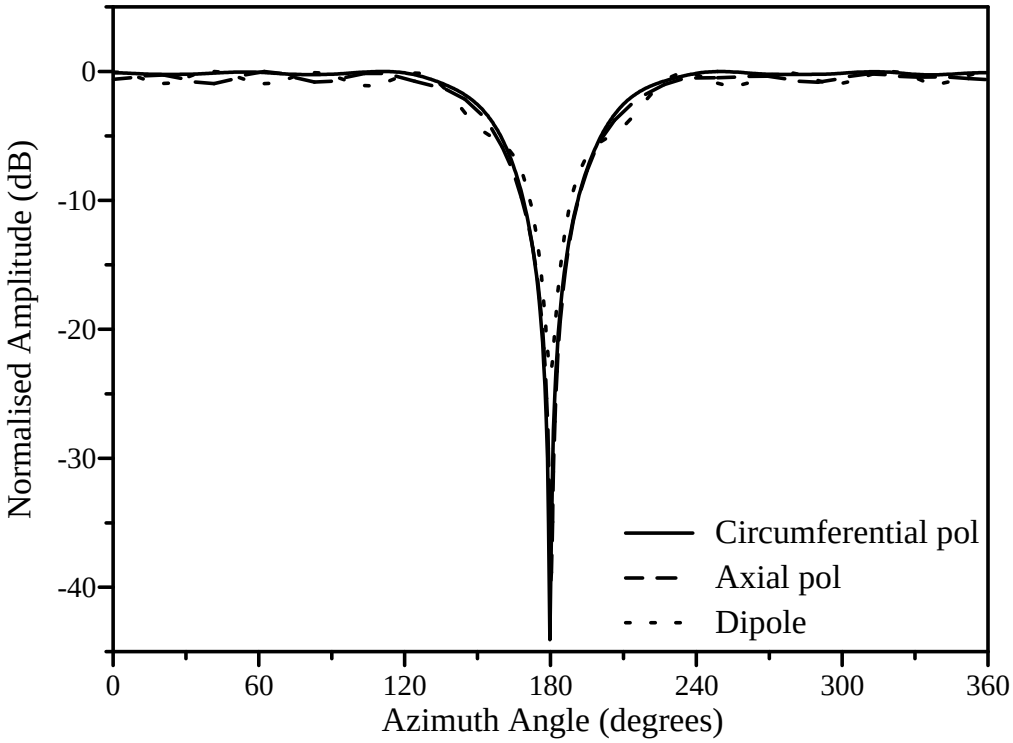

Figure 3.4: Radiation pattern of a cylindrical array (N=10 and $d_\phi = 0.5\lambda_0$) with a single null

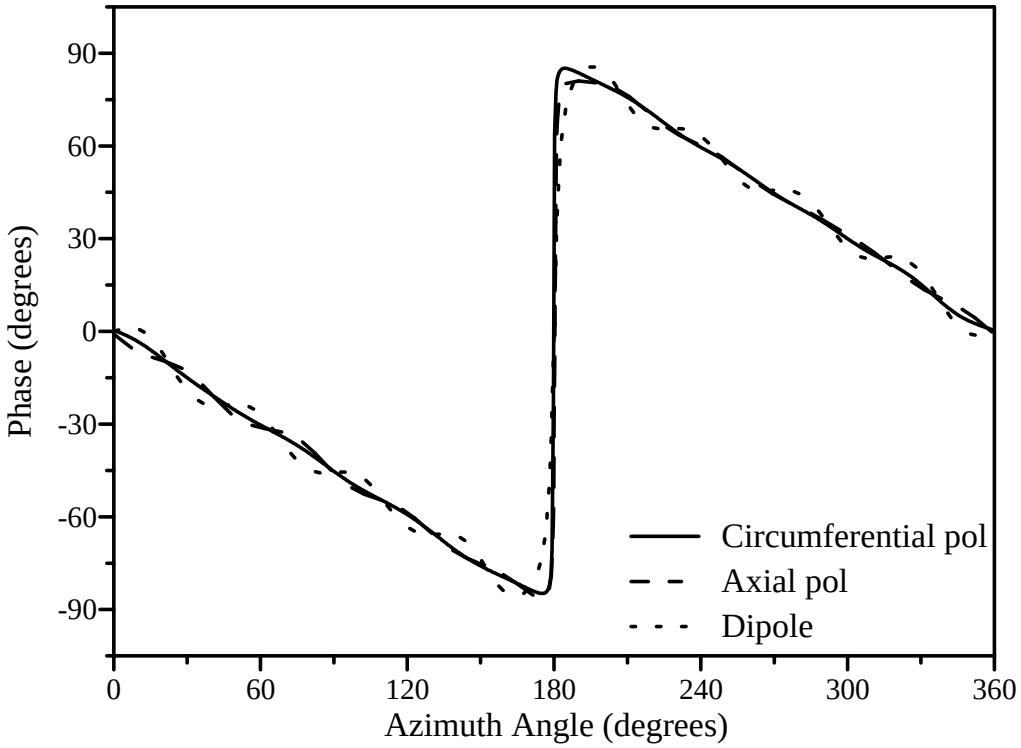

Figure 3.5: Phase of the radiation pattern for a cylindrical array (N=10 and $d_\phi = 0.5\lambda_0$) with a single null

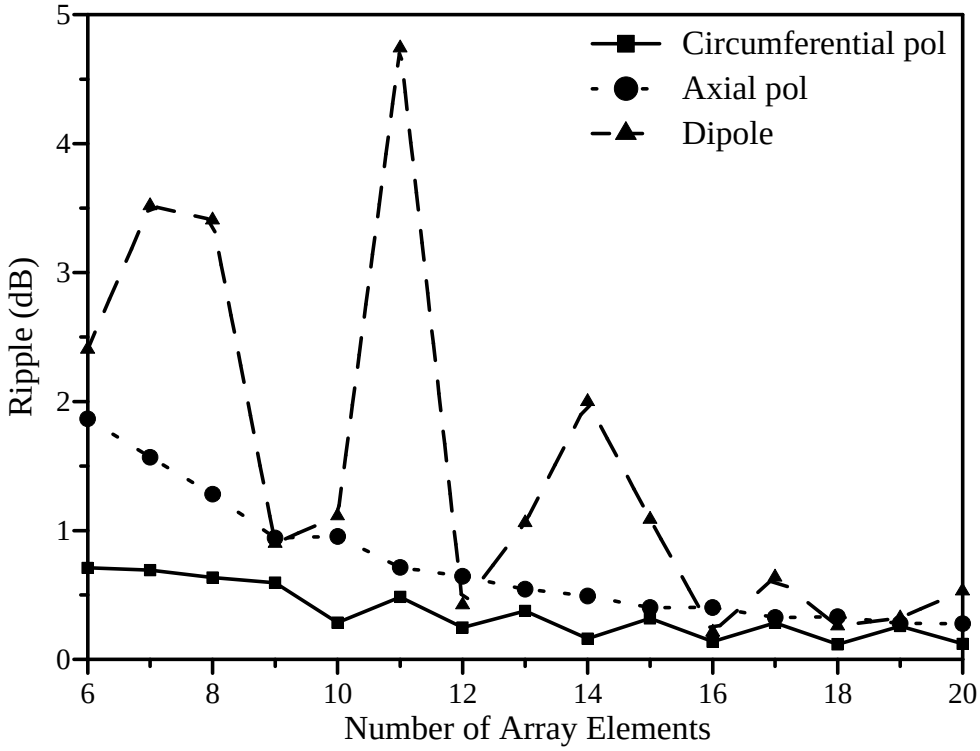

Figure 3.6: Resulting ripple of a single null in the radiation pattern of a cylindrical array with $d_\phi = 0.5\lambda_0$

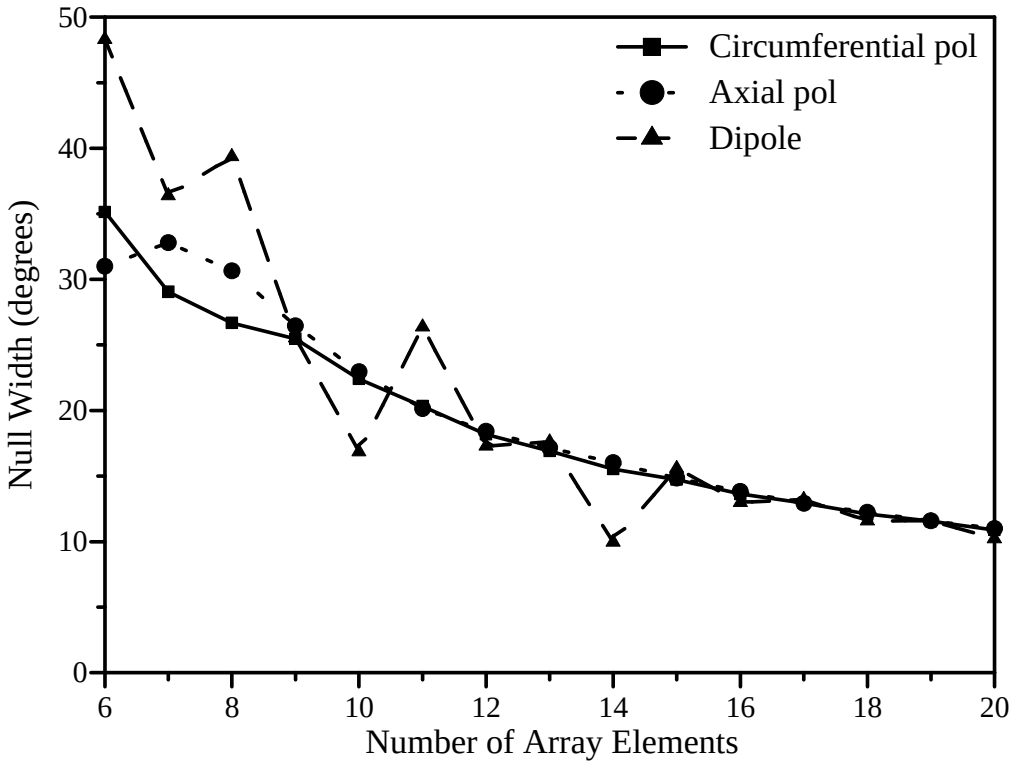

Figure 3.7: Resulting null width of a single null in the radiation pattern of a cylindrical array with $d_\phi = 0.5\lambda_0$

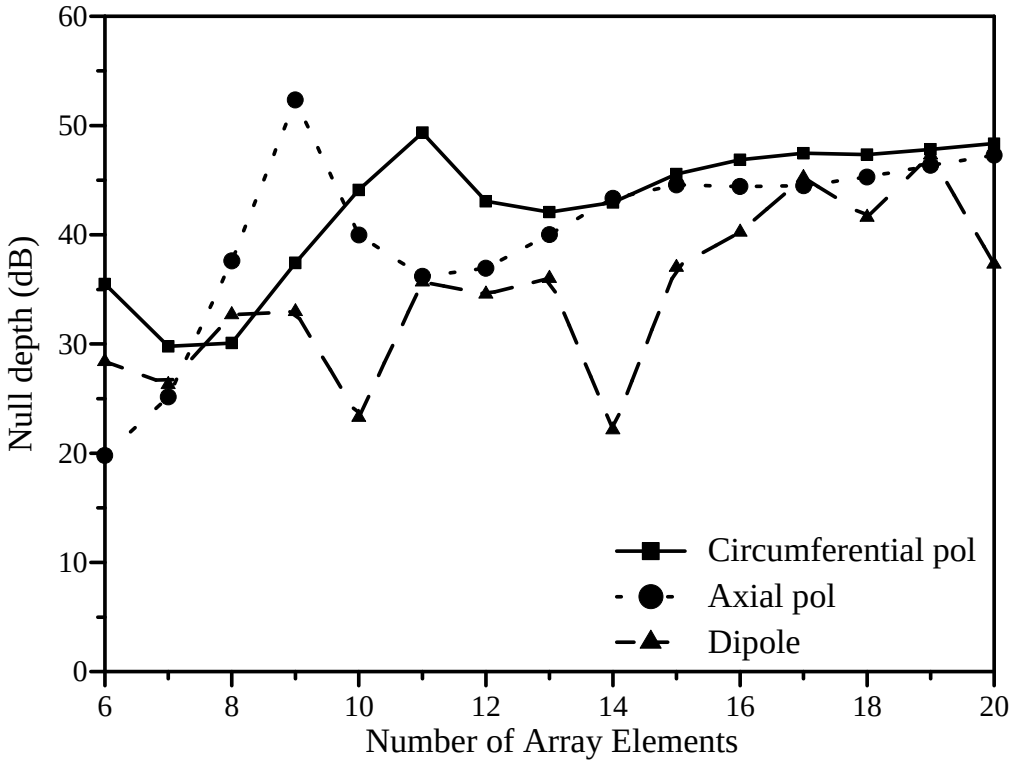

Figure 3.8: Resulting null depth of a single null in the radiation pattern of a cylindrical array with $d_\phi = 0.5\lambda_0$

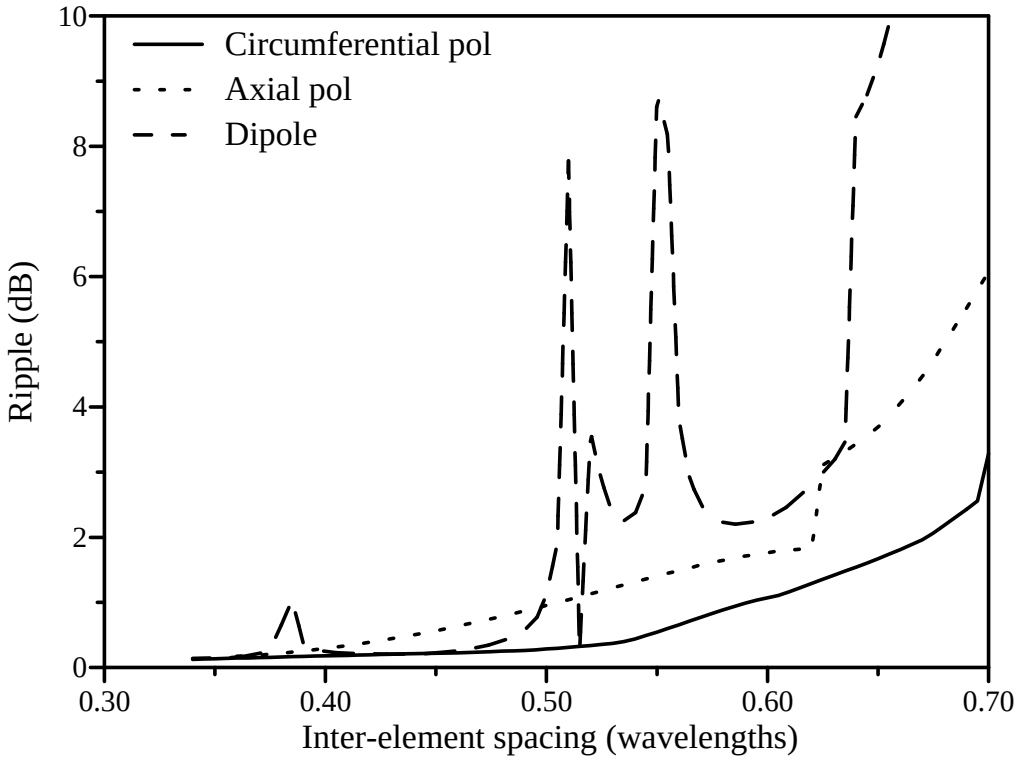

Figure 3.9: Resulting ripple of a single null in the radiation pattern of a cylindrical array with $N = 10$

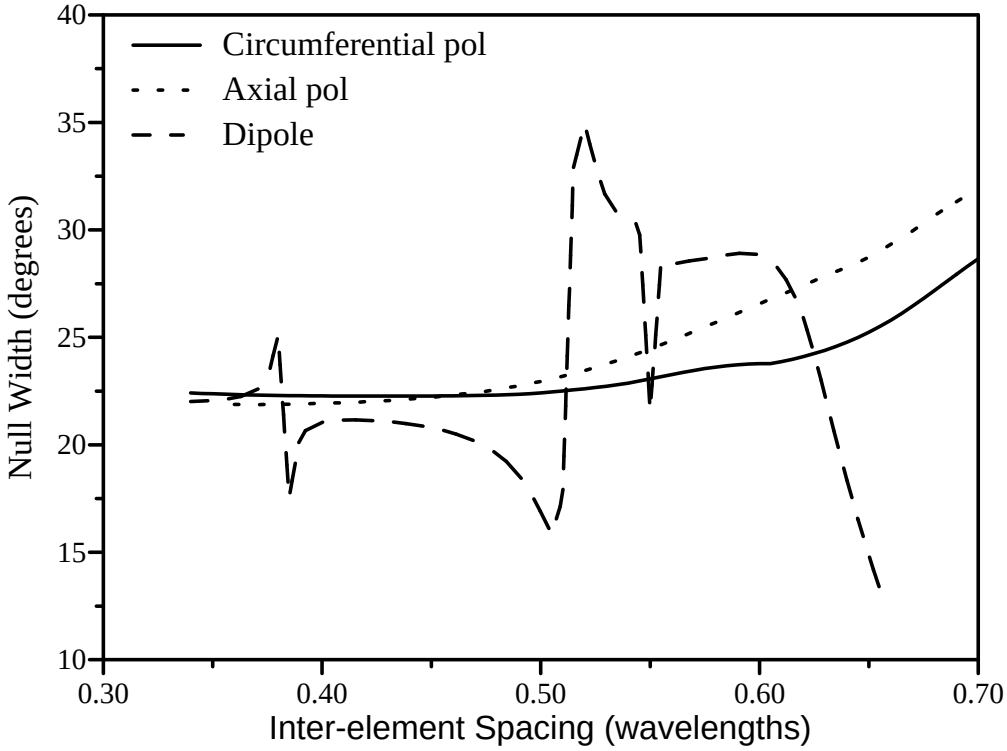

Figure 3.10: Resulting null width of a single null in the radiation pattern of a cylindrical array with $N = 10$

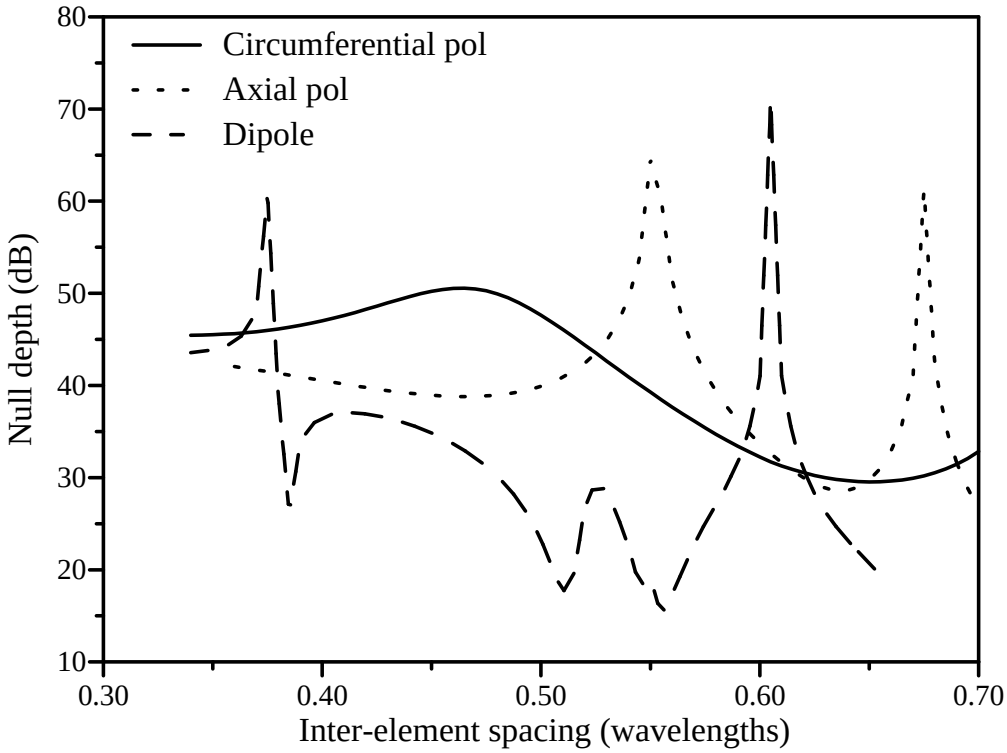

Figure 3.11: Resulting null depth of a single null in the radiation pattern of a cylindrical array with $N = 10$

increased in the axially polarised patch array. In contrast to the behaviour of the patch arrays, the gain ripple in the amplitude pattern of the dipole array depends highly on the inter-element spacing. For certain inter-element spacings, the interference between the elements yields large gain ripple values.

Figure 3.10 shows that the null widths of the resulting nulls increase gradually as the inter-element spacing is increased in both patch arrays. On the other hand, the utilisation of the dipole array may result in a maximum or minimum null width, depending on the inter-element spacing. All three arrays yield different null depth results using the orthogonal projection method, as seen in Figure 3.11. A maximum null depth of 49 dB at $d_\phi = 0.465\lambda_0$ may be obtained with the circumferentially polarised patch array. With the axially polarised patch array a maximum null depth of 64 dB can be obtained at $d_\phi = 0.55\lambda_0$, while the dipole array yields a maximum null depth of 71 dB at $d_\phi = 0.61\lambda_0$.

3.2 Objective weighting method

The orthogonal projection method provides an optimal array pattern with the least pattern error (in a least square sense). The optimal array pattern may not have the desired pattern characteristics, since the amplitude and phase of the radiation pattern are optimised simultaneously. Some of the amplitude pattern characteristics may be improved by applying a windowing function to the resulting element excitations. While some characteristics may improve, other characteristics are degraded.

This implies that a multi-objective optimisation approach has to be followed. In stead of minimising the array pattern error, a global performance function can be defined by utilising the amplitude pattern error and the phase pattern error. The minimum of this performance function is then sought after.

3.2.1 Performance function and Pareto optimality

In the objective weighting method a global performance function is obtained by means of a linear combination of the multi-objective functions of the optimisation scenario [97].

The performance function for an array pattern may be defined as:

$$P = c_1 e_a + c_2 e_p, \tag{3.1}$$

where c_1 and c_2 are weighting factors and e_a and e_p are the amplitude and phase pattern errors, respectively. The amplitude pattern error e_a is defined as:

$$e_a(\mathbf{A}) = \int_0^{2\pi} \left(|F(\phi;\mathbf{A})| - |F_0(\phi)|\right)^2 d\phi, \tag{3.2}$$

while the phase pattern error e_p is defined as:

$$e_p(\mathbf{A}) = \int_0^{2\pi} \left(\angle F(\phi;\mathbf{A}) - \angle F_0(\phi)\right)^2 d\phi. \tag{3.3}$$

The multi-objective optimisation problem can be solved by finding the minimum of P. Using the above definition, P will be independent of the minima of the objective functions e_a and e_p. It can also be observed from Equation 3.1, that the resulting values of e_a and e_p, which are obtained after finding the minimum of P, will depend on the ratio c_2/c_1. Thus, the ratio c_2/c_1 should be properly defined. The critical value of the ratio c_2/c_1 can be obtained through observing the behaviour of e_a and e_p when minimising different performance functions.

Figure 3.12 illustrates an example of an optimisation problem with different minima in a criterion space for different performance function definitions. The minima of P was found for different ratios c_2/c_1, which is indicated on the graph. For each minimum, the resulting values of e_a and e_p is shown. The curve formed by the resulting e_a and e_p is referred to as the Pareto optimal front which contains Pareto optimal points. A Pareto optimal point has been obtained when no other points exist in the variable domain for which the value of one of the two objective functions decreases and the other function does not increase [95–97]. The critical ratio (0.5), where $\sqrt{(e_a^2 + e_p^2)}$ is at a minimum, is circled on the graph. This Pareto optimal point is the most reasonable choice in a least square sense when trying to minimise both the amplitude and phase pattern errors.

The objective weighting method can thus be applied in a null synthesis technique to improve the amplitude pattern and consequently the amplitude pattern error. As indicated by the Pareto optimal front, the trade-off will be a gain in the phase pattern error for a loss in the amplitude pattern error.

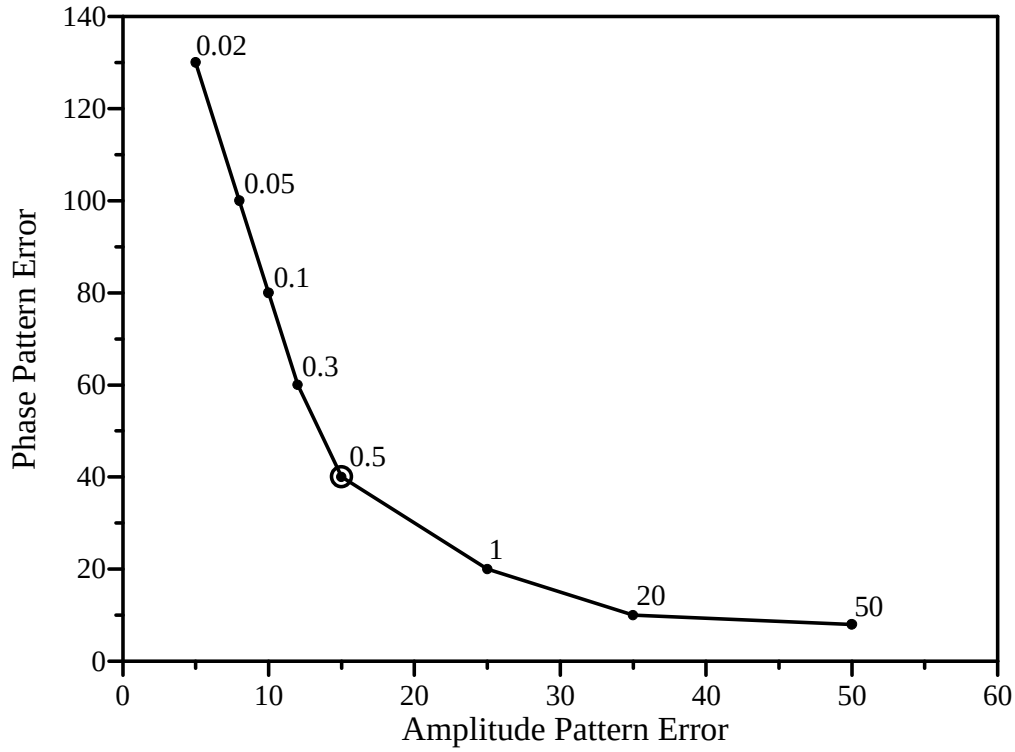

Figure 3.12: Example of different minima in a criterion space for different definitions of the performance function

The method is applied after the optimum element excitation vector $\mathbf{A}$ has been obtained from the projection method. An unconstrained non-linear minimisation algorithm [99] is used to find the minimum of each performance function P using this excitation vector as the starting vector. The algorithm applies a quasi-Newton optimisation method which incorporates a cubic-quadratic polynomial line search method. For each array configuration, the critical ratio c_2/c_1 and consequent function P has to be found. The excitation vector which minimises this P, is then used to form the omnidirectional radiation pattern with a null. In the next subsection, the objective weighting method is applied using the resulting excitation vectors of the projection method described in the previous section.

3.2.2 Results of the objective weighting method

The objective weighting method is applied using the unconstrained optimum excitation vectors obtained from the orthogonal projection method as starting values. The minima of P with different weight ratios are found using an unconstrained least square

optimisation algorithm. Figures 3.13 and 3.14 show examples of the Pareto optimal fronts for an axially and a circumferentially polarised patch array, respectively. The Pareto optimal fronts are shown for arrays with $N = 10$ and $d_\phi = 0.5\lambda_0$. An omnidirectional radiation pattern with a single infinitely deep null at 180° was required. In Figure 3.15 the optimal front for a dipole array with the same array configuration is shown. The objective weight ratios for each P is indicated along each point and the critical ratios are circled on all three graphs. For these array configurations, the axially and circumferentially polarised arrays have the same critical ratio of $c_1/c_2 = 0.1384$, while the dipole array has a critical ratio of $c_1/c_2 = 0.5904$.

After obtaining the excitations vectors which minimise P at the critical ratios, the resulting amplitude radiation patterns in Figure 3.16 were formed. The circumferentially polarised patch array forms the null with the least ripple, whereas the axially polarised patch array forms the deepest null. When comparing the results in Figure 3.16 to the results of the projection method in Figure 3.4, one can observe the decrease in null width and the increase in null depth for all three array types. On the other hand, the ripple in the omniregion increased in all three patterns. In Figure 3.17 the phase of the radiation patterns are shown. The increase in the ripple of the phase pattern can be seen when this figure is compared to Figure 3.5. The objective weighting method thus decreases the amplitude pattern error while increasing the phase pattern error. This is due to the trade-off that exists between the two pattern errors for optimal points on the Pareto optimal front - a decrease in one objective will result in an increase in the other objective.

The resulting gain ripple, null width and null depth are compared for different numbers of array elements in Figures 3.18, 3.19 and 3.20, respectively. The inter-element spacing was kept constant at $d_\phi = 0.5\lambda_0$ and an infinitely deep null at 180° was required. The ripple in Figure 3.18 gradually decreases to a value close to 1 dB as the number of elements increases. This value is higher than the ripple of 0.5 dB or lower, which was obtained with the orthogonal projection method for $N = 20$ in Figure 3.6. The null width also decreases as the number of elements is increased. Compared to the results of the projection method in Figure 3.7, the objective weighting method forms nulls with smaller null widths. Figure 3.20 shows that deep nulls can be obtained by using only a small number of array elements. Using the projection method, as seen in Figure 3.8, lower null depths were obtained for small numbers of elements.

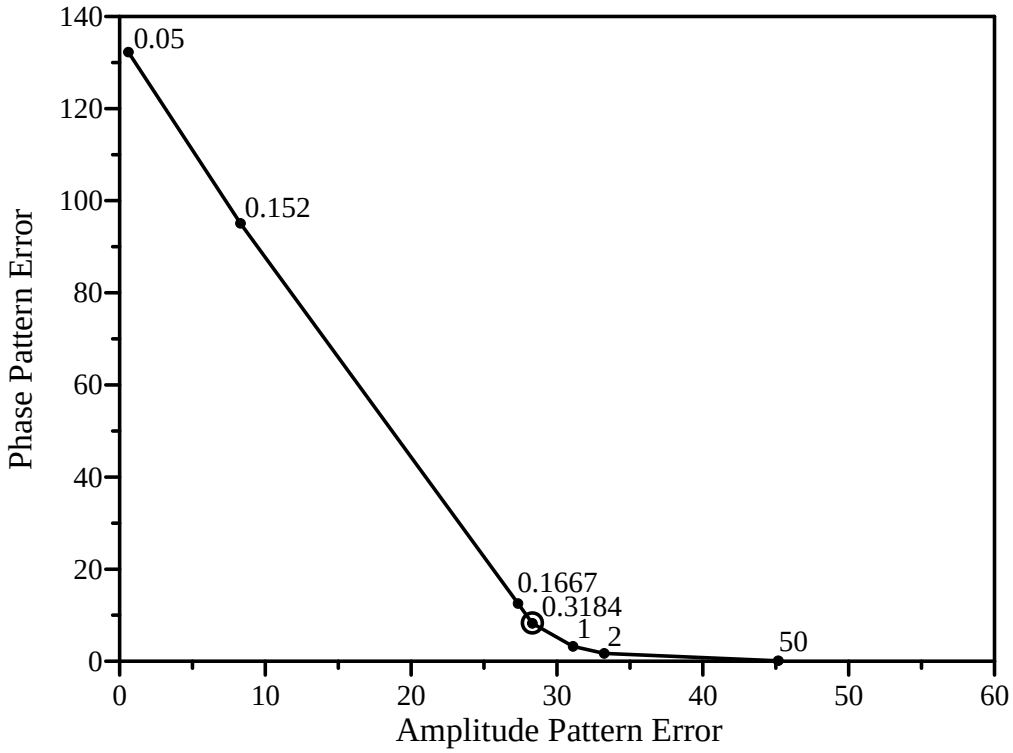

Figure 3.13: Minima for different definitions of the performance function for a cylindrical array of axially polarised patches with $N = 10$ and $d_\phi = 0.5\lambda_0$

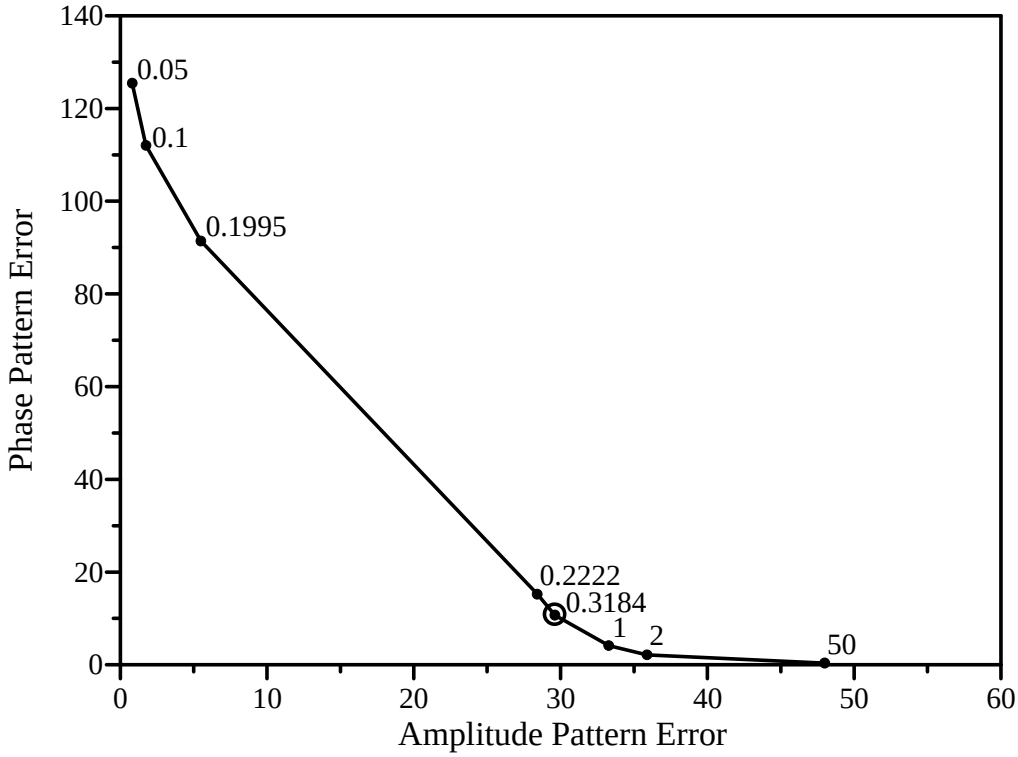

Figure 3.14: Minima for different definitions of the performance function for a cylindrical array of circumferentially polarised patches with $N = 10$ and $d_\phi = 0.5\lambda_0$

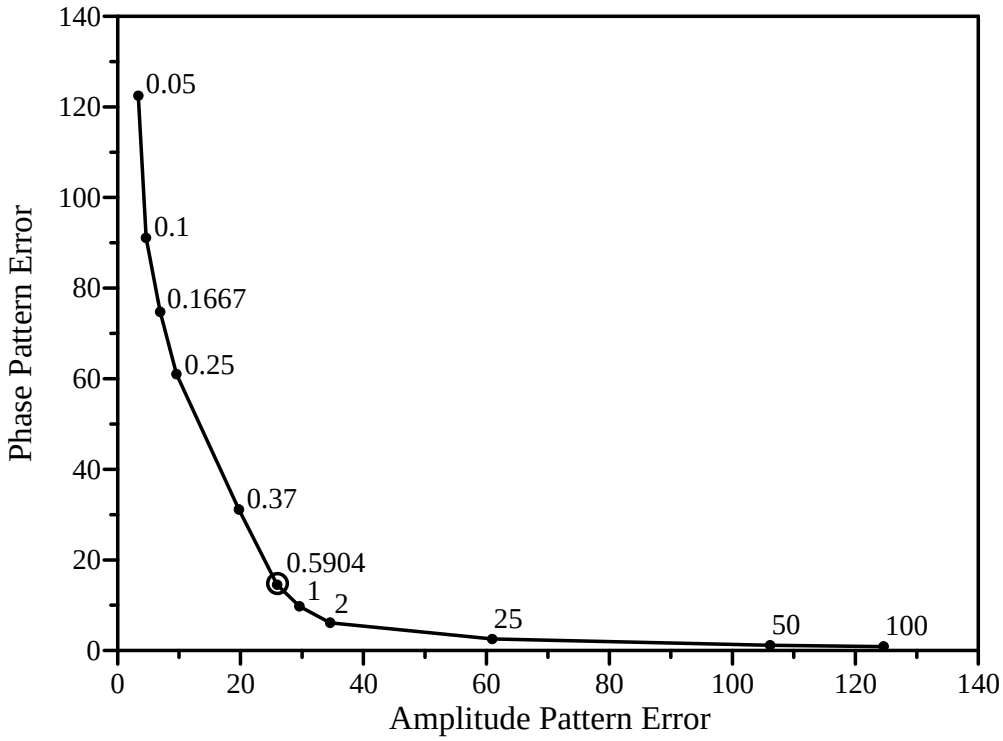

Figure 3.15: Minima for different definitions of the performance function for a cylindrical array of dipoles with $N = 10$ and $d_\phi = 0.5\lambda_0$

While keeping the number of array elements constant at $N = 10$, the inter-element spacing of the arrays was varied. The resulting ripple, null width and null depth are compared for the different types of arrays in Figures 3.21, 3.22 and 3.22, respectively. For the dipole array with $d_\phi = 0.55\lambda_0$, the objective weighting function could not yield a critical ratio value for P due to the high ripple in the omni-region. No results for this inter-element spacing could thus be shown in the figures.

For patch arrays with $d_\phi \geq 0.45\lambda_0$, the ripple increases as the inter-element spacing is increased in Figure 3.21. In Figure 3.22, the resulting null width for a circumferentially polarised patch array decreases as the inter-element spacing increases for $d_\phi \leq 0.55\lambda_0$. For $d_\phi \geq 0.6\lambda_0$, the null width starts to increase for increasing inter-element spacing. The null width for an axially polarised patch array firstly decreases with increasing inter-element spacing up to $d_\phi = 0.5\lambda_0$ before it increases for increasing inter-element spacing. Using the objective weighting method, maximum null depths can be obtained with inter-element spacings of $d_\phi = 0.625\lambda_0$ and $d_\phi = 0.675\lambda_0$ for circumferentially and axially polarised patch arrays, respectively.

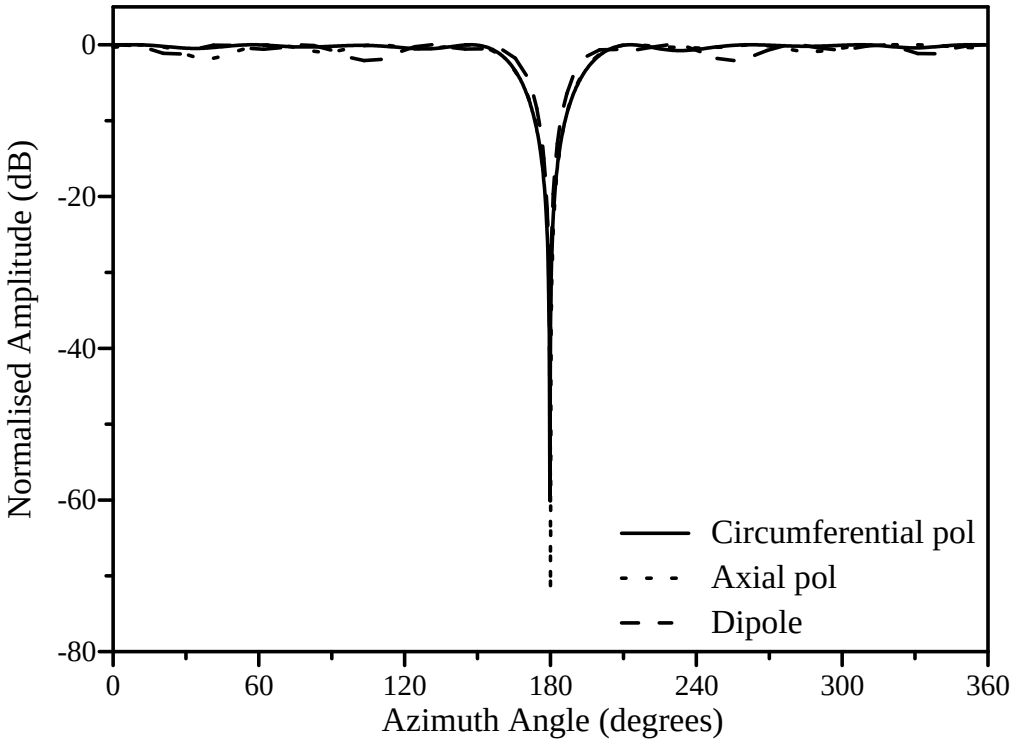

Figure 3.16: Radiation pattern of a cylindrical array (N=10 and $d_\phi = 0.5\lambda_0$) with a single null, using the objective weighting method

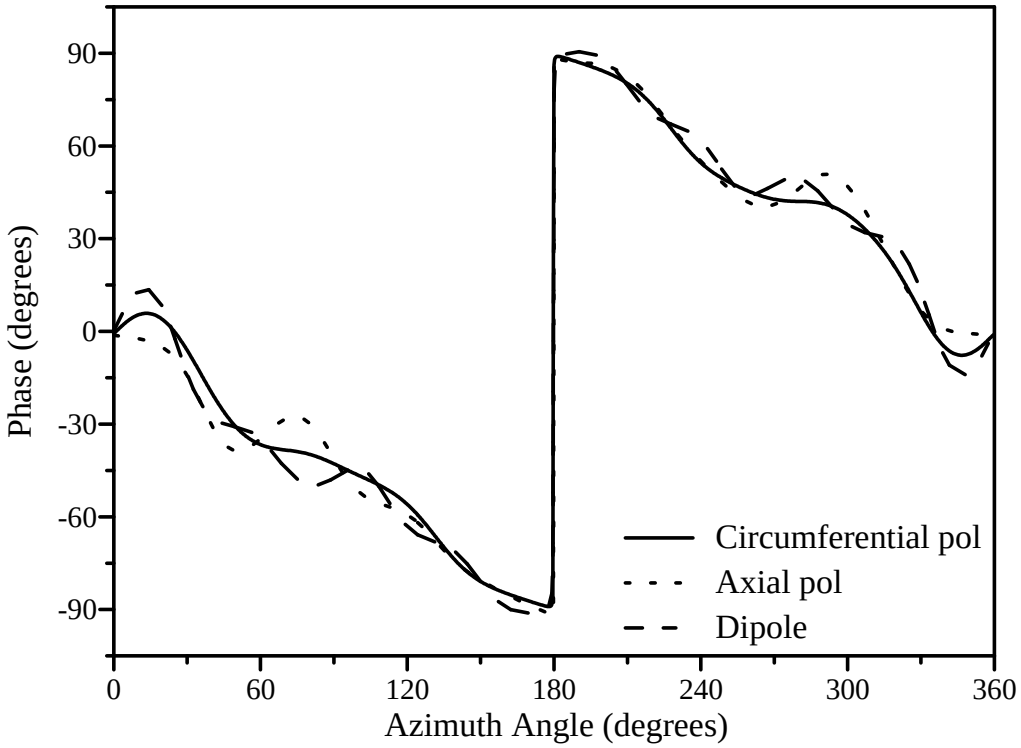

Figure 3.17: Phase of the radiation pattern for a cylindrical array (N=10 and $d_\phi = 0.5\lambda_0$) with a single null, using the objective weighting method

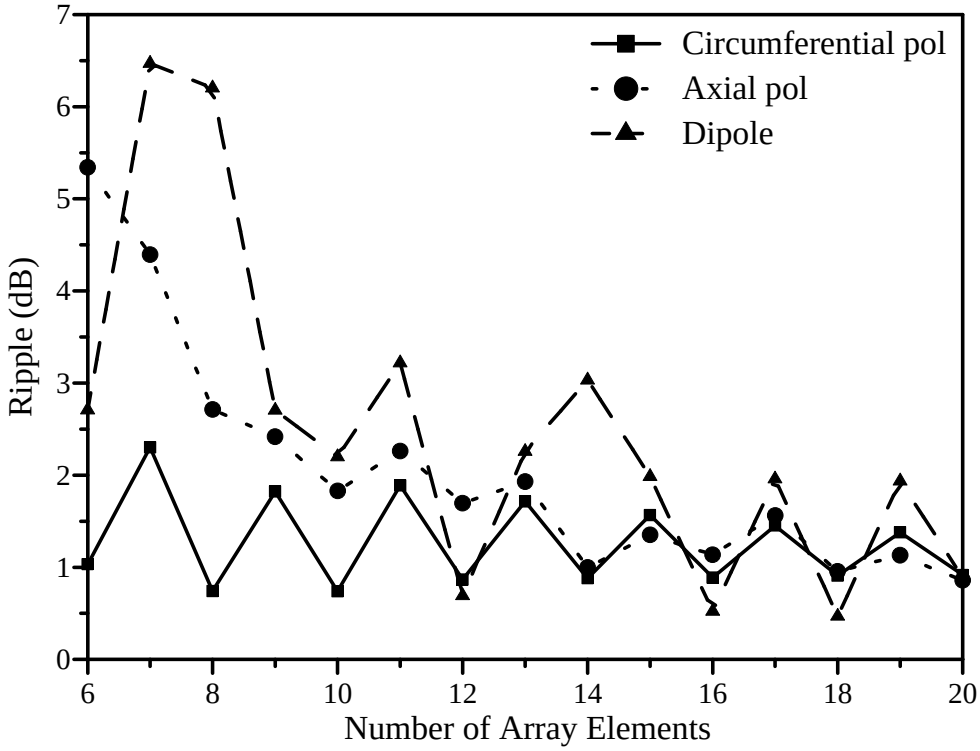

Figure 3.18: Resulting ripple of a single null in the radiation pattern of a cylindrical array with $d_\phi = 0.5\lambda_0$, using the objective weighting method

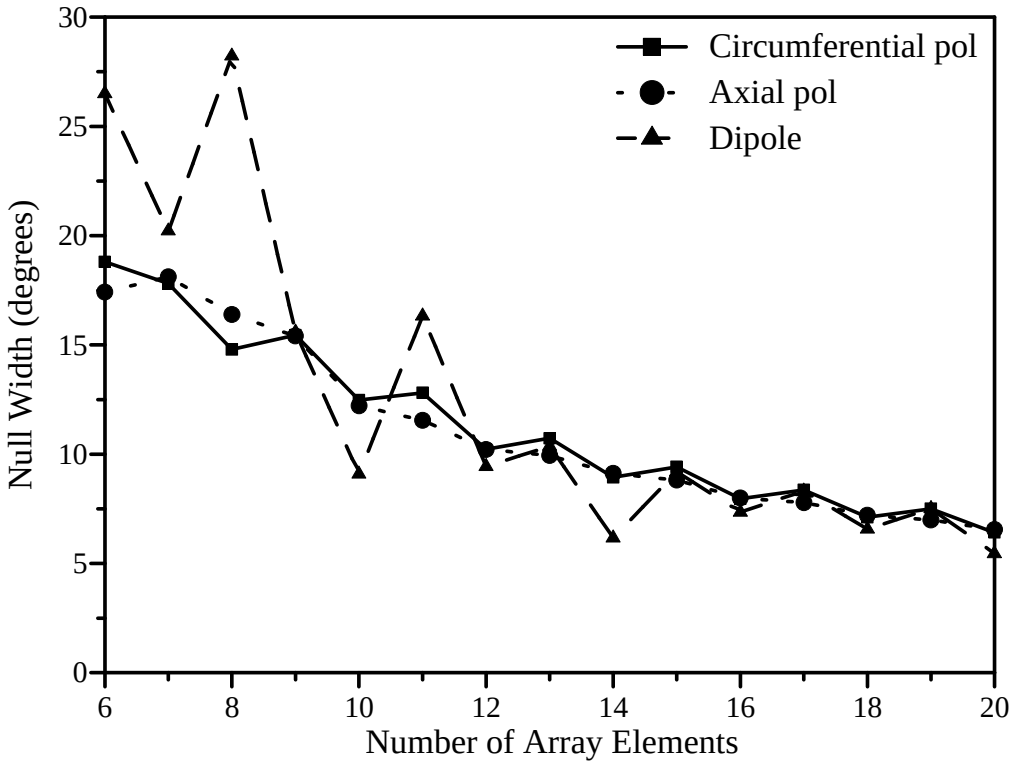

Figure 3.19: Resulting null width of a single null in the radiation pattern of a cylindrical array with $d_\phi = 0.5\lambda_0$, using the objective weighting method

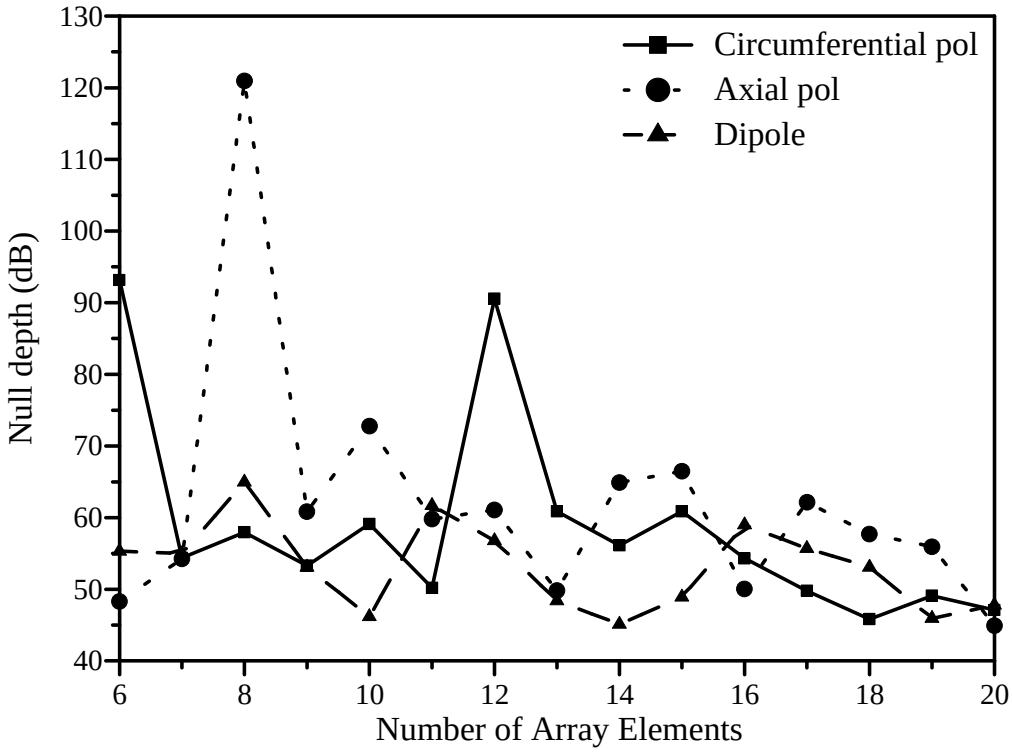

Figure 3.20: Resulting null depth of a single null in the radiation pattern of a cylindrical array with $d_\phi = 0.5\lambda_0$, using the objective weighting method

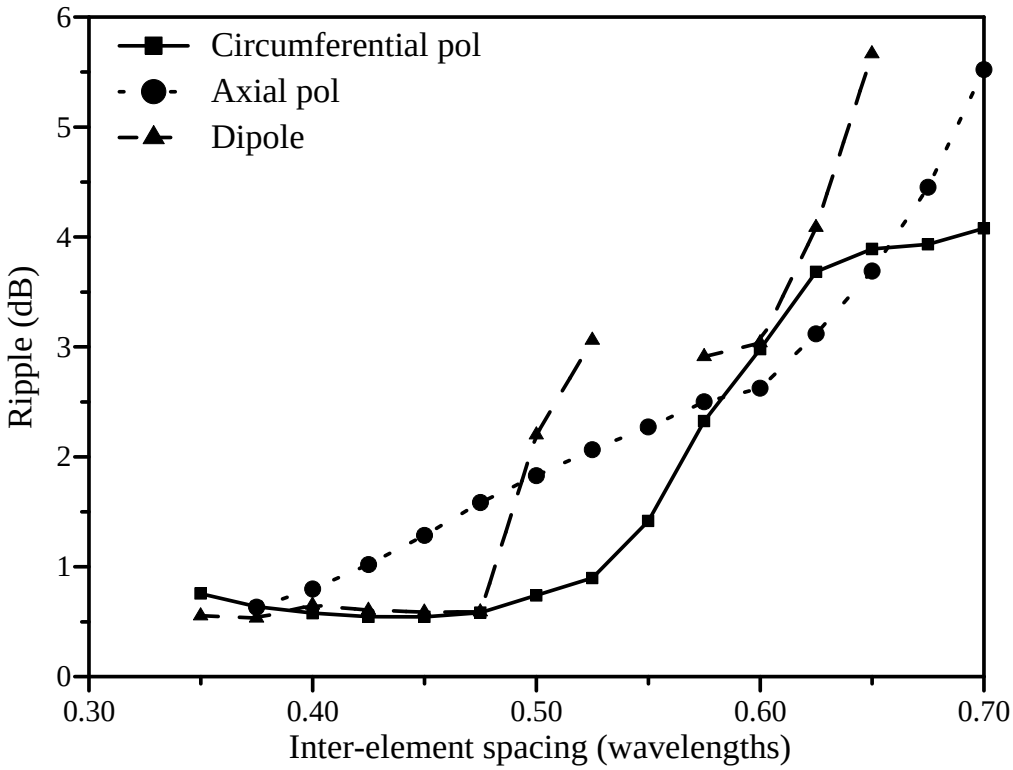

Figure 3.21: Resulting ripple of a single null in the radiation pattern of a cylindrical array with $N = 10$, using the objective weighting method

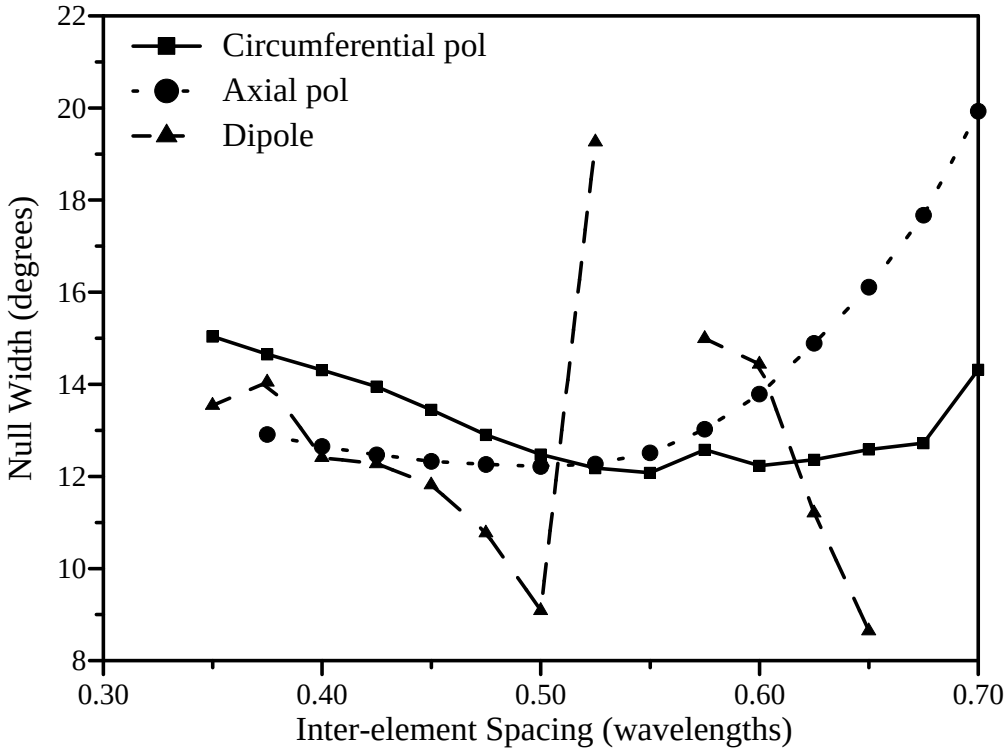

Figure 3.22: Resulting null width of a single null in the radiation pattern of a cylindrical array with $N = 10$, using the objective weighting method

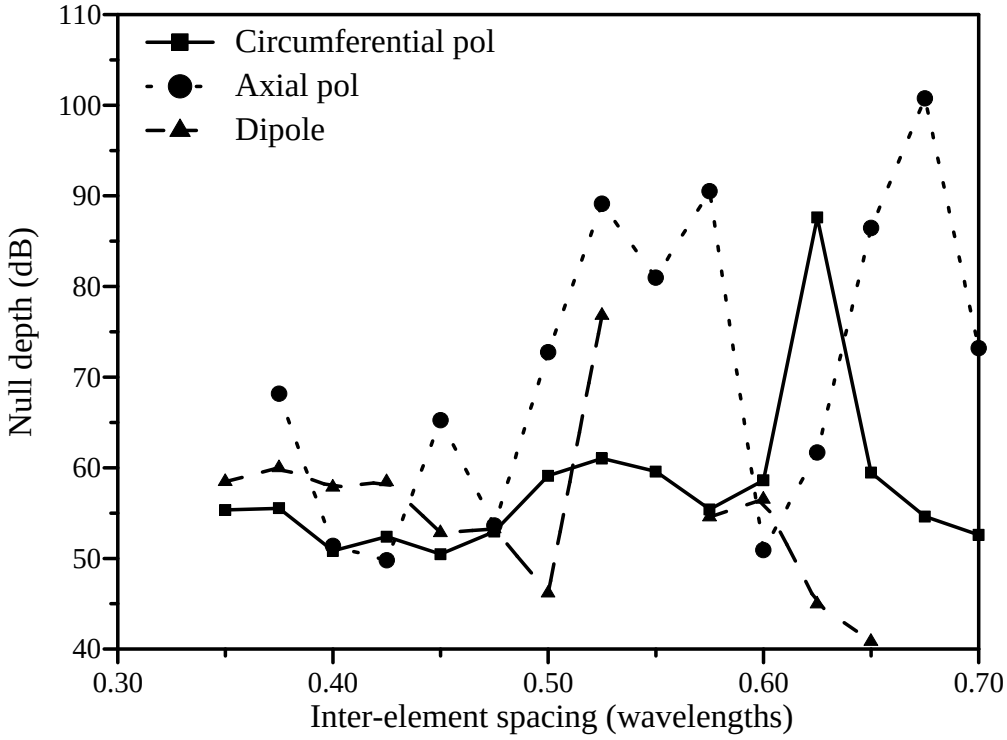

Figure 3.23: Resulting null depth of a single null in the radiation pattern of a cylindrical array with $N = 10$, using the objective weighting method

3.3 Constrained optimisation

The objective weighting method provides a way of improving the characteristics of the amplitude radiation pattern. This improvement is mostly manifested in a decreased null width and an increased null depth when an infinitely deep null is considered. On the other hand, the gain ripple in the omni-region increases.

Another way of improving the resulting amplitude pattern would be to provide control over the individual characteristics. In some applications, the degree of suppression needs to be specified through a controllable null depth. As discussed previously, Abele [54] proposed a variable phase step to provide control over the null depth. The accuracy of the resulting null depth depends on the array configuration and the desired null depth.

Constrained optimisation provides a method of constraining the different attributes of the amplitude pattern while minimising the array pattern error. All the attributes or combinations of attributes can thus be controlled.

3.3.1 Results of the constrained optimisation

A constrained optimisation algorithm [99] is employed to find an excitation vector which yields the minimum pattern error under the constraints specified for certain amplitude pattern characteristics. The choice of the starting values for the excitations vector fulfils a very important role in the success of the optimisation. When these values are chosen carefully, the optimisation time can be limited and local minima can be avoided. The excitation vector obtained from the orthogonal projection method yields an optimum radiation pattern with the minimum pattern error and is therefore chosen as the starting value. The resulting vector from the constrained optimisation will produce a radiation pattern with a pattern error as close as possible to this minimum pattern error while satisfying the constraints.

The algorithm allows the placement of constraints on the gain ripple, the null depth and the null width. These constraints are set equal to the desired values of the characteristics. Two additional constraints are also placed on the amplitudes and phases of the element excitations:

$$|a_n| \leq 1, \tag{3.4}$$

and

$$|\angle a_n| \leq 180°. \tag{3.5}$$

The above constraints effectively decrease the variable space to the normalised excitation amplitudes and one 360° phase cycle for the excitation phases. The execution time of the optimisation algorithm is consequently decreased.

Different combinations of constraints were used to illustrate the performance of the algorithm. The antenna element configuration of the previous sections was applied in a circumferentially polarised patch array. A -40 dB null at 180° was desired. The various constrained optimisation study cases and their results are summarised in Table 3.1. Figure 3.24 shows the resulting amplitude patterns for study cases 1 to 3, while the amplitude patterns of study cases 4 to 6 are shown in Figure 3.25. The amplitude pattern of the last study case is presented in Figure 3.26. Table 3.1 shows that either individual characteristics or combinations of characteristics are controllable using the constrained optimisation. When the ripple is not constrained to be 1 dB, the resulting ripple is between 1.63 and 1.72 dB. The unconstrained null depth is between -22.1 and -23 dB, while the unconstrained null width varies from 13.11° to 13.6°.

Table 3.1: Study cases for constrained optimisation

Case	**Constraints**			**Results**		
	Null depth (dB)	Ripple (dB)	Null width (°)	Null depth (dB)	Ripple (dB)	Null width (°)
1	-40	none	none	-40.0	1.70	13.54
2	none	1	none	-22.8	1	13.11
3	none	none	13	-23.0	1.63	13.00
4	-40	1	none	-40.0	1	13.60
5	none	1	13	-22.1	1	13.00
6	-40	none	13	-40.0	1.72	13.00
7	-40	1	13	-40.0	1	13.00

Case study 4 was extended to investigate the effect of different numbers of elements and inter-element spacings on the resulting unconstrained null width. Figure 3.27 compares the resulting null width for the different types of arrays as the number of elements is varied. The inter-element spacing was kept constant at $d_\phi = 0.5\lambda_0$. As the number of elements is increased while the desired null depth and ripple are constrained, the

null width gradually decreases. Arrays with an uneven number of elements produce wider null widths than arrays with an even number of elements for $N \geq 9$. The circumferentially and axially polarised patch arrays show similar null widths for $N > 11$, while for a large number of array elements ($N > 16$), the null widths of all three arrays become similar.

While keeping the number of elements constant at $N = 10$, the inter-element spacing was varied, yielding the results in Figure 3.28. Due to the high distortion in the far-field of the dipole array, a gain ripple of less than 1 dB could not be obtained with the dipole array, while the axially and circumferentially polarised patch arrays could not form the null with a 1 dB ripple for $d_\phi > 0.65\lambda_0$ and $d_\phi > 0.675\lambda_0$, respectively. The circumferentially polarised patch array patterns have the smallest null widths for $d_\phi > 0.5\lambda_0$.

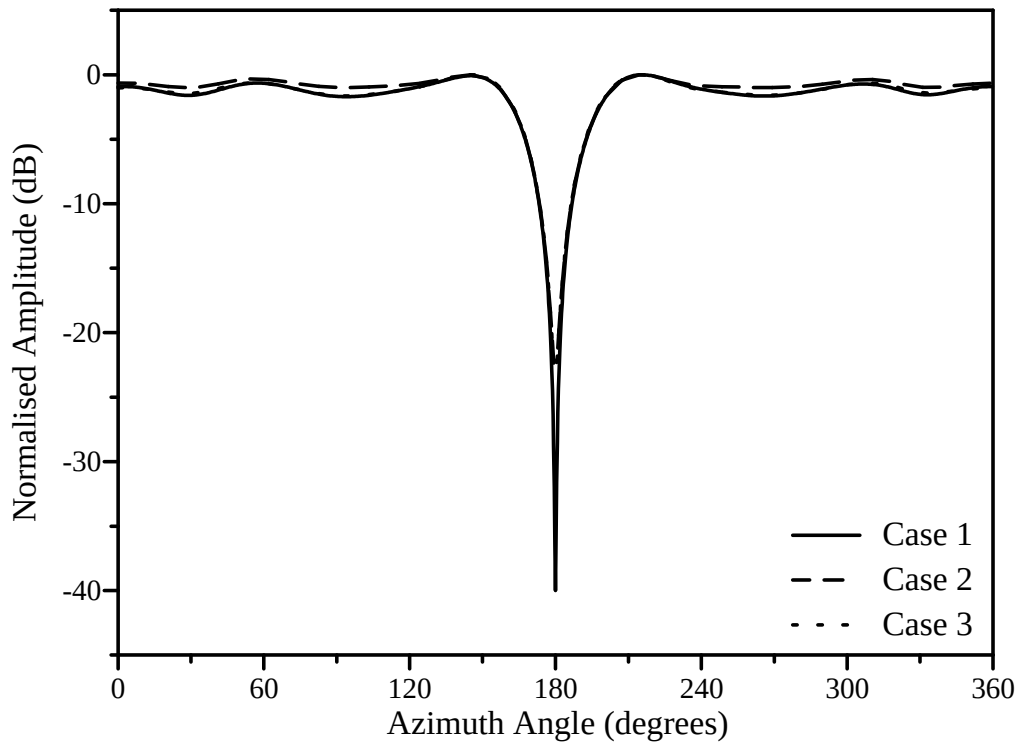

Figure 3.24: Radiation pattern of a cylindrical array (N=10 and $d_\phi = 0.5\lambda_0$) with a single null, using the constrained optimisation method for cases 1, 2 and 3

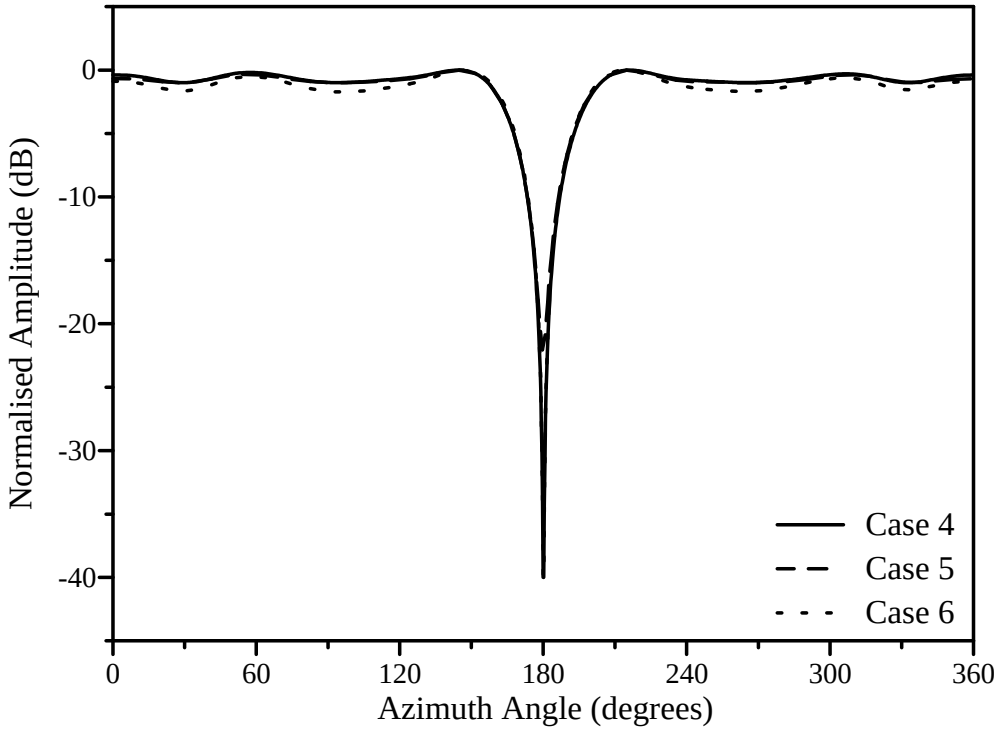

Figure 3.25: Radiation pattern of a cylindrical array (N=10 and $d_\phi = 0.5\lambda_0$) with a single null, using the constrained optimisation method for cases 4, 5 and 6

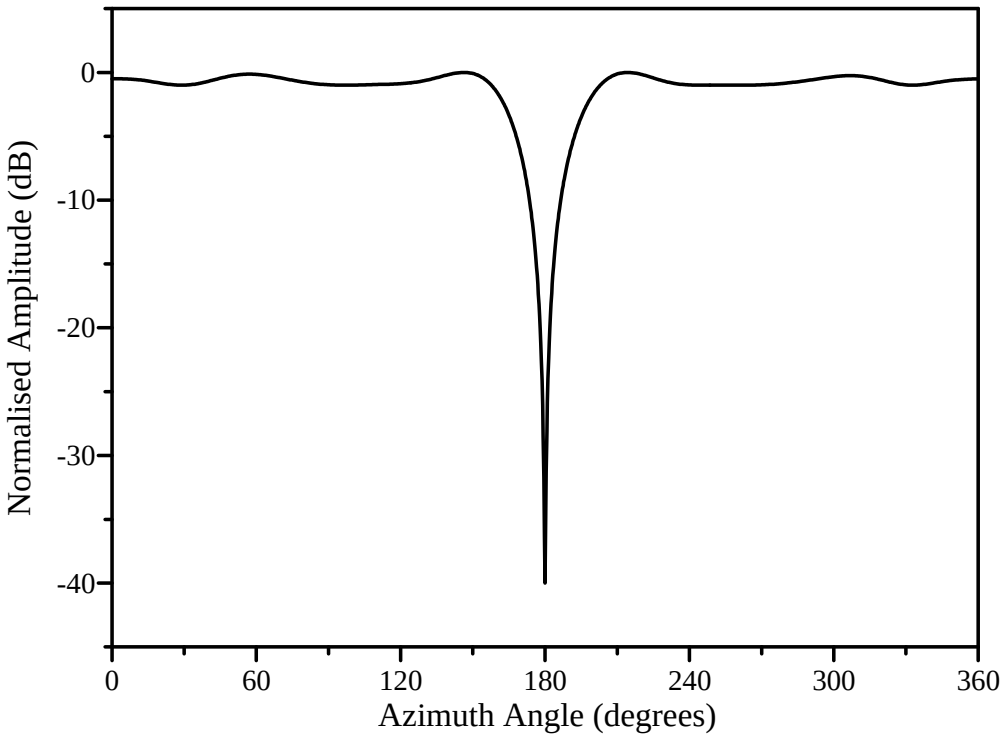

Figure 3.26: Radiation pattern of a cylindrical array (N=10 and $d_\phi = 0.5\lambda_0$) with a single null, using the constrained optimisation method for case 7

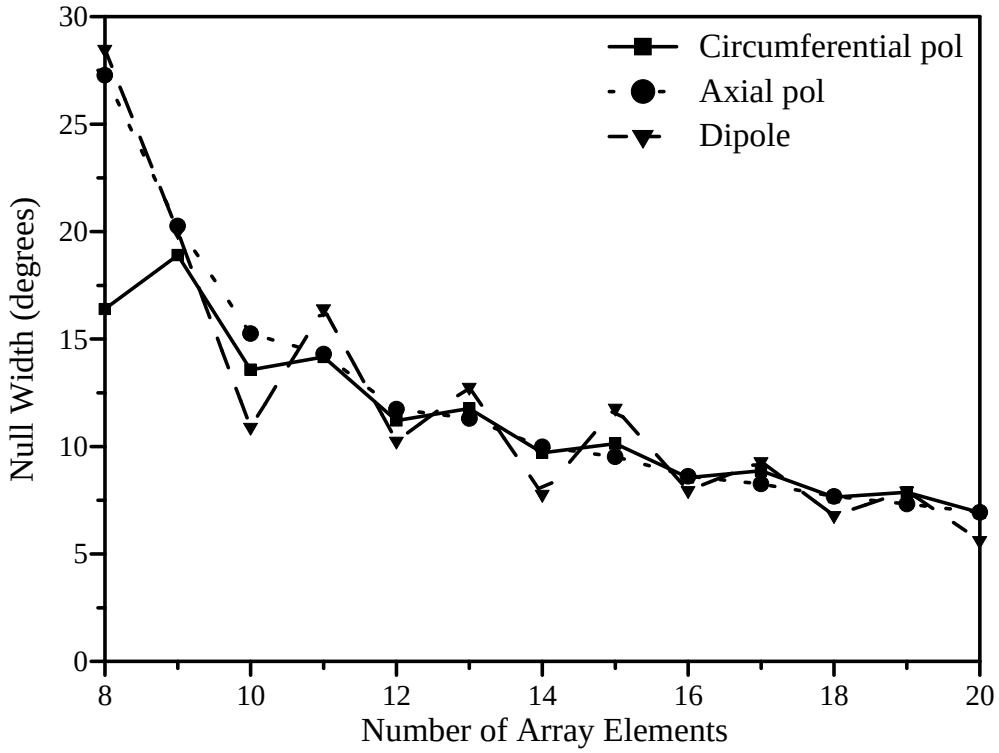

Figure 3.27: Resulting null width of a single null (40 dB depth, 1 dB ripple) in the radiation pattern of a cylindrical array with $d_\phi = 0.5\lambda_0$

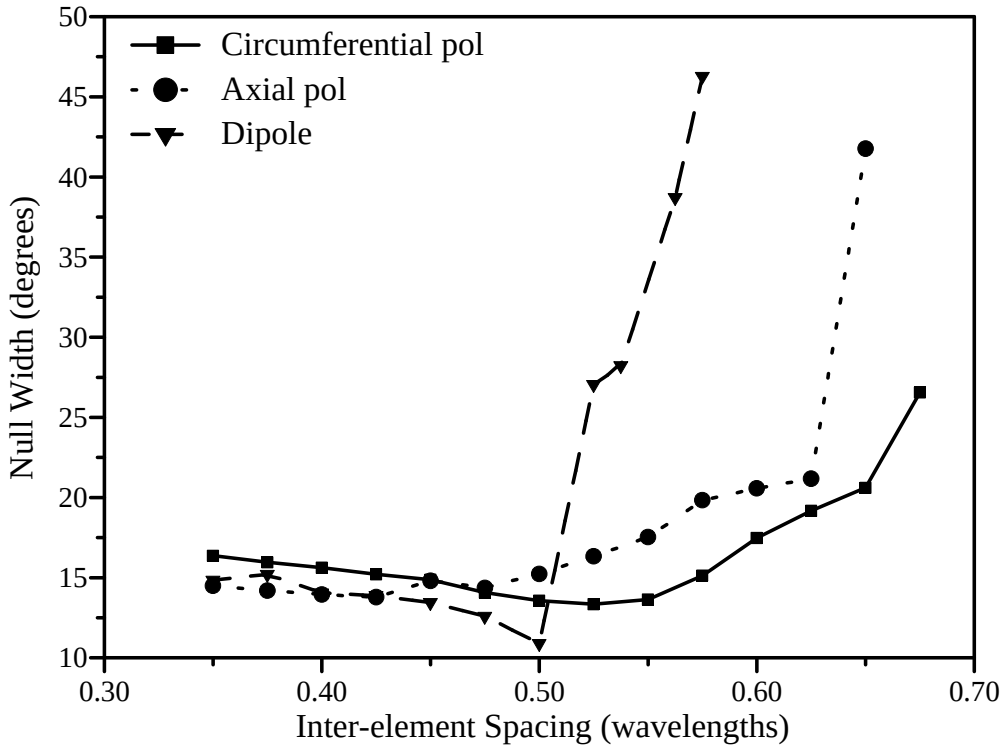

Figure 3.28: Resulting null width of a single null (40 dB depth, 1 dB ripple) in the radiation pattern of a cylindrical array with $N = 10$

3.4 Comparison of null synthesis methods

Each of the optimisation methods proposed in the previous sections have different advantages and disadvantages. To compare the results of the three methods, a single -40 dB null at 180° was specified as the desired null. The orthogonal projection method was used to obtain the starting excitation vector for all the methods. The results of the different optimisation methods for different types of arrays ($N = 10$ and $d_\phi = 0.5\lambda_0$) are compared in Table 3.2. In the first method, a window function was applied to reduce the ripple in the omni-region. Figures 3.29, 3.30 and 3.31 compare the resulting amplitude patterns of the first three optimisation methods for a circumferentially polarised patch array, an axially polarised patch array and a dipole array, respectively.

For each array configuration, the projection method forms the null with the least gain ripple, but with the largest null width. The objective weighting method produces a null with the least null width, but the resulting null is deeper than required. When the constrained method is used with only one constraint placed on the null depth, the resulting gain ripple for the patch arrays is higher than the gain ripple obtained from the projection and objective weighting methods. The obtained null width is also slightly higher than the null width produced by the objective weighting method. By constraining the ripple as well, the null width remains almost the same for the circumferentially polarised patch array, but slightly increases for the axially polarised patch array.

When only a low gain ripple is of concern, the orthogonal projection method with a window function can be used. On the other hand, the objective weighting method can be applied to obtain a narrow null when a higher gain ripple is tolerable. The resulting null depth for these two methods will depend on the number of elements as well as the inter-element spacing. The constrained optimisation method can be used to control both the null depth and the ripple, while obtaining a null width close to the null width resulting from the objective weighting method.

In the next section, the constrained optimisation method will be used to form multiple nulls in an otherwise omnidirectional pattern.

Table 3.2: Results of different optimisation methods for cylindrical arrays with $N = 10$ and $d_\phi = 0.5\lambda_0$

Array type	**Method**	**Null depth (dB)**	**Ripple (dB)**	**Null width (°)**
Circumferentially polarised patches	Projection with windowing	-36.1	0.27	22.31
	Objective weighting	-48.0	0.68	12.50
	Constraint: -40 dB	-40.0	1.70	13.54
	Constraints: -40 dB, 1dB ripple	-40.0	1.00	13.51
Axially polarised patches	Projection with windowing	-34.3	0.97	23.28
	Objective weighting	-81.9	1.85	12.21
	Constraint: -40 dB	-40.0	2.66	13.81
	Constraints: -40 dB, 1dB ripple	-40.0	1.00	15.25
Dipoles	Projection with windowing	-34.3	0.98	23.32
	Objective weighting	-46.5	2.05	9.10
	Constraint: -40 dB	-40.0	1.70	13.74
	Constraints: -40 dB, 1dB ripple	-40.0	1.00	10.89

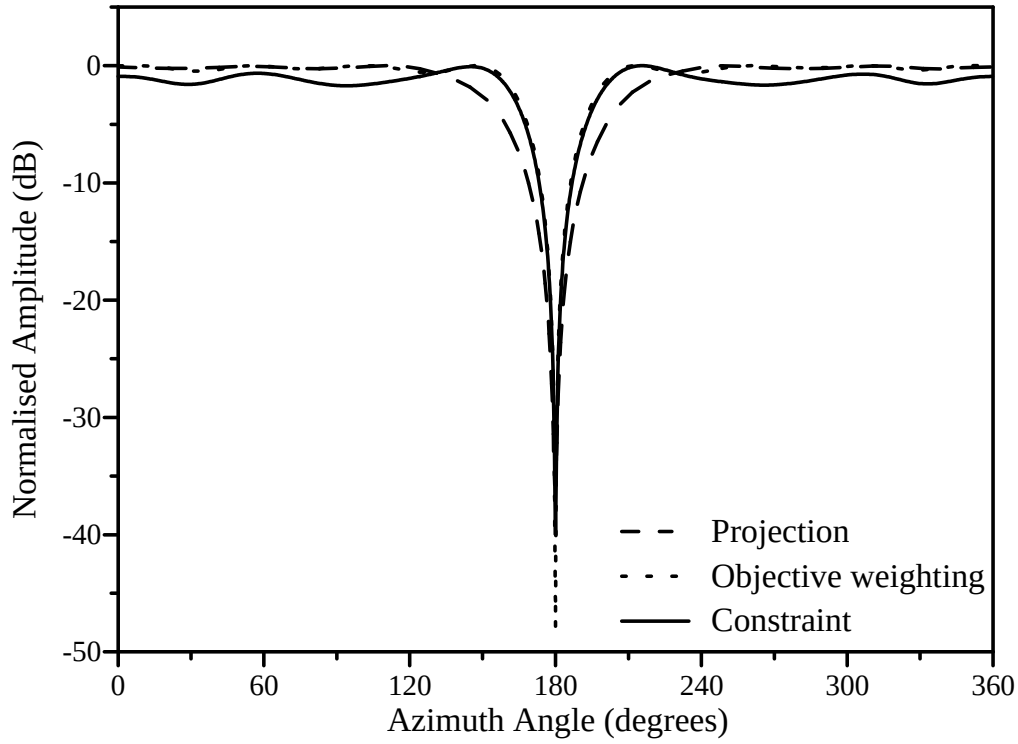

Figure 3.29: Radiation pattern of a circumferentially polarised patch array (N=10 and $d_\phi = 0.5\lambda_0$) with a single null using different methods

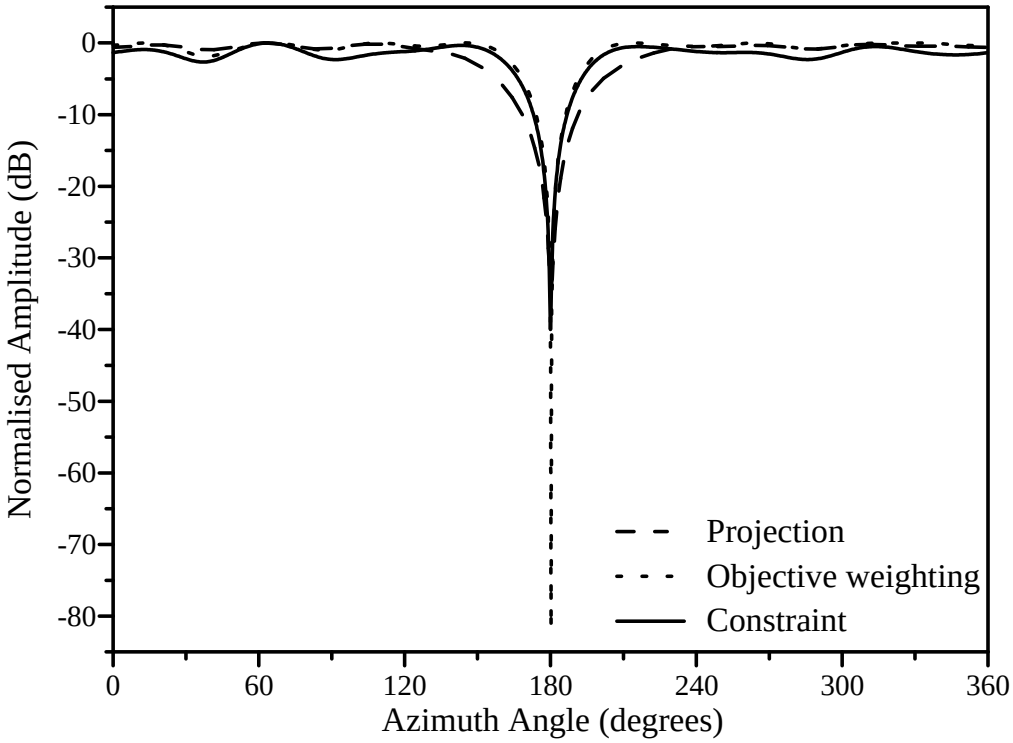

Figure 3.30: Radiation pattern of an axially polarised patch array (N=10 and $d_\phi = 0.5\lambda_0$) with a single null using different methods

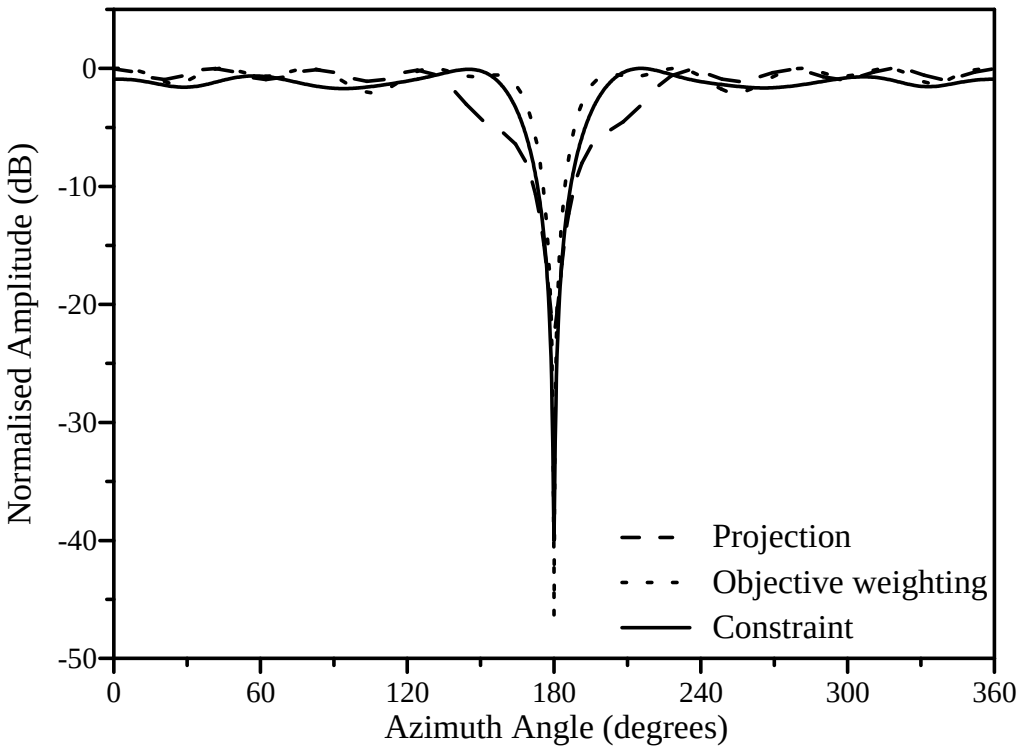

Figure 3.31: Radiation pattern of a cylindrical dipole array (N=10 and $d_\phi = 0.5\lambda_0$) with a single null using different methods

3.5 Multiple null synthesis

Where more than one interference should be suppressed, multiple null synthesis is required. The constrained optimisation method can be extended to perform the multiple null synthesis by adding the necessary constraints. The orthogonal projection method is used to obtain the optimum excitation vector, which is used as the starting vector for the optimisation.

In the first example, an omnidirectional radiation pattern with -40 dB nulls at 72° and 252° was specified. Constraints were specified for the two null depths as well as the ripple (1 dB or less). Figure 3.32 shows the amplitude pattern formed by the resulting excitation vector. The two nulls are present at the desired locations while the specified constraints are satisfied. Three -40 dB nulls were desired in the second example at 90°, 180° and 270°. A third constraint was added to the optimisation method for the additional null and the resulting amplitude pattern is shown in Figure 3.33. The pattern contains all three nulls at the specified locations with the desired null depths (-40 dB) and gain ripple (1 dB) between the nulls.

Cases with variable null depths were also studied. Firstly, two nulls were desired at 72° and 252° with null depths of -10 dB and -20 dB, respectively. The orthogonal projection method with the necessary variable phase steps in the idealised pattern was applied to form the starting excitation vector for the optimisation. The resulting radiation pattern is shown in Figure 3.34. The pattern contains the nulls with the desired null depths at the specified locations and the gain ripple is equal to 1 dB. An omnidirectional pattern containing three nulls with different null depths was also required. The nulls were desired at 90°, 180° and 270° with null depths of -10 dB, -15 dB and -20 dB, respectively. Figure 3.35 presents the resulting pattern with the three nulls at their desired locations. The null depths and gain ripple (1 dB) meet the required specifications.

The constrained optimisation method is thus able to form multiple nulls with different null depths while constraining the gain ripple in the omni-region. Since the null depths and ripple can be controlled, these characteristics are independent of the number of elements and the inter-element spacing. The null widths of the multiple nulls will, however, vary with the number of elements and inter-element spacing if they are not constrained as well.

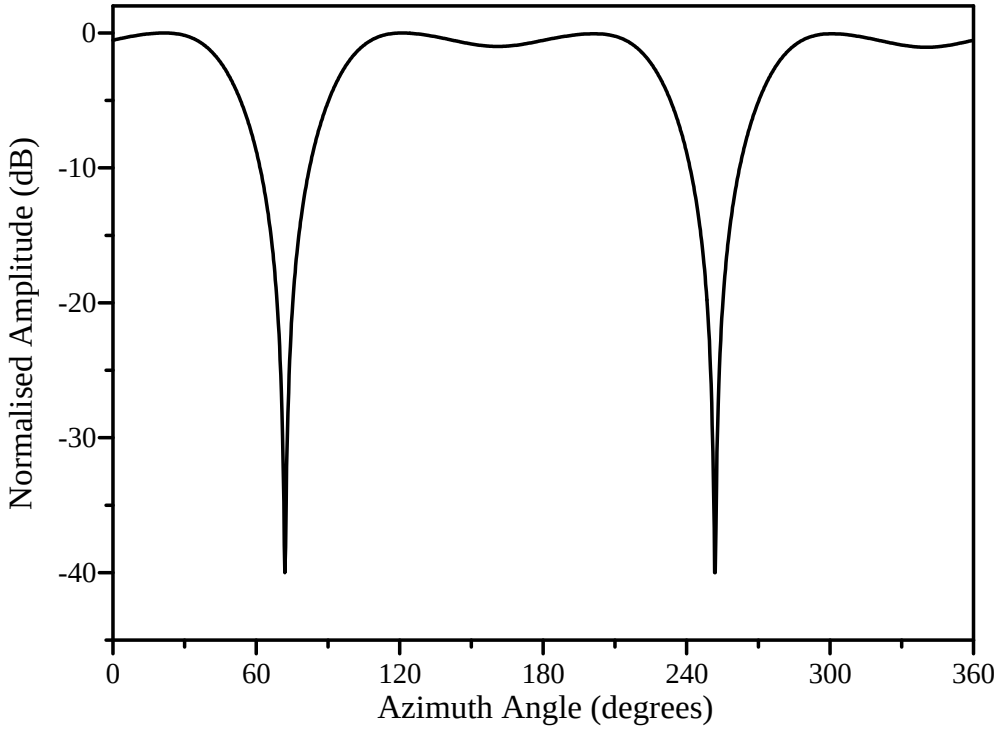

Figure 3.32: Radiation pattern of a circumferentially polarised patch array (N=10 and $d_\phi = 0.5\lambda_0$) with two nulls (72° and 252°), using constrained optimisation

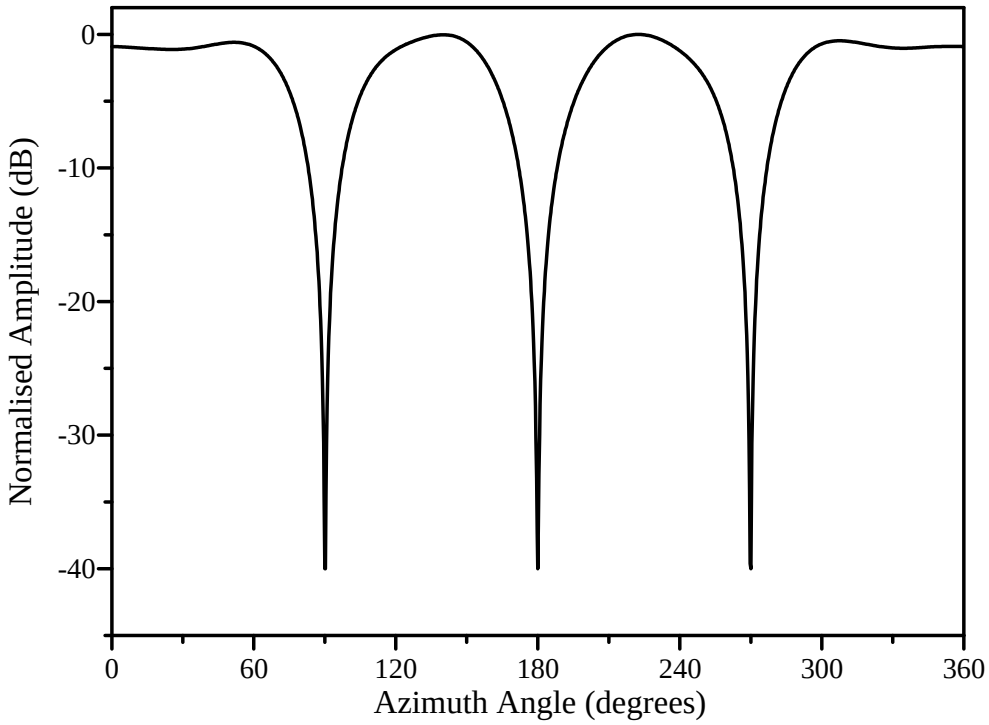

Figure 3.33: Radiation pattern of a circumferentially polarised patch array (N=10 and $d_\phi = 0.5\lambda_0$) with three nulls (90°, 180° and 270°), using constrained optimisation

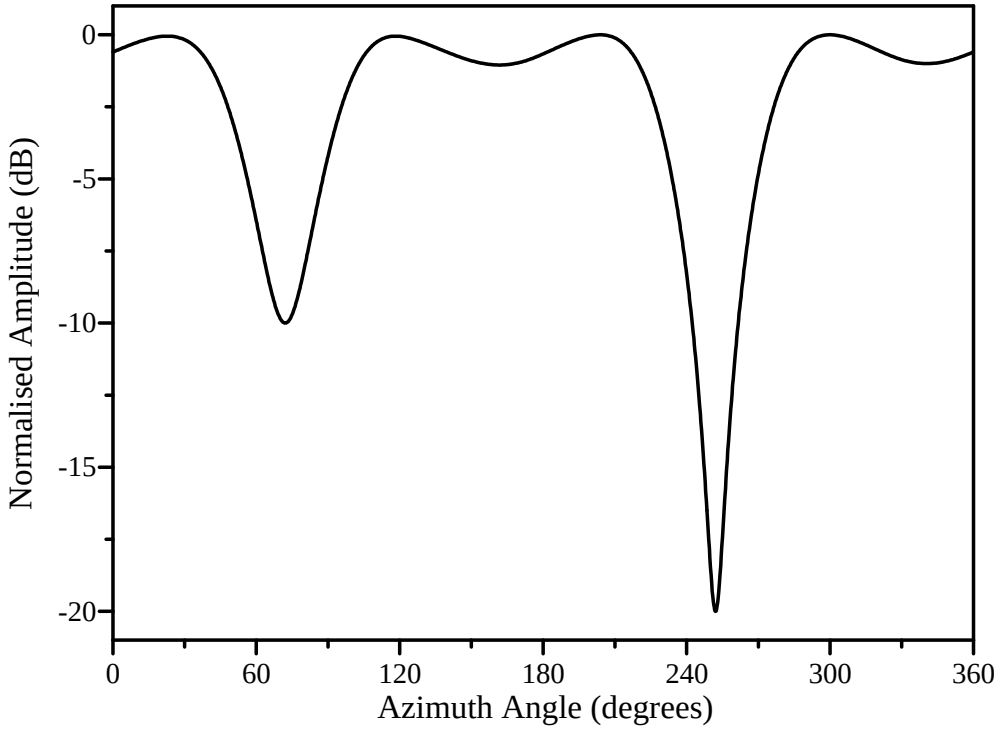

Figure 3.34: Radiation pattern of a circumferentially polarised patch array (N=10 and $d_\phi = 0.5\lambda_0$) with two nulls (72° and 252°), using constrained optimisation

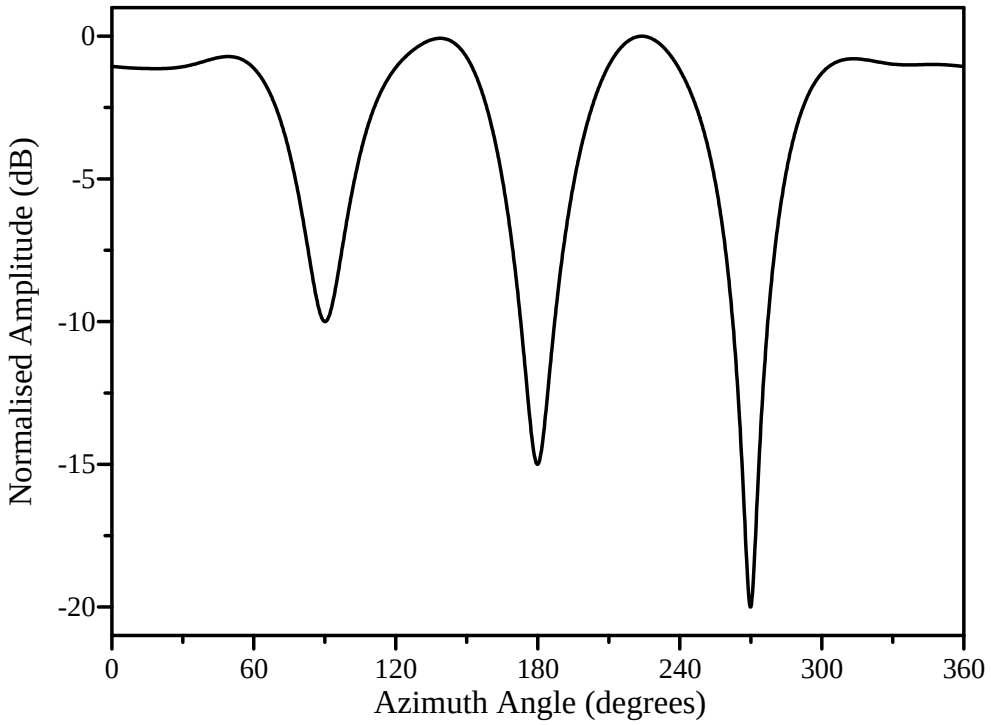

Figure 3.35: Radiation pattern of a circumferentially polarised patch array (N=10 and $d_\phi = 0.5\lambda_0$) with three nulls (90°, 180° and 270°), using constrained optimisation

3.6 Influences of the antenna element characteristics

The characteristics of the resulting null pattern may be influenced by the characteristics of the array as well as the attributes of the antenna element. The influence of the array characteristics such as the number of elements and the inter-element spacing have been shown in Section 3.3.1. Since the antenna element pattern varies with the height of the patch and the dielectric constant of the substrate, the resulting null pattern may also change due to variations in these characteristics. Different patch antenna elements were used to study the effects of element characteristics on the resulting null pattern.

3.6.1 Influence of the dielectric constant

Three different cylindrical patch antennas were designed to study the influence of using substrates with different dielectric constants. All three patches were designed for a resonant frequency of 1.8 GHz for the dominant mode and had a substrate height of $h = 1.6$ cm. For the first patch antenna, air was used as the substrate ($\varepsilon_r = 1$). The dimensions were $L = 7.97$ cm and $W = 8.2$ cm for the axial polarisation and vice versa for the circumferential polarisation. A substrate with $\varepsilon_r = 4.4$ was used to design the second patch antenna with dimensions of $L = 3.87$ cm and $W = 4.75$ cm for the axial polarisation; for the circumferential polarisation $W = 3.87$ cm and $L = 4.75$ cm. The results using these two patch antenna elements were compared with the results in the previous sections using the patch antenna with $\varepsilon_r = 2.3$ ($L = 5.44$ cm and $W = 6$ cm).

An omnidirectional pattern with a single null of -40 dB at 180° was specified. In each case the orthogonal base was modified to include the radiation pattern of the specific patch antenna element. Firstly, the constrained optimisation method was used without constraining the gain ripple. Figures 3.36 and 3.37 compare the amplitudes of resulting radiation patterns for the circumferential and axial polarisation, respectively. The axially polarised array using the air substrate forms the widest null with the most gain ripple. The other two axially polarised arrays form nulls with similar characteristics. The null width is almost the same for all three axial polarisation cases. For the circumferential polarisation, the resulting pattern of the array using the substrate with $\varepsilon_r = 4.4$ has the highest gain ripple. The null widths of all three patterns differ by less

than 0.5°.

The ripple was also constrained (1 dB or less) to yield the resulting patterns in Figures 3.38 and 3.39 for the circumferential and axial polarisation, respectively. In the circumferential and axial polarisations, the air substrate array produces the widest and narrowest nulls, respectively. On the other hand, the array with the $\varepsilon_r = 4.4$ substrate, yields the narrowest and widest nulls in the circumferential and axial polarisations, respectively. From these results, it can be concluded that the choice of the dielectric constant of the substrate will have an effect on the resulting null pattern characteristics. This is mainly due to the differences in element patterns when using different substrates.

3.6.2 Influence of the height of the substrate

Another attribute of the patch antenna elements which modifies the element pattern, is the height of the substrate. Two patch antenna elements with different heights were used to illustrate the influence of the height of the substrate. A foam based substrate with $\varepsilon_r = 1.024$ was used to design the two patches with $h = 1.6$ mm and $h = 5$ mm, respectively. Both patches were designed for a resonant frequency of 1.8 GHz. The dimensions for both patches were $L = 7.36$ cm and $W = 7.6$ cm for the axial polarisation and vice versa for the circumferential polarisation. The cavity model was used to obtain the element pattern of the patch with $h = 1.6$ mm. For the patch with $h = 5$ mm, a FDTD software package [101] was used to compute the element pattern.

The constrained optimisation method was used to determine the excitation vectors for a -40 dB null at 180°. Figures 3.40 and 3.41 compare the amplitude of the resulting radiated fields when only the null depth is constrained for the circumferential and axial polarisations, respectively. For $h = 5$ mm, a wider null with a higher gain ripple is formed for the circumferential polarisation. In contrast, the results are very similar when the two axial polarisation patterns are compared. When the gain ripple is constrained to 1dB or less, the resulting amplitude pattern in Figures 3.42 and 3.43 are obtained for the circumferential and axial polarisations, respectively.

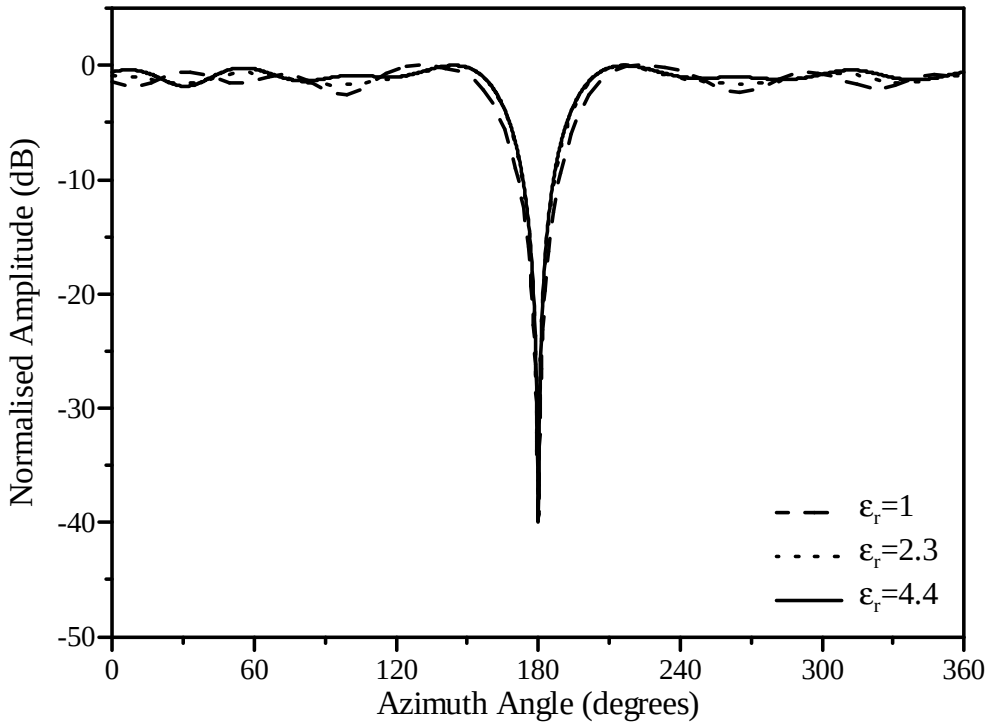

Figure 3.36: Comparison of the radiation patterns of circumferentially polarised patch arrays (N=10 and $d_\phi = 0.5\lambda_0$) using antenna elements with different substrates

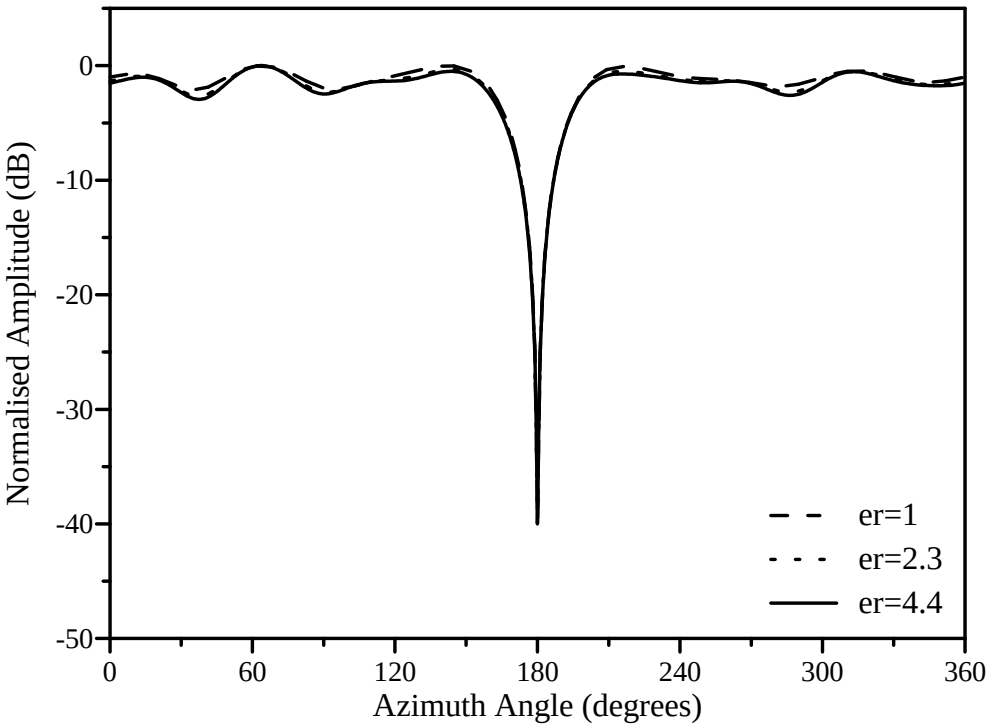

Figure 3.37: Comparison of the radiation patterns of axially polarised patch arrays (N=10 and $d_\phi = 0.5\lambda_0$) using antenna elements with different substrates

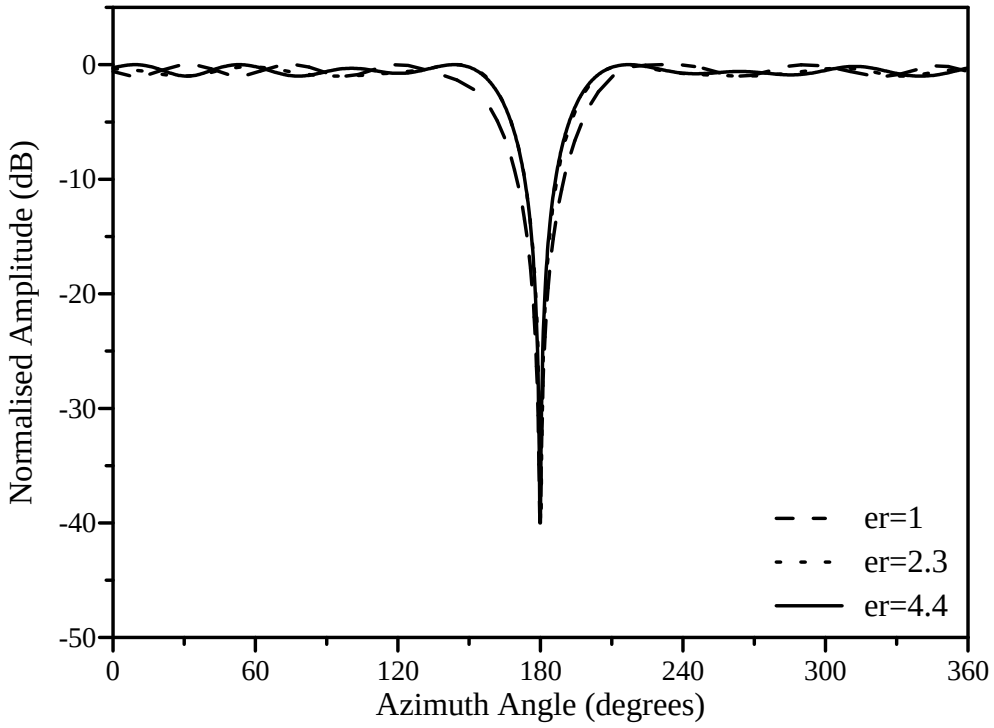

Figure 3.38: Comparison of the radiation patterns of circumferentially polarised patch arrays (N=10 and $d_\phi = 0.5\lambda_0$) using antenna elements with different substrates

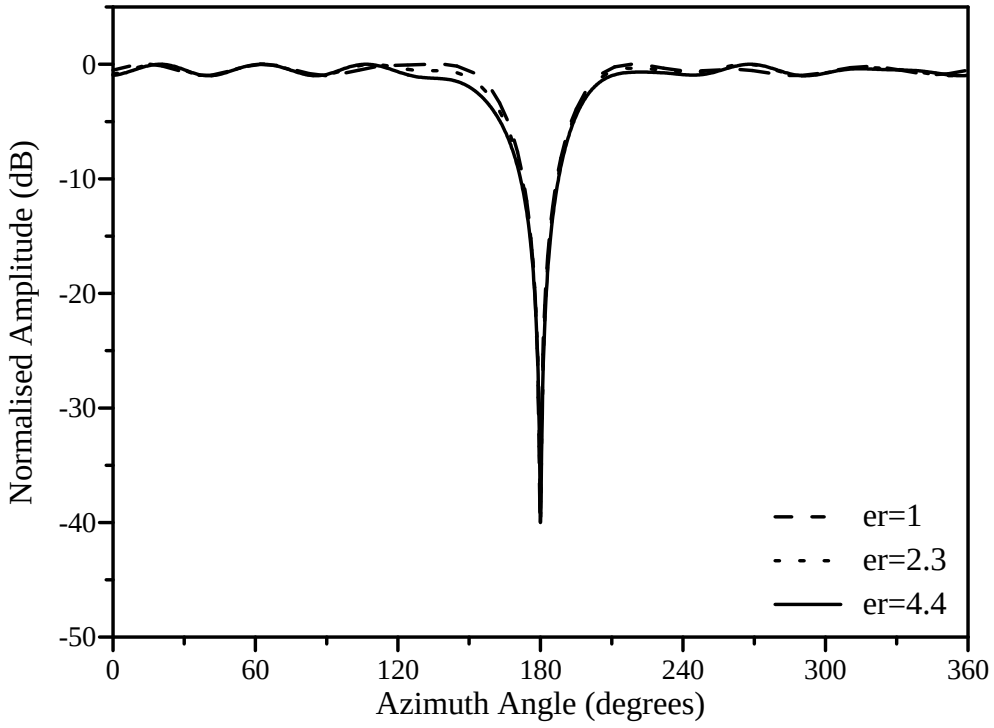

Figure 3.39: Comparison of the radiation patterns of axially polarised patch arrays (N=10 and $d_\phi = 0.5\lambda_0$) using antenna elements with different substrates

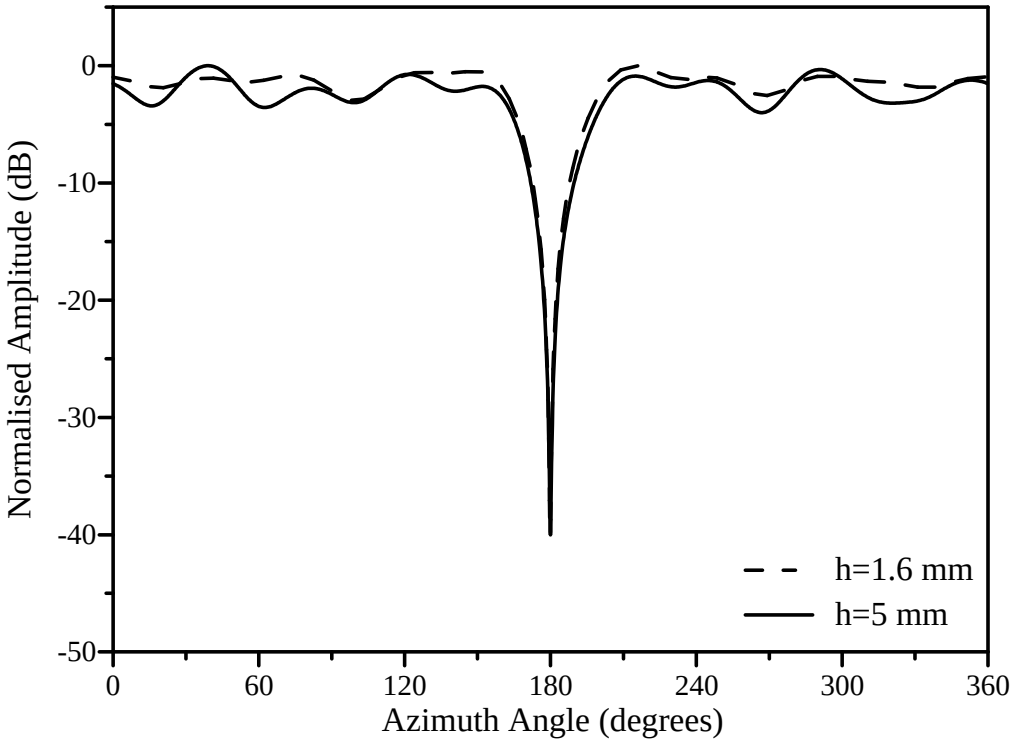

Figure 3.40: Comparison of the radiation patterns of circumferentially polarised patch arrays (N=10 and $d_\phi = 0.5\lambda_0$) using antenna elements with different substrate heights

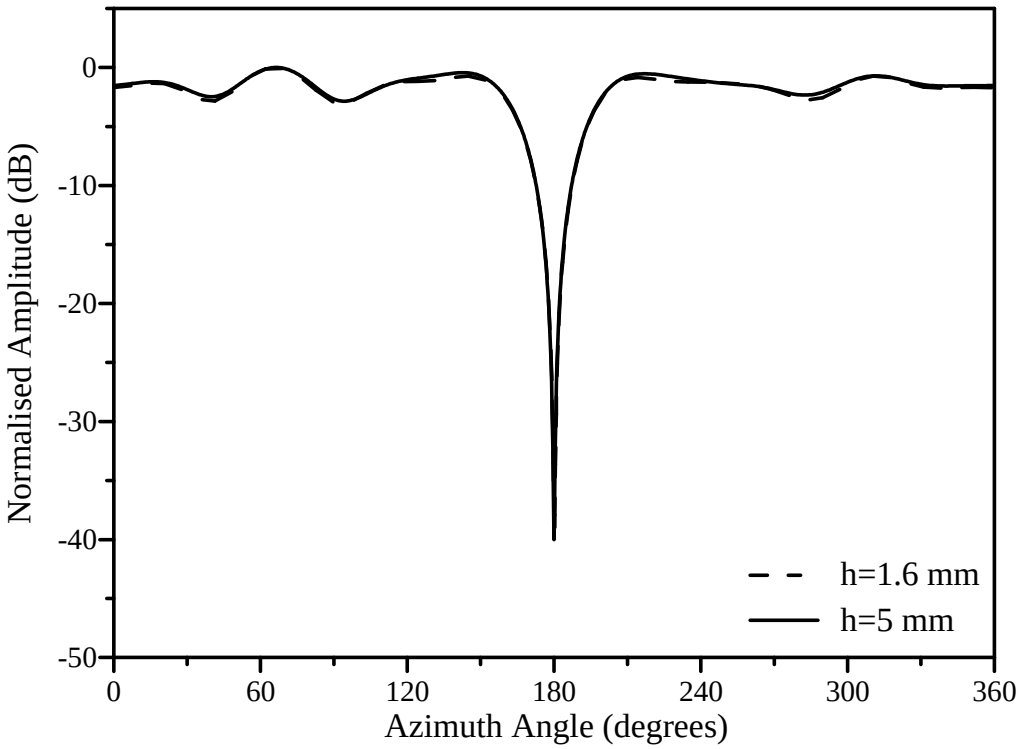

Figure 3.41: Comparison of the radiation patterns of axially polarised patch arrays (N=10 and $d_\phi = 0.5\lambda_0$) using antenna elements with different substrate heights

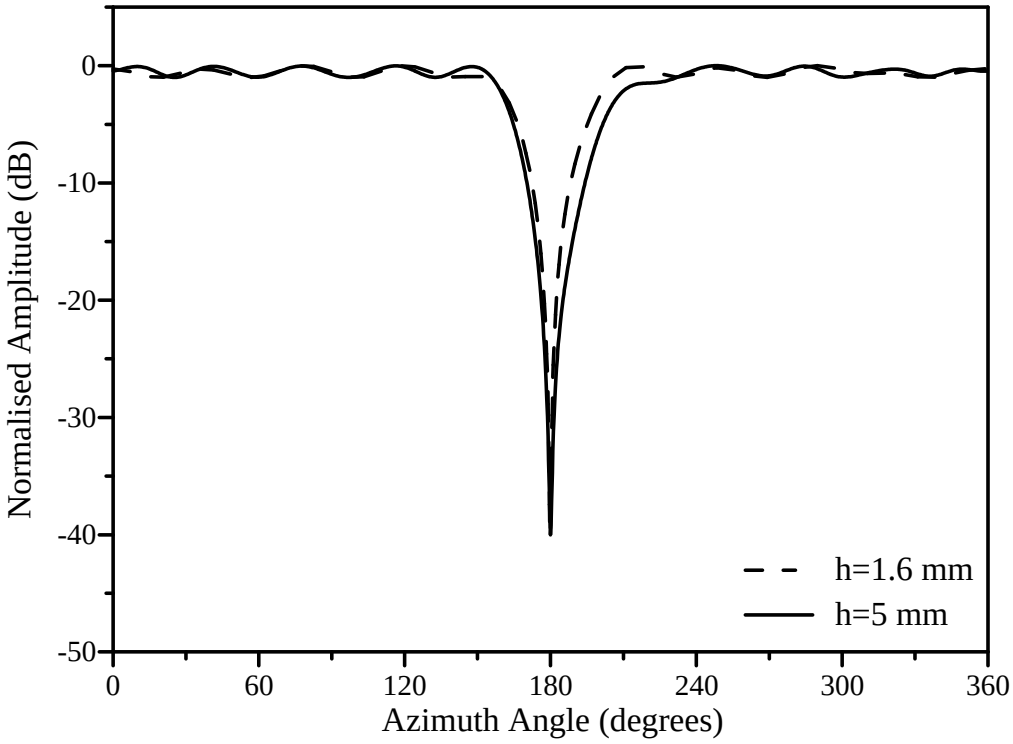

Figure 3.42: Comparison of the radiation patterns of circumferentially polarised patch arrays (N=10 and $d_\phi = 0.5\lambda_0$) using antenna elements with different substrate heights

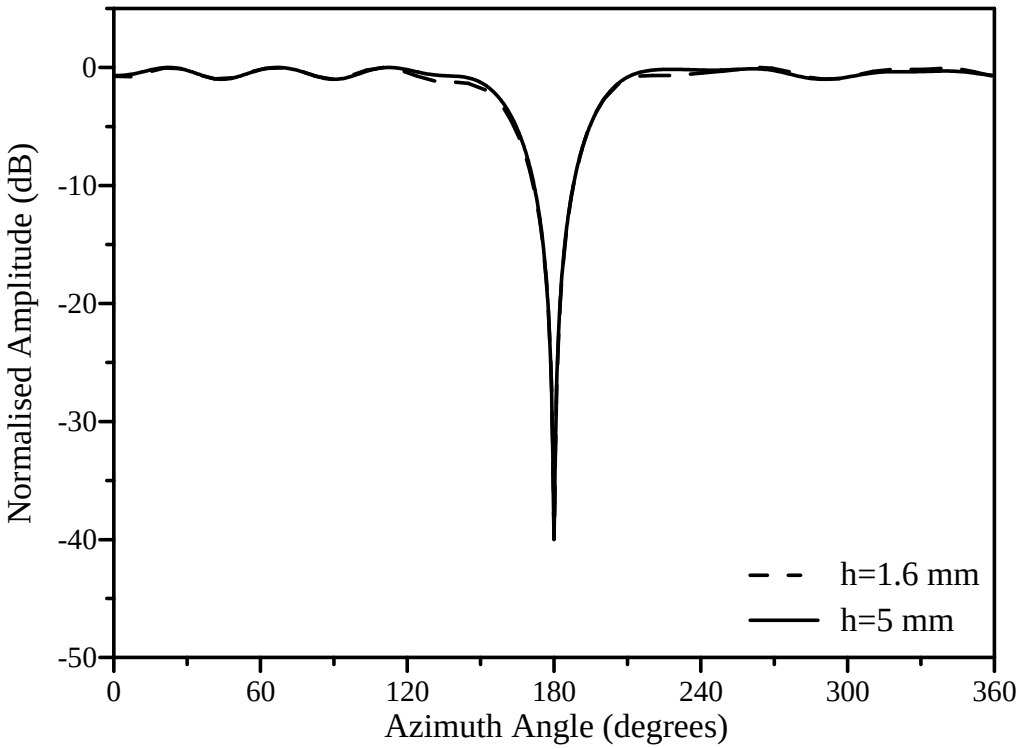

Figure 3.43: Comparison of the radiation patterns of axially polarised patch arrays (N=10 and $d_\phi = 0.5\lambda_0$) using antenna elements with different substrate heights

A null width difference of 7.04° exists between the two resulting circumferential polarisation patterns with the pattern for $h = 5$ mm having the widest null. The axial polarisation patterns differ only slightly. The choice of the substrate height has a greater influence on the resulting null width and gain ripple in the circumferential polarisation, since the element patterns for this polarisation differ more for different substrate heights. For this polarisation, a low substrate height is recommended when a narrow null is preferred.

3.7 Results for various null positions

Depending on the available degrees of freedom, the resulting characteristics of a null pattern may vary as the angular position of the null is changed. When a large number of elements is used, the variation in the null pattern will be low. On the other hand, the variations in the pattern characteristics may be higher when a small number of elements is used.

To study the influence of the position of the null, a -40 dB null was formed at different angular positions using patch arrays with N=10 and $d_\phi = 0.5\lambda_0$. Table 3.3 compares the resulting null pattern characteristics as the null position is varied for the different polarisations and the various constraints used in the constrained optimisation method. The angular position of the null is changed from ϕ_n to $\phi_n + \pi/N$ at 180° and 198°, respectively. The resulting amplitude patterns are compared in Figures 3.44 and 3.45 for circumferential and axial polarisations, respectively. These patterns are obtained when the null depth and the gain ripple are constrained to -40 dB and 1 dB, respectively.

The values of the pattern characteristics for a null at 180° and 198° do not differ much for the circumferential polarisation. Using this polarisation, the maximum gain ripple and null width occur when a null is desired at 189° ($\phi_n + \pi/2N$). When the axially polarised array is utilised and only the null depth is constrained, the gain ripple increases while the null width decreases as the null position is varied from 180° to 198°. A maximum null width is obtained at 198° when the gain ripple is constrained as well. In this case, the null width increased by 2.04° when the desired angular null position was changed from 180° to 198°.

Table 3.3: Results for cylindrical arrays with $N = 10$ and $d_\phi = 0.5\lambda_0$ using the constrained optimisation method for different null positions

Array type	**Constraints**	**Null position (°)**	**Ripple (dB)**	**Null width (°)**
Circumferentially polarised patches	-40 dB depth	180	1.70	13.54
		189	1.86	13.73
		198	1.72	13.47
	-40 dB depth 1dB ripple	180	1.00	13.58
		189	1.00	13.74
		198	1.00	13.55
Axially polarised patches	-40 dB depth	180	2.66	13.81
		189	2.72	13.49
		198	2.93	13.28
	-40 dB depth 1dB ripple	180	1.00	15.25
		189	1.00	14.58
		198	1.00	17.29

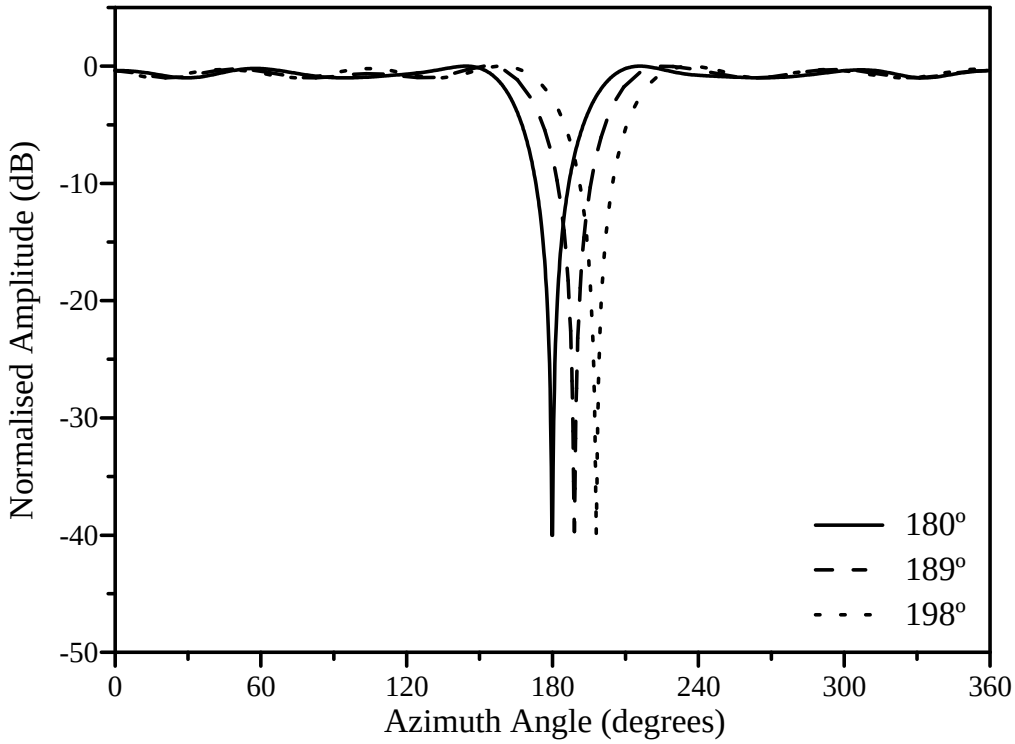

Figure 3.44: Comparison of the radiation patterns of a circumferentially polarised patch array (N=10 and $d_\phi = 0.5\lambda_0$) when the null position is varied

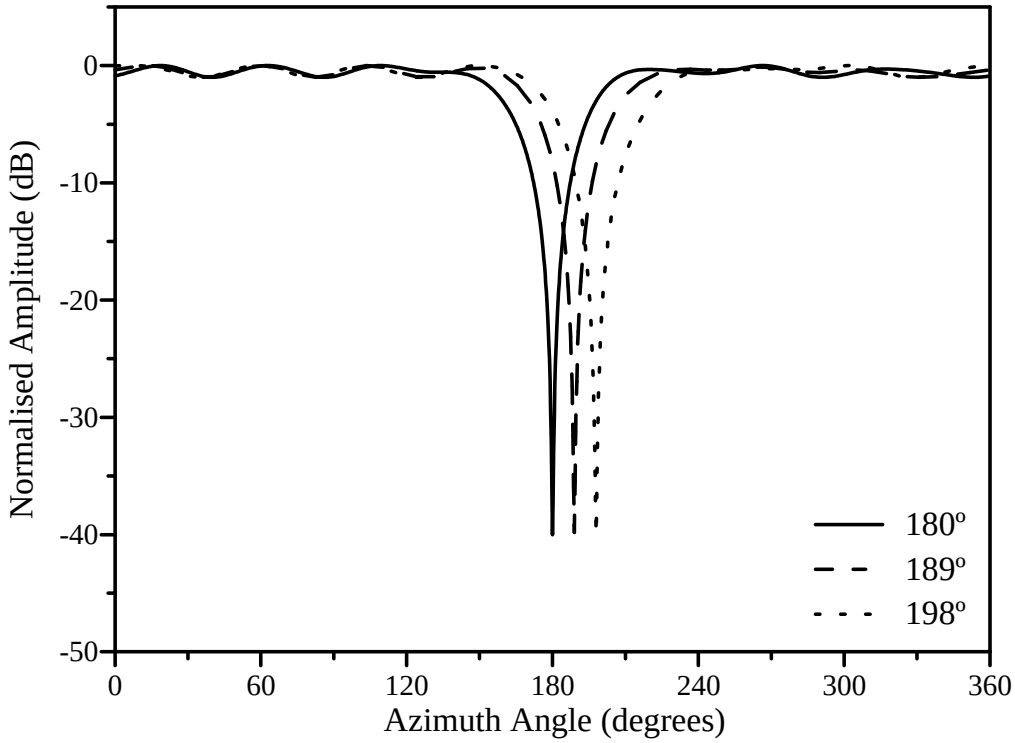

Figure 3.45: Comparison of the radiation patterns of an axially polarised patch array (N=10 and $d_\phi = 0.5\lambda_0$) when the null position is varied

The degree to which the characteristics of the resulting null pattern change as the null position is varied, depends on the utilised polarisation. The variations in the pattern characteristics consequently depend on the element pattern that is incorporated. By carefull selection of the element pattern, the sensitivity of the pattern characteristics to a change in the null position, can thus be minimised.

3.8 Summary

Abele *et al.* [53] introduced a null synthesis technique for a cylindrical dipole array. The technique utilised the orthogonal projection method and projected an idealised null pattern onto the orthogonal base of realisable array patterns. The resulting array pattern was an omni-directional pattern with one or more nulls. Vescovo [56] extended the orthogonal projection method for an arc array with theoretical directional elements. A beam pattern was formed through the projection method and additional nulls were introduced in the pattern with null constraints to reduce the side lobe level. In this chapter the null synthesis technique of Abele was extended to incorporate the radiation

patterns of conformal microstrip patches.

In this chapter, the null synthesis technique of Abele [53] was used to form an omnidirectional radiation pattern with nulls at specified locations for a cylindrical microstrip patch array. The orthogonal projection method was extended by modifying the orthogonal base for the space of realisable array pattern to include the radiation pattern characteristics of microstrip patch antennae mounted on a conducting cylinder. For electrically thin patches, the cavity model was used to compute the element pattern of the cylindrical patches. A FDTD software package [101] was used to calculate the element pattern of electrically thick cylindrical patches. The unconstrained optimum element excitations obtained from the orthogonal projection method provided an optimal array pattern with the minimum pattern error (in a least square sense).

The resulting radiation pattern contained the desired null at the specified angular location in the otherwise omnidirectional pattern. By applying a Hamming window to the sequence excitations before the element excitations are computed, the gain ripple in the omniregion was reduced. The resulting null pattern characteristics were also influenced by the array configuration parameters such as the number of elements and the inter-element spacing. When an infinitely deep null was desired, the resulting gain ripple and null width gradually decreased while the null depth increases as the number of elements were increased for both axially and circumferentially polarised microstrip patch arrays. As the inter-element spacing was increased, the gain ripple and null width increased as well. For a large number of elements the yielded null widths became comparable to the null widths obtained with dipoles as the array elements. In most cases, the microstrip patches yielded better gain ripple due to the high level of gain ripple in the radiated field of cylindrical dipole arrays.

Since the amplitude and phase of the radiation pattern were optimised simultaneously, the optimal array pattern may not have had the desired characteristics. Although the ripple was successfully decreased by using the windowing function, the resulting null width was increased. Instead of only minimising the array pattern error, a multi-objective optimisation approach was followed [95–97]. The Objective Weighting method, previously applied in other fields of computational electromagnetic problems [96, 97], was used to improve the amplitude pattern characteristics. A global performance function was defined by utilising both the amplitude pattern error and the phase pattern error. The optimisation problem was solved by finding the critical

ratio of the weights that were assigned to the two errors in the performance function. Each performance function was minimised by using an unconstrained minimisation algorithm [99]. The excitation vector obtained from the orthogonal projection method yielded an optimum radiation pattern with the minimum pattern error and was therefore chosen as the starting vector. The resulting excitation vector that minimised the performance function formed with the critical weight ratio, was used to form the radiation pattern.

Compared to the results of the windowing method, the objective weighting method provided a null pattern with a narrower and deeper null and with a higher gain ripple in the omni-region. An increase in the phase pattern error was observed due to the trade-off that existed between the two pattern errors in the performance function. When infinitely deep nulls were desired, the method could synthesise deep nulls utilising only a small number of elements.

Constrained optimisation methods have been used previously to form beam patterns with cylindrical arrays [45, 52, 56]. Prasad [45] applied the least squares optimisation method to circular and arc arrays to form a beam pattern with a specified beamwidth. Additional nulls were also placed in the sidelobe region by using null constraints while minimising the mean square difference between the desired pattern and the optimum pattern. The Hook and Jeeves algorithm was also used to perform an iterative search to find the optimum excitation vector while satisfying the null constraints. During the search, the sidelobe level was minimised. Ares *et al.* [52] used a simulated annealing technique to produce beam patterns for a circular arc array on a cylinder. A cost function, which could include terms to control the radiation pattern, was minimised. Terms which placed constraints on the excitations, could also be included in the cost function. The sidelobe level was also decreased by placing null constraints in the region near the main lobe [56]. In this chapter, constrained optimisation was also used to yield an excitation vector which minimises the pattern error under the constraints specified for the different amplitude pattern characteristics. The minimum pattern error was found using a constrained minimisation algorithm [99]. The optimum element excitation vector, which was obtained from the projection method, was used as the starting vector.

Individual characteristics as well as combinations of characteristics were controlled using the constrained optimisation. Compared to the above methods, the constrained

optimisation algorithm obtained a null width close to the null width resulting from the objective weighting method, while controlling both the null depth and gain ripple in the omni-region. The method was also able to form multiple nulls with different null depths while constraining the gain ripple. Due to the control provided by the algorithm, the resulting pattern characteristics could be made independent of the number of elements and the inter-element spacing.

Since the element pattern can not be factorised out of the array factor, any change in the element pattern may influence the characteristics of the resulting array pattern. While controlling certain null pattern characteristics, the influence of changes in the antenna element configuration on the remaining unconstrained pattern characteristics, was studied. The effects of the changes in the dielectric constant and the height of the substrate are different for the circumferentially and axially polarisations. The null pattern characteristics for the axial polarisation are only slightly influenced by a change in substrate height. When the null depth is constrained, the resulting ripple and null width for both polarisations are influenced by a change in the dielectric constant. The degree to which the unconstrained characteristics of the resulting null pattern change as the null position is varied, also depend on the utilised polarisation. The sensitivity of the resulting null pattern characteristics to a change in the desired null position or an antenna element characteristic, can be minimised by a careful selection of the element pattern.

The above three null synthesis methods determines the necessary element excitations without considering the mutual coupling between the elements. If the inter-element spacing is chosen large enough or the height of the patch elements is low in terms of wavelength, the mutual coupling factor is small and has very little effect on the resulting pattern. On the other hand, the mutual coupling between closely spaced patch antenna elements with high substrate heights, is large enough to distort the resulting radiation pattern. Consequently, the mutual coupling must be compensated for. In most systems, the driving impedances of the patch antenna elements also need to be matched to the input system. In the next chapter, a mutual coupling compensation technique is employed which alter the patch antenna element geometries to simultaneously correct the resulting null pattern and the driving impedances of the antenna elements.

CHAPTER 4

IMPLEMENTATION OF CYLINDRICAL MICROSTRIP PATCH ARRAYS

The null synthesis techniques proposed in the previous chapter do not consider the mutual coupling between the antenna elements and it is also assumed that the antenna elements do not disturb each other's current distributions. Each element's radiation pattern is thus considered to be identical to the radiation pattern of an isolated antenna in both shape and radiation strength. The input impedance of each antenna element is furthermore assumed to be matched to the impedance of its port in the feeding network.

These assumptions are valid when large inter-element spacings and low substrate heights are used to minimise the effects of the mutual coupling. In Chapter 3, it was seen that the utilisation of large inter-element spacings leads to wide nulls with high gain ripple in the omni-region. The use of a low substrate height is also not favoured since it decreases the realisable bandwidth. Small inter-element spacings and higher substrate heights are therefore preferred to yield null patterns with a reasonable bandwidth within the pattern specifications.

When small inter-element spacings are used, distortion of the excitations may occur due to the mutual coupling. The desired radiation pattern is consequently deteriorated due to the errors in the element excitations [72, 73]. During null synthesis, these erroneous

excitations lead to null filling and null position errors [53, 74]. The nulls introduced in the beam patterns of linear monopole arrays were found to be shifted or filled due to the mutual coupling [74]. Abele [54] studied the effect of the mutual coupling on the null pattern of a cylindrical dipole array and found that the coupling needed to be compensated for to prevent distortion of the null characteristics.

In this chapter, an investigation into the extent to which the mutual coupling has an influence on the null pattern of a cylindrical microstrip patch array will be done. When it is established that the mutual coupling may not be neglected for a specific array configuration and null pattern, a technique to compensate for the mutual coupling will be needed.

Yang *et al* [86] proposed a mutual coupling compensation technique to obtain the desired bandwidth and voltage standing wave ratio (VSWR) at the resonant frequency for an electromagnetically coupled (EMC) dipole antenna array. For a given set of excitation voltages, the dipole lengths and dipole offsets from the microstrip feed line were altered to obtain the prescribed driving admittances seen by the feed lines. As a result, a good similarity was also found between the desired and measured radiation patterns. Chen *et al* proposed a similar technique for a linear array of parallel dipoles [88]. The lengths and the radii of the dipoles were changed to obtain equal driving impedances for all the dipoles. Consequently, the desired radiation pattern was obtained. In this chapter, the mutual coupling compensation technique is applied to both linear and cylindrical microstrip patch arrays.

In the first section, the design of a cylindrical microstrip patch element for both polarisations will be discussed. The effect of the mutual coupling on the bandwidth of a linear microstrip patch array will be investigated firstly. This investigation was conducted in order to study the improvement in the bandwidth due to the use of the mutual coupling compensation technique. Afterwards, the effect of coupling on the array imbedded element pattern of the cylindrical microstrip patch element will be shown. The influence of the mutual coupling on the null pattern of a cylindrical microstrip patch will also be investigated for various inter-element spacings and both polarisations. The mutual coupling compensation technique will be used for both the linear and cylindrical microstrip patch arrays. The improvement in the characteristics of the linear and cylindrical patch arrays due to the compensation technique will be discussed using two test cases.

4.1 Design of cylindrical microstrip patch element

In the investigation of the cylindrical microstrip patch arrays, probe-fed microstrip patches were also utilised as the array elements. To assist with the design of the array elements, a commercial electromagnetic software package which apply the Finite Difference Time Domain (FDTD) method [101], was used. To verify the results of the software package, a single element was designed, manufactured and measured. The measured results were then compared with the simulated results.

Figure 4.1 illustrates the cylindrical microstrip patch element (axially polarised) on a copper cylinder, as well as the probe feeding mechanism. The patch element consisted of a 5mm layer of air, a thin layer of FR4 ($\varepsilon_r = 4.17$) and a 36 μm layer of copper. The patch was etched onto the thin layer of FR4 (with a thickness of 0.127mm) and conformally shaped to the patch along the surface of the cylinder.

The FDTD software package uses conforming cell elements in the xy-plane, and rectangular cell elements in the xz- and yz-planes. To make use of the conforming cells, the axes of the cylinder were thus aligned with the z-axis. The three main considerations during the design of the single element using the software, were the simulation of the probe feeding, the thin layer of copper and the thin layer of FR4.

When the thin layers of FR4 and copper were used in the simulation, a very large number of cells was generated during the meshing of the problem. This high number of cells exceeded the simulation capability of the software and an alternative method for the simulation of the problem was thus needed. The effect of the thin layer of FR4 was simulated by combining the layers of air and FR4 into one layer. The characteristics of the combined layer were found by simulating and comparing the input impedances of a planar patch with the two layers and a planar patch with a combined layer. A single layer with a height of 4.77mm and $\varepsilon_r = 1.0705$ were found to yield similar results compared to the double layer. The thickness of the copper layer was increased to 1mm in order to reduce the number of cells.

The probe-feed was simulated using a square co-axial probe. The dimensions of the probe-feed were designed for $S_{11} = S_{22} = 0$ and $S_{12} = S_{21} = 1$. The resulting centre conductor had a diameter of 0.8mm. The outer conductor had an outer diameter of 4mm and a thickness of 0.45mm. The dielectric material in the coax had an ε_r of 2.3.

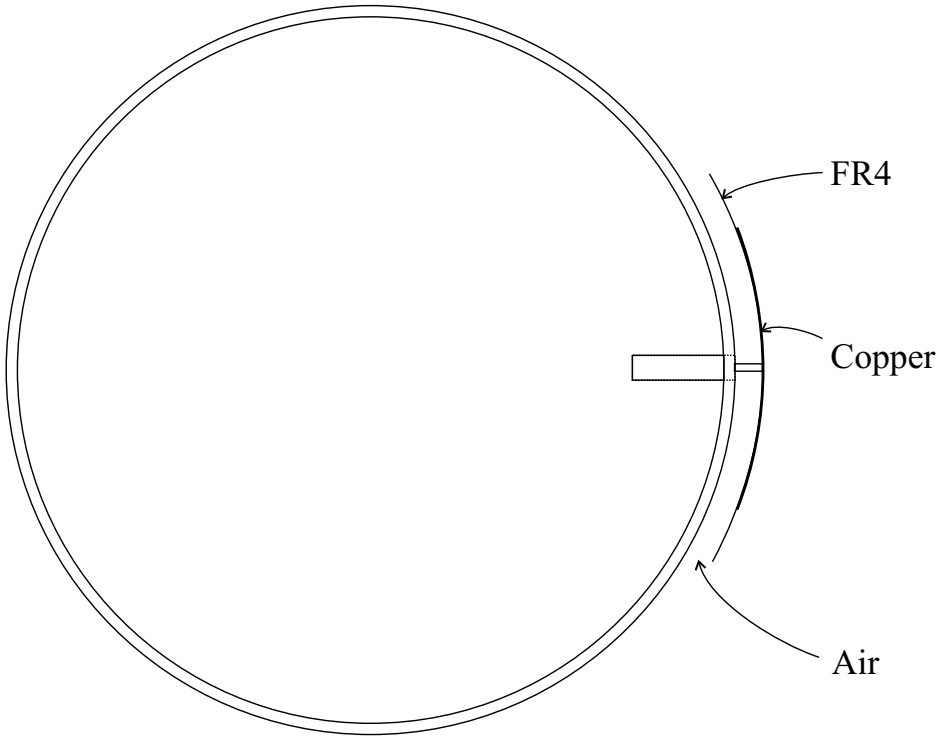

Figure 4.1: Top view of cylindrical microstrip patch on a copper cylinder with a radius of 127 mm and a thickness of 2 mm

The effects of the above approximations on the simulated results were studied by designing a single element and by comparing the simulated and measured results. A planar patch was designed for a resonant frequency of 1.8 GHz, with resulting dimensions of $L = 73.1$ mm, $W = 76$ mm and $y = 20.85$ mm. The planar patch was simulated with a copper thickness (t) of 0mm (using a perfectly conducting boundary) and 1mm. The same patch element was also used to form the axially polarised cylindrical patch element and was simulated with the above mentioned approximations. A 250mm high cylinder with $a = 127$ mm and $h = 2$ mm was used. Both the planar and cylindrical patch elements were manufactured and their reflection coefficients were measured.

Figure 4.2 compares the simulated and measured reflection coefficients for the planar and cylindrical patch elements. For the planar patch, the simulation yielded a lower resonant frequency (1.774 GHz) for $t = 0$ mm compared to the measured resonant frequency of 1.798 GHz. For the thicker layer of copper ($t = 1$ mm), the resonant frequency is even lower at 1.744 GHz. This decrease in the resonant frequency is due to the wider fringing fields. The simulation for the cylindrical patch with $t = 1$ mm yielded a resonant frequency of 1.735 GHz. In comparison, a higher resonant

frequency of 1.808GHz was obtained from the measurements of the cylindrical patch. The resonant frequencies of the measured planar and cylindrical patches differed by only 10 MHz.

The lower resonant frequency of the simulated reflection coefficient must thus be taken into account when designing the cylindrical patch element. The reflection coefficients of the simulated and measured cylindrical patch elements also differ by 7.7 dB, which must also be considered during the design.

The simulated and measured radiation patterns of the axially polarised patch element were also compared. The comparison of the patterns at the respective resonant frequencies can be seen in Figure 4.3. The radiation pattern was measured with the centre of the cylindrical patch pointing towards 0°. In the main beam region, between −100° and 100°, the patterns are very similar. At 180° the radiation patterns differ by 3.2 dB.

The effect of the approximations was also studied for a circumferentially polarised cylindrical patch element. The thin layer of FR4 and the 5mm layer of air were also combined into one layer and the copper patch had a thickness of 1mm in the simulations. The dimensions of the patch element were $L = 75$ mm and $W = 76$ mm. The feed position was at 16.9 mm in the ϕ-direction from the centre of the patch. The simulated and measured results for the reflection coefficients are compared in Figure 4.4. The resonant frequency of the measured results (1.779 GHz) was also higher than the resonant frequency (1.727 GHz) yielded by the simulation. The simulated and measured reflection coefficients at their respective resonant frequencies differed by 6.8 dB.

Figure 4.5 compares the measured and simulated radiation patterns for the circumferentially polarised patch. The two patterns compared well in the main beam region between −60° and 60°, but differ slightly outside this angular range.

The above shifts in the resonant frequencies and changes in the input impedances can consequently be applied to refine the design of the axially and circumferentially polarised patch elements for the desired resonant frequency and input impedance. Manufacturing tolerances will however still have an influence on the measured results.

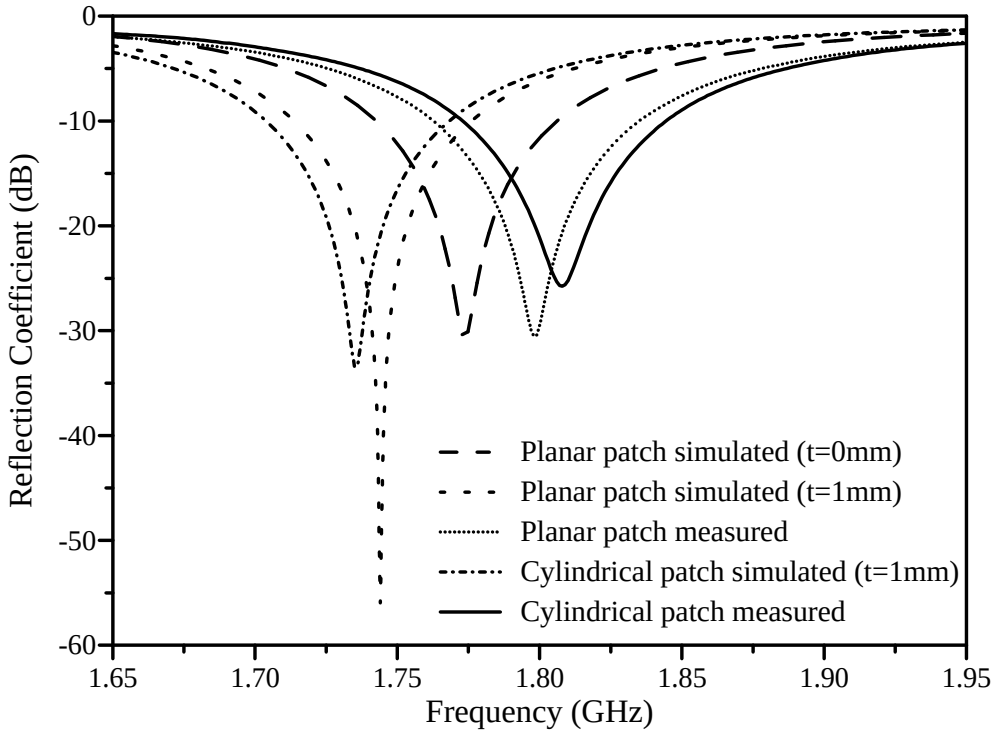

Figure 4.2: Simulated and measured reflection coefficients for planar and cylindrical patch (axially polarised) elements

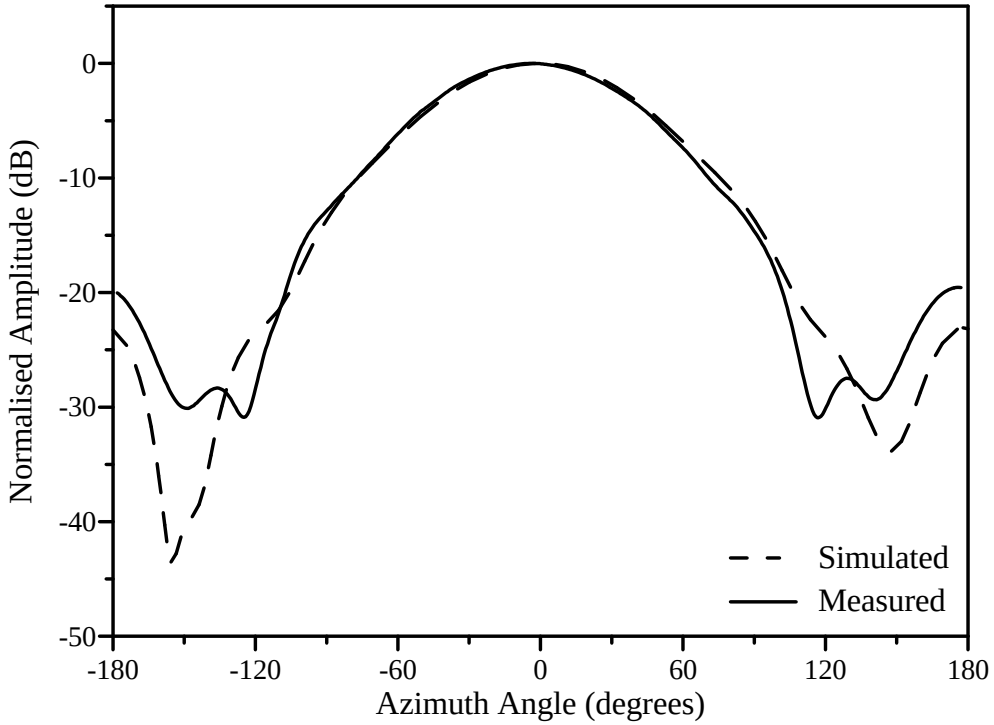

Figure 4.3: Simulated and measured radiation patterns for the axially polarised patch element

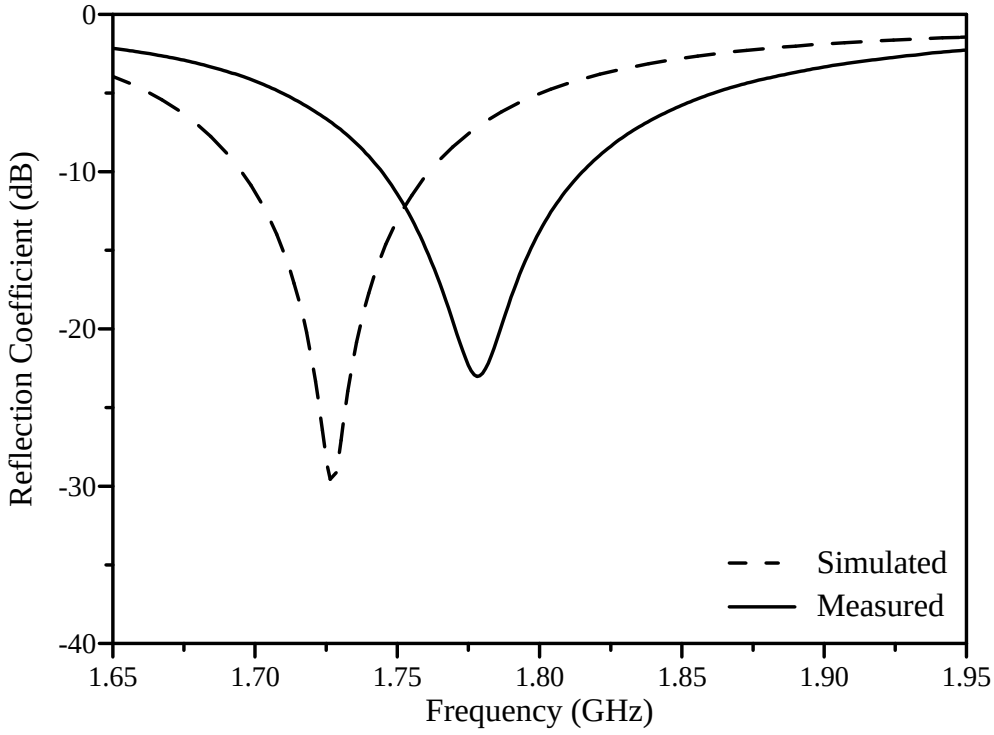

Figure 4.4: Simulated and measured reflection coefficients for the circumferentially polarised patch element

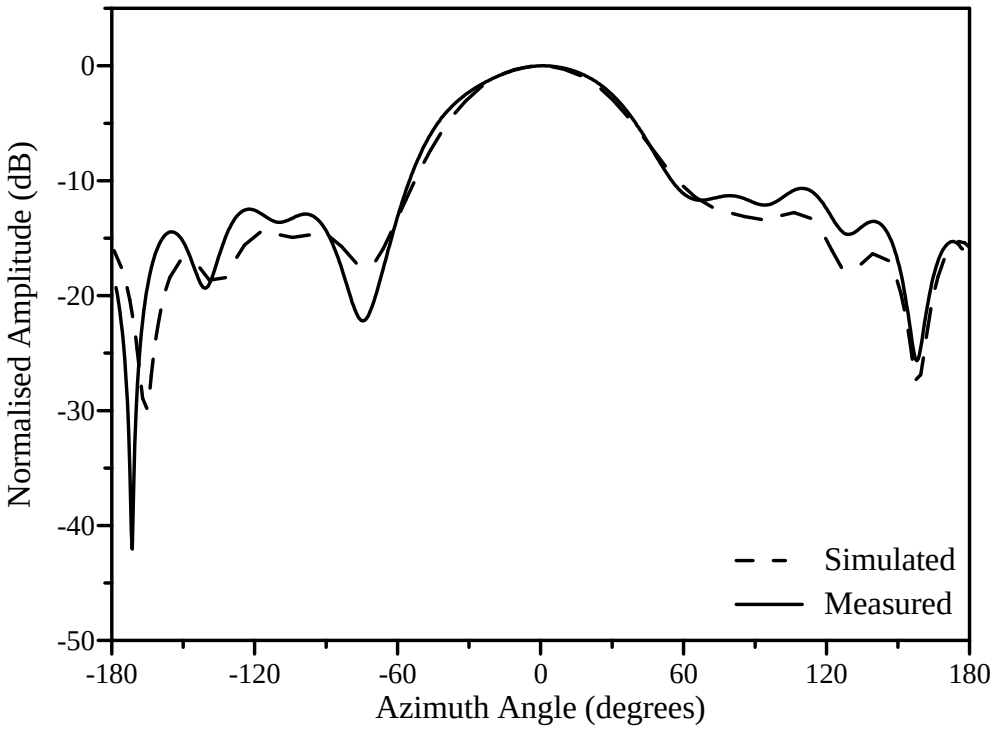

Figure 4.5: Simulated and measured radiation patterns for the circumferentially polarised patch element

4.2 Effect of mutual coupling

4.2.1 Effect of mutual coupling for linear patch arrays

The effect of the mutual coupling on the bandwidth and resonant frequency of a linear microstrip patch array was investigated. The investigation was done for specific array configurations and co-operate feed networks were used to excite the elements. The results of this investigation will be used to study the improvement in the bandwidth and resonant frequency of a linear patch array when a mutual coupling compensation technique is used, which will be discussed later in this chapter.

Probe-fed microstrip patch antennas are considered as narrowband antenna elements with bandwidths smaller than 5% for a voltage standing wave ratio (VSWR) of 1.5. Bandwidth enlargement may be obtained by increasing the height of the patch antenna, which on the other hand leads to an increase in the inductive reactance of the probe. The high reactance prevents the matching of the antenna element's input impedance by varying only the remaining physical parameters of the antenna.

Due to the narrowband nature of the elements, mutual coupling may significantly degrade the performance of an array. For linear arrays two types of mutual coupling are defined [62]. E-plane coupling refers to the mutual coupling existing between end coupled patches forming a linear array in the E-plane of the antenna radiation. The coupling between parallel coupled patches, forming a linear array in the H-plane of the antenna radiation, is referred to as H-plane coupling.

To investigate the influence of the E-plane mutual coupling, a uniform four element linear microstrip patch array as shown in Figure 4.6 was used. Without any mutual coupling compensation, the probe-fed microstrip patch antenna elements were designed for a resonant frequency of 1.8 GHz. For a single isolated patch a simulated bandwidth of 2.9% for a VSWR of 1.5 was obtained with 5mm air and 1.6mm dielectric substrate with $\varepsilon_r = 4.4$. L_n, W_n and y_n in Figure 4.6 were 62.8mm, 65mm and 12.9mm for all n, respectively. A simple cooperate feed network with 50Ω ports was designed to excite the four patches with equal amplitude and phase. Only 50Ω microstrip lines were used in the cooperate feed network.

Four identical patches were used to form arrays with different inter-element spacings, d, to study the effect of the mutual coupling on the reflection coefficient. The simulated

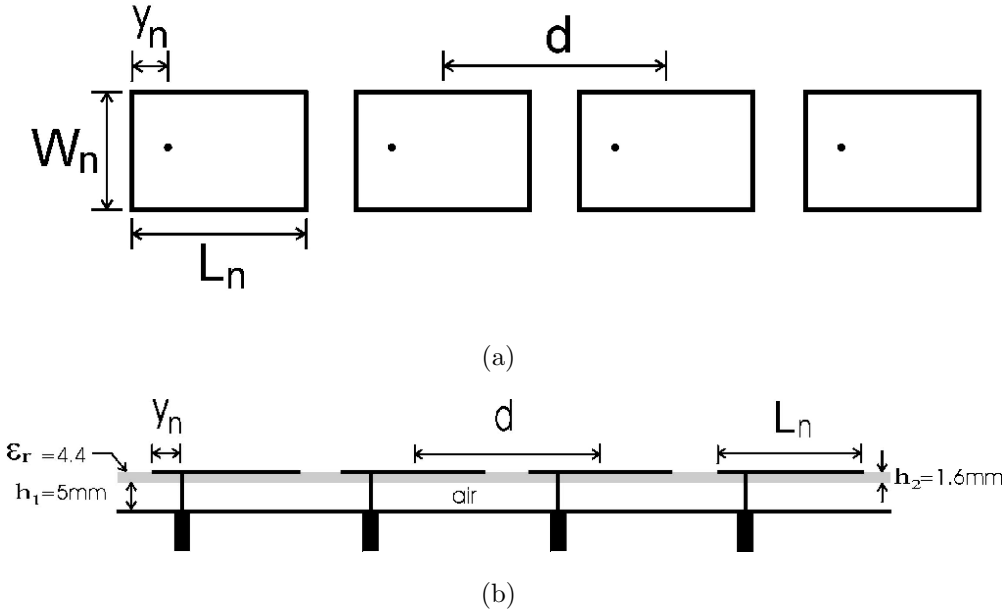

Figure 4.6: Four element linear microstrip patch array: (a) Top view, (b) Side view

reflection coefficients at the input ports of the feeding networks for the arrays with different inter-element spacings are shown in Figure 4.7. It is seen that both the minimum of the reflection coefficient and the resonant frequency are influenced by the mutual coupling. For $d = 0.5\lambda_0$, the resonant frequency shifted by 2.8%, which is close to the bandwidth of an isolated patch. In this case, there is also no measurable bandwidth for a VSWR of 1.5. As the inter-element spacing increases, the coupling between the antenna elements decreases and has less effect on the bandwidth and resonant frequency. Table 4.1 summarises the magnitude of the E-plane coupling and the resulting characteristics for the different inter-element spacings. The tabulated coupling is the coupling between two neighbouring patch antennae.

The effect of H-plane mutual coupling was also studied by rotating the four antenna elements individually by 90°. Figure 4.8 compares the simulated reflection coefficients at the input ports of the feeding networks for arrays with different inter-element spacings. Due to the smaller magnitude of the H-plane coupling, the resonant frequency and bandwidth are less influenced. The bandwidth of the array with an inter-element spacing of $d = 0.5\lambda_0$ decreased by 0.7% to 2.2%. The coupling magnitude and the resulting characteristics are also summarised in Table 4.1.

It is evident that the characteristics of these narrowband arrays are effected by the mutual coupling. A high coupling factor can alter the resonant frequency to such an

extent that the active bandwidth of the array falls outside the desired bandwidth. The bandwidth at a VSWR of 1.5 decreases as the mutual coupling increases. An increasing coupling also causes the minimum reflection coefficient at the resonant frequency to increase. A technique is thus needed to match the desired and active characteristics.

Table 4.1: Characteristics at the input port of a linear microstrip patch arrays

Coupling	**Spacing** (λ_0)	**Coupling factor (dB)**	**Resonant frequency (GHz)**	**Reflection coefficient (dB)**	**Bandwidth** (%)
E-plane	0.5	-10.4	1.748	-13.9	0.00
	0.6	-17.3	1.785	-16.0	2.13
	0.7	-23.4	1.800	-18.9	2.73
	0.8	-28.2	1.804	-23.3	2.94
H-plane	0.5	-16.2	1.800	-16.5	2.20
	0.6	-21.3	1.805	-18.6	2.77
	0.7	-25.1	1.809	-22.7	2.99
	0.8	-27.9	1.809	-30.7	2.99

4.2.2 Effect of mutual coupling on the amplitude pattern of cylindrical patch arrays

Similar to the planar microstrip patch arrays, the coupling between two cylindrical patches is referred to as either E-plane or H-plane coupling depending on the orientation of the patches [66]. For axially polarised patch arrays, the coupling is called H-plane coupling. E-plane coupling exists between two circumferentially polarised patches.

The coupling in an array has an effect on both the array imbedded radiation pattern of the element as well as the element excitations [17, 19, 72]. To illustrate the effect of the coupling on the array imbedded element pattern, an axially polarised patch array was manufactured on a cylinder with $a = 127$ mm and $h = 2$ mm. The array had 10 elements with an inter-element spacing of $d_\phi = 0.5\lambda_0$. The axially polarised patch element had dimensions of $L = 73.1$ mm and $W = 76$ mm. The feed position was 20.85 mm in the z-direction from the bottom of the patch element.

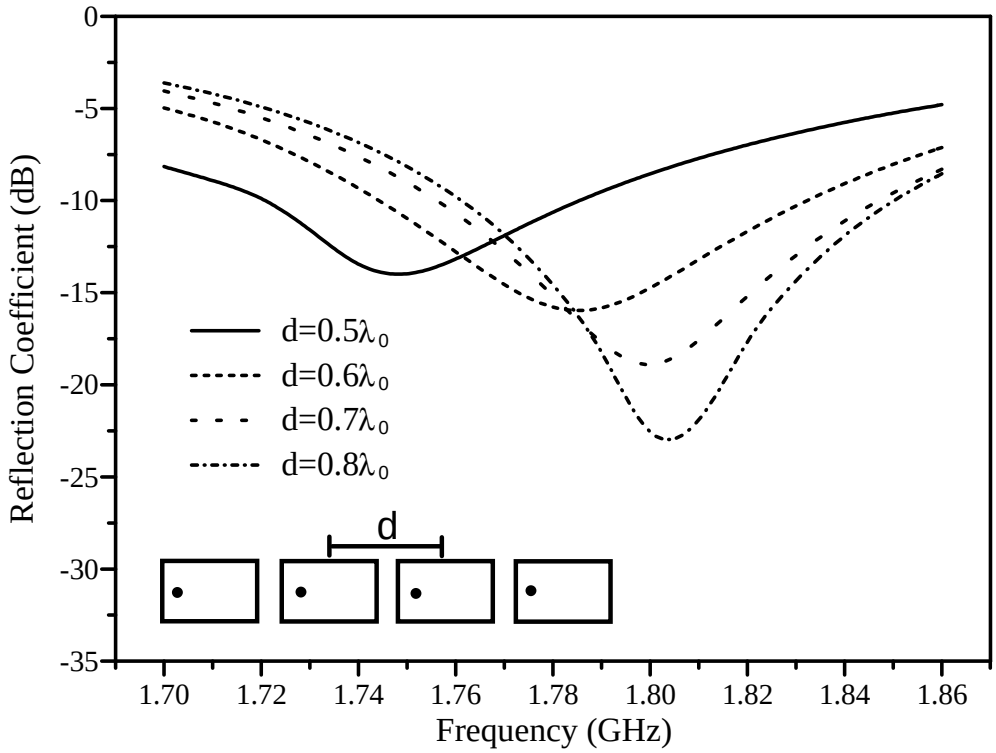

Figure 4.7: Simulated reflection coefficient at the feeding network input port of a horisontal polarised array (E-plane coupling) for different inter-element spacings

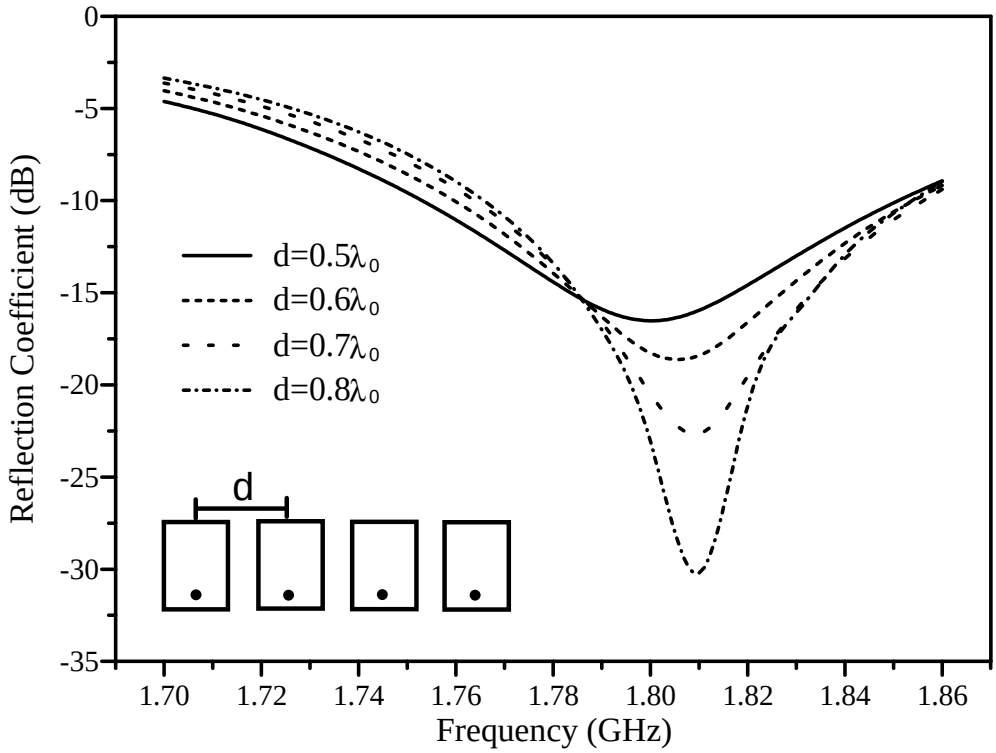

Figure 4.8: Simulated reflection coefficient at the feeding network input port of a vertically polarised array (H-plane coupling) for different inter-element spacings

The array imbedded element pattern was measured by exciting only one element while terminating the remaining elements with 50Ω loads. The same procedure was followed for the simulation of the active pattern. Figure 4.9 compares the measured and simulated active element radiation patterns with the radiation pattern of a single element. The simulated and measured patterns compare well within the region of the main beam and differ slightly in the region of the back lobe.

It is evident that the main beam of the element pattern is broader due to the mutual coupling between the patch elements. To prevent distortion of the resulting array pattern, it is thus important to use the active element pattern when determining the excitation coefficients for a specified array radiation pattern.

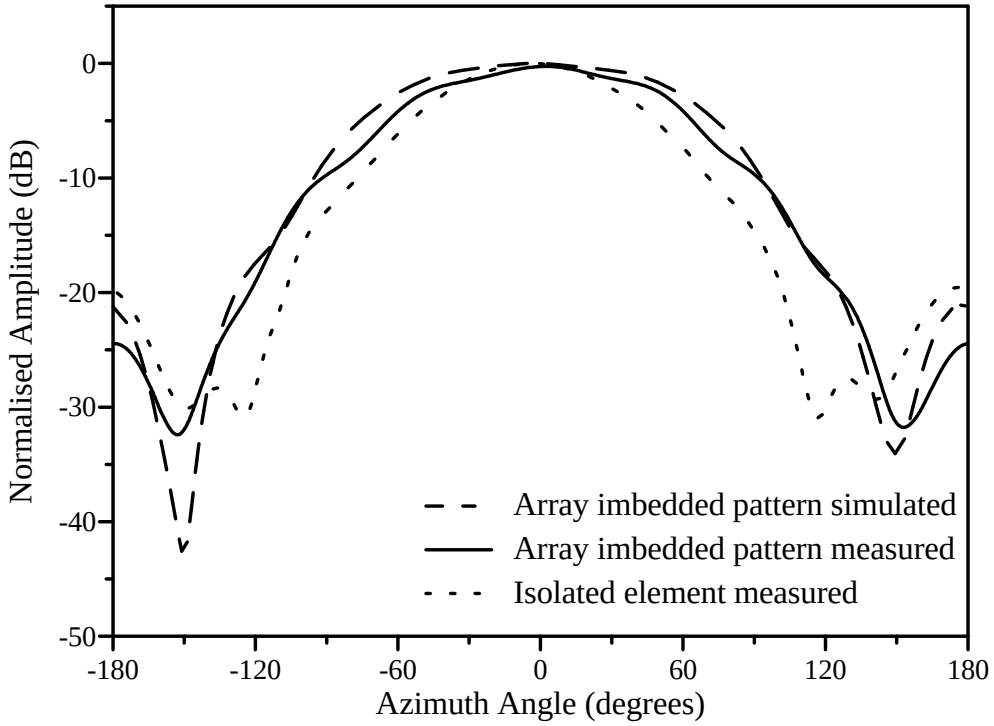

Figure 4.9: Simulated and measured array imbedded radiation patterns of an axially polarised patch in a cylindrical array with $d_\phi = 0.5\lambda_0$

The effect of the mutual coupling on a desired null pattern was also studied. A cylindrical patch array of 10 elements was simulated to study the influence of the mutual coupling on an omnidirectional radiation pattern with a single null. The same substrates as those used in the previous study, were used to form the patch elements. For both the axial and circumferential polarisations, the patch dimensions were $L = 73.1$ mm and $W = 76$ mm. The position of the feed was 15.7 mm in the z-direction from

the centre of the patch for the axial polarisation. For the circumferential polarisation, the feed was at 15.7 mm in the ϕ-direction from the centre of the patch.

The desired element excitations to form a null, with a null depth of 20 dB at 180°, were obtained from the constrained optimisation method. The gain ripple in the omni-region was constrained to 1 dB and no constraint was placed on the -10 dB null width. The element excitations for both polarisations were calculated without considering mutual coupling. Afterwards, the active driving currents were computed using the simulated admittance matrix in Equation 2.79 to study the influence of the mutual coupling on the null pattern. The array imbedded patterns of the axially and circumferentially polarised patches at their respective resonant frequencies of 1.735 GHz and 1.765 GHz, were used.

The simulated results for a circumferentially polarised patch array with an inter-element spacing of $0.5\lambda_0$ are shown in Figure 4.10. The resulting null pattern when there is no mutual coupling is compared with the resulting null pattern due to the active driving currents when mutual coupling is present. It can be seen that the mutual coupling increased the ripple and null width, while decreasing the maximum suppression of 20 dB to 16.7 dB. The position of the null was also changed by 3.25°, which consequently decreased the suppression at 180° by 4.36 dB. For this array configuration, Table 4.2 compares the normalised driving currents when there is no mutual coupling to the normalised active driving currents when mutual coupling is present.

Table 4.2: Influence of the mutual coupling on the driving currents for a circumferentially polarised patch array with $d_\phi = 0.5\lambda_0$ and $N = 10$

Element	**No Coupling**	**With Coupling**
1	$0.84\angle 4.19°$	$0.91\angle -25.07°$
2	$0.65\angle -73.20°$	$0.89\angle -41.09°$
3	$1.00\angle -22.09°$	$0.97\angle -60.70°$
4	$0.77\angle -78.80°$	$0.79\angle -82.15°$
5	$0.16\angle 63.21°$	$0.14\angle -2.31°$
6	$0.98\angle 68.67°$	$0.87\angle 54.78°$
7	$0.81\angle 89.29°$	$1.00\angle 43.57°$
8	$0.77\angle 48.62°$	$0.97\angle 23.16°$
9	$0.78\angle 44.89°$	$0.93\angle 8.94°$
10	$0.76\angle 23.36°$	$0.91\angle -8.32°$

Figure 4.11 shows the simulated patterns for a circumferentially polarised patch array with an inter-element spacing of $0.65\lambda_0$. For this larger inter-element spacing, the mutual coupling was smaller and the most significant observed change was in the ripple in the omni-region of the null pattern. For this case, the ripple increased from 1 dB to 2.86 dB, when the active element excitations are used. The results for the different inter-element spacings are summarised in Table 4.3 and Table 4.4. The coupling coefficients in these tables are the mutual coupling between an element and its nearest neighbour.

For the axially polarised patch array with an inter-element spacing of $0.5\lambda_0$, the results are shown in Figure 4.12. The resulting null pattern when there is no mutual coupling is compared with the resulting null pattern due to the active driving currents when mutual coupling is present. Both the ripple and null width were increased by the mutual coupling, while the maximum suppression was decreased by 1.46 dB. Table 4.5 compares the normalised driving currents when there is no mutual coupling to the normalised active driving currents when mutual coupling is present.

Figure 4.13 shows the resulting patterns for this array with an inter-element spacing of $0.65\lambda_0$. Although the mutual coupling is less for this larger inter-element spacing, the distortion of null pattern is more significant. In this case, the ripple and maximum suppression changed by 2.55 dB and 4.06 dB, respectively. Table 4.6 and Table 4.7 summarises the results for the different inter-element spacings.

The desired radiation pattern could not be obtained for inter-element spacings larger than $0.7\lambda_0$ and $0.65\lambda_0$ for the circumferentially and axially polarised arrays, respectively. This is due to the high ripple in the omnidirectional radiation pattern when large inter-element spacings are utilised.

Greater changes in the null positions and null widths are observed for the circumferentially polarised patch array. The change in the suppression at 180° and the change in the maximum suppression decreases as the spacing increases and the mutual coupling decreases for $d_\phi \leq 0.65\lambda_0$. For the larger inter-element spacing, as seen for $d_\phi = 0.7\lambda_0$, the element excitations tend to be more sensitive to the mutual coupling, although it is less than -20 dB. For the axial polarisation, the change in the suppression at 180° increases although the coupling decreases. For this polarisation, the increasing inter-element spacing thus makes the element excitations more sensitive to the mutual coupling.

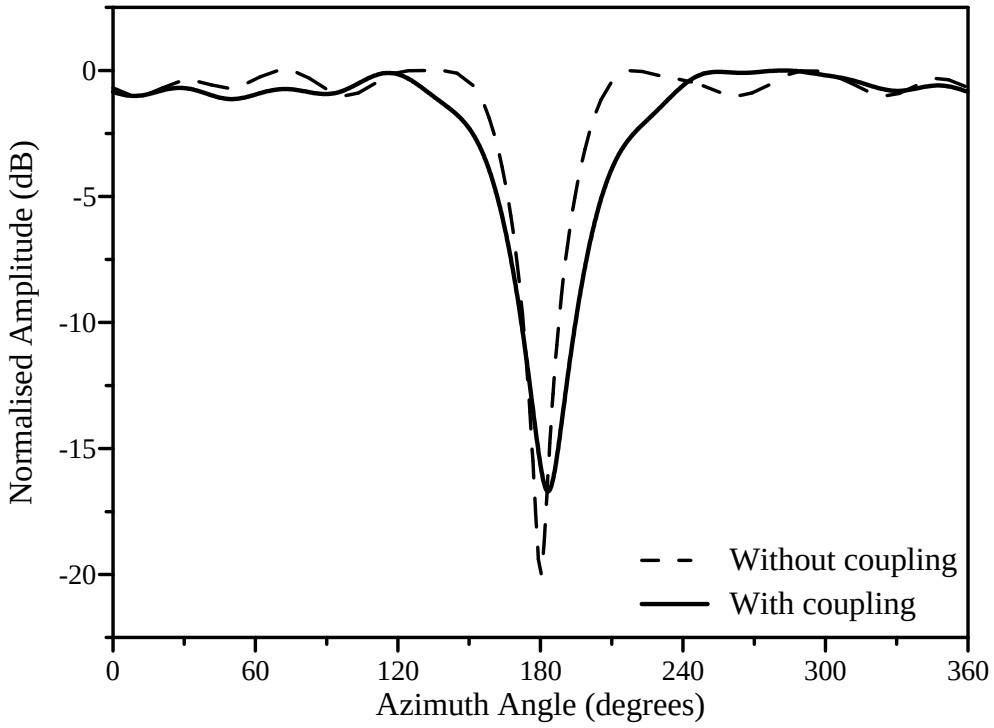

Figure 4.10: Normalised amplitude patterns of a circumferentially polarised patch array with $d_\phi = 0.5\lambda_0$ and $N = 10$

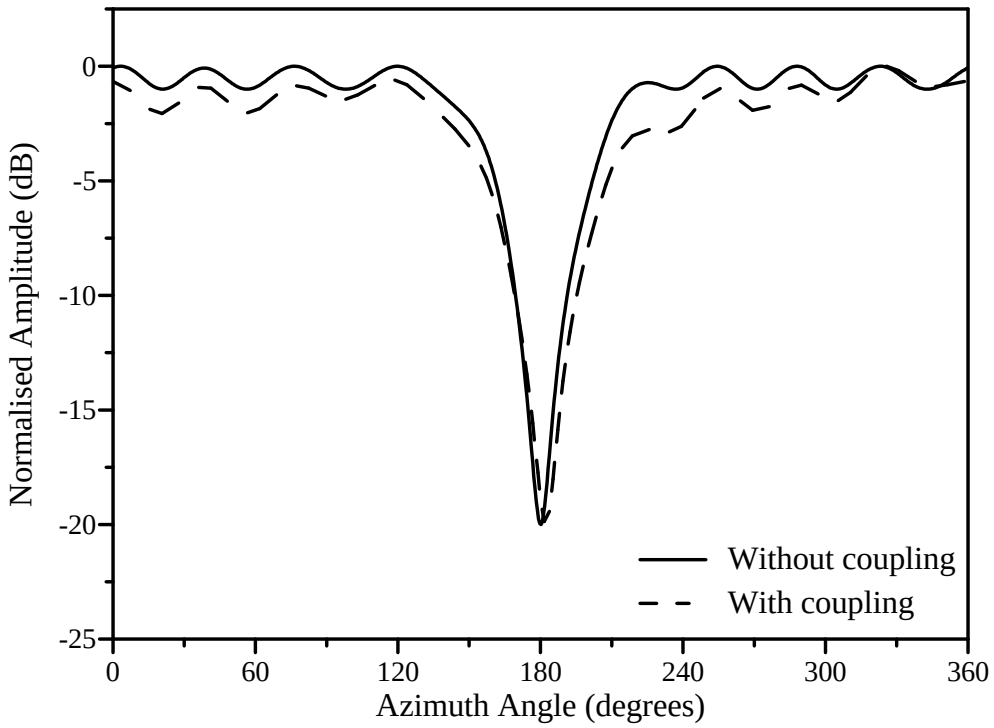

Figure 4.11: Normalised amplitude patterns of a circumferentially polarised patch array with $d_\phi = 0.65\lambda_0$ and $N = 10$

Table 4.3: Influence of the mutual coupling on the desired null pattern for a circumferentially polarised patch array

Spacing (λ_0)	**Coupling (dB)**	**Change in suppression at** 180° **(dB)**	**Change in maximum suppression (dB)**
0.5	-10.7	4.36	3.3
0.55	-13.3	4.23	1.95
0.6	-16.1	1.37	0.05
0.65	-18.8	1.21	-0.01
0.7	-21.1	4.3	3.52

Table 4.4: Influence of the mutual coupling on the desired null pattern for a circumferentially polarised patch array (continued)

Spacing (λ_0)	**Change in ripple (dB)**	**Change in null position (deg)**	**Change in null width (deg)**
0.5	0.14	3.25	7.80
0.55	0.40	4	7.69
0.6	1.51	2.25	6.69
0.65	1.86	2.25	4.34
0.7	4.63	2	-3.45

The inter-element spacing thus plays an important role in the choice of an array configuration. For small inter-element spacings in a circumferentially polarised array, the larger coupling between the elements has a greater influence on the radiation pattern. On the other hand, the use of large inter-element spacings makes the desired element excitations more sensitive to the mutual coupling for both polarisations. The coupling between axially polarised patches is smaller and the radiation pattern is less effected for small inter-element spacing.

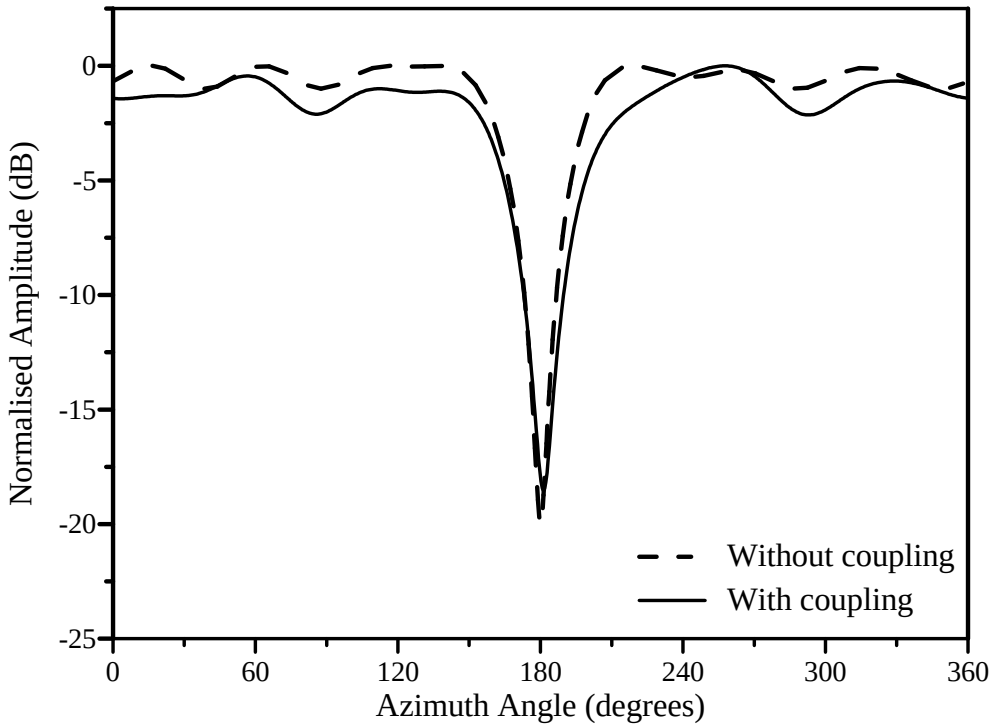

Figure 4.12: Normalised amplitude patterns of an axially polarised patch array with $d_\phi = 0.5\lambda_0$ and $N = 10$

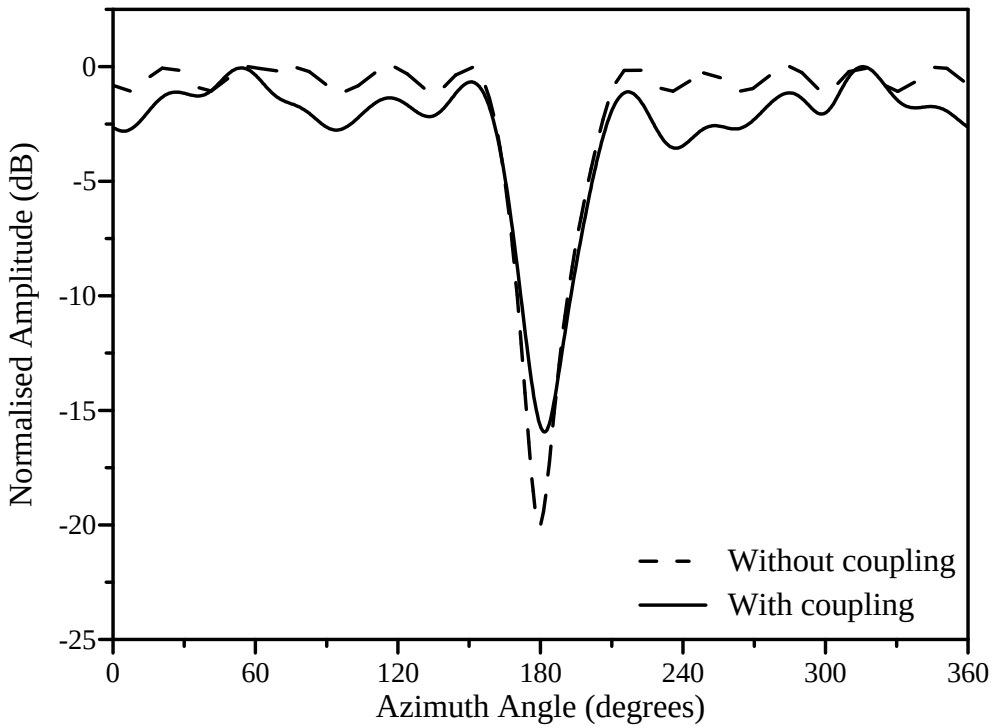

Figure 4.13: Normalised amplitude patterns of an axially polarised patch array with $d_\phi = 0.65\lambda_0$ and $N = 10$

Table 4.5: Influence of the mutual coupling on the driving currents for a axially polarised patch array with $d_\phi = 0.5\lambda_0$ and $N = 10$

Element	**No Coupling**	**With Coupling**
1	$0.79\angle 12.14°$	$0.81\angle -5.27°$
2	$0.70\angle -6.55°$	$0.84\angle -22.51°$
3	$0.95\angle -16.17°$	$0.84\angle -35.48°$
4	$0.75\angle -71.78°$	$0.79\angle -73.28°$
5	$0.18\angle 62.69°$	$0.13\angle 58.73°$
6	$1.00\angle 78.36°$	$1.00\angle 72.14°$
7	$0.73\angle 91.40°$	$0.76\angle 60.52°$
8	$0.81\angle 59.14°$	$0.92\angle 47.32°$
9	$0.76\angle 45.93°$	$0.77\angle 28.57°$
10	$0.77\angle 28.71°$	$0.88\angle 12.09°$

Table 4.6: Influence of the mutual coupling on the desired null pattern for a axially polarised patch array

Spacing (λ_0)	**Coupling (dB)**	**Change in suppression at** $180°$ **(dB)**	**Change in maximum suppression (dB)**
0.5	-17.6	2.08	1.46
0.55	-20.1	2.67	2.08
0.6	-22.5	2.67	1.83
0.65	-24.3	4.31	4.06

From Table 4.3 and Table 4.4, it is observed that for small inter-element spacing in the circumferential polarisation, the mutual coupling must be compensated for in order to obtain the desired radiation pattern. The compensation is also needed to correct the degree of suppression in a specified direction for all inter-element spacings and both polarisations.

Table 4.7: Influence of the mutual coupling on the desired null pattern for a axially polarised patch array (continued)

Spacing (λ_0)	**Change in ripple (dB)**	**Change in null position (deg)**	**Change in null width (deg)**
0.5	1.14	1.25	3.28
0.55	1.47	1	1.22
0.6	1.47	1.75	0.08
0.65	2.55	1.75	-0.23

4.3 Mutual coupling compensation

4.3.1 Mutual coupling compensation for linear patch arrays

Paragraph 2.4.3 discusses a technique in which the geometries of the elements are varied to provide matched and equal driving impedances for all the antenna elements, given a required set of element excitations. From Equation 2.80, the driving impedances may be written as:

$$Z_m^a = Z_{mm}^s(L_m, y_m) + \sum_{\substack{n=1 \\ n \neq m}}^{N} Z_{mn}(L_n, L_m, y_n, y_m)\frac{I_n}{I_m}, \tag{4.1}$$

where L_m and y_m are the length and feed position of the m-th patch antenna element, respectively. The length and feed position of the n-th neighbouring antenna element are represented by L_n and y_n, respectively. Both the self impedance and mutual impedances are expressed as functions of the length and feed positions. Although the above impedances also vary with the widths and heights of the patch antennae, these dimensions are kept constant to reduce the dimensionality of variable space.

A commercial electromagnetic software package [100] which utilises the method of moments, is used to obtain Z_{mm}^s and Z_{mn} for different lengths and feed positions. For the linear array configuration in Figure 4.6, Z_{mn} has a low sensitivity to small variations in the feed positions and the dimensionality of Z_{mn} can thus be even further reduced. The self and mutual impedances are computed for linearly spaced values

of the lengths and feed positions and are placed in two lookup tables. One lookup table is populated with the self impedance values with respect to the lengths and feed-positions of a single antenna element. Another lookup table is populated with the mutual impedance values with respect to the lengths of two neighbouring antenna elements. A least squares optimisation algorithm is used to determine the lengths and feed positions at which the driving impedances of all the patches are equal to 50Ω. N lengths and N feed positions are used as the variables and the algorithm interpolates between the computed impedance values using a bicubic spline algorithm. For each antenna element an error in the real part of impedance as well as an error in the imaginary part of the impedance is calculated. The cost function is then determined as the sum of the $2N$ squared errors. The least squares optimisation algorithm determines the N lengths and N feed positions which minimise this cost function.

An example in which the mutual compensation technique is applied to a linear patch array, is incorporated into the test case in paragraph 4.4.1.

4.3.2 Mutual coupling compensation for cylindrical arrays

The mutual coupling compensation technique described in paragraph 4.3.1 for the linear patch array will also be used for the cylindrical patch arrays. For the cylindrical arrays, L_m and y_m in equation 4.1 are respectively the length and feed position of the m-th patch element along the direction of its polarisation.

The look-up table, which is used to search for the necessary lengths and feed positions to adjust the active driving impedances to 50Ω, is populated using simulation results from the FDTD software.

As an example, the lengths and feed positions were found to correct the null pattern in Figure 4.10 for the axially polarised array with $d_\phi = 0.5\lambda_0$ and $N = 10$. The starting values used by the optimisation algorithm for all n elements, were L_n=73.1 mm and y_n=20.85 mm. A graphical representation of the variable space for the self-impedance is shown on a Smith chart in Figure 4.14. The variable space is shown for 71.6mm $\leq L_n \leq$ 74.6mm and 4.85mm $\leq y_n \leq$ 26.85mm. During the search for the appropriate lengths and feed positions, it was assumed that small changes in the lengths and feed positions, do not have a significant effect on the mutual coupling and was considered to stay constant. The resulting lengths and feed positions needed to

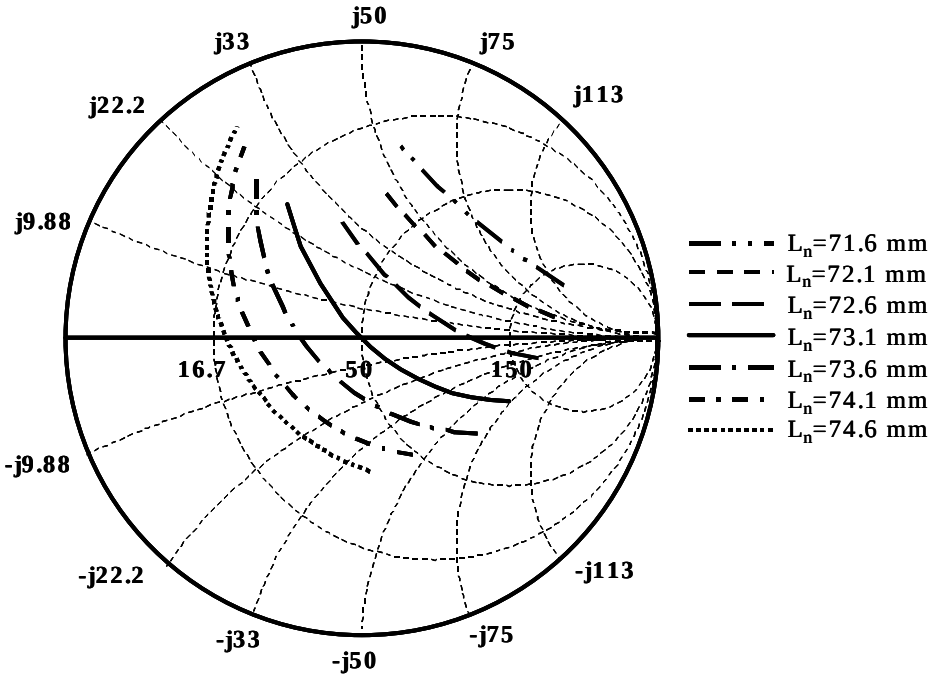

Figure 4.14: Self-impedance of the axially polarised patch antenna element for different L_n and $4.85mm \leq y_n \leq 26.85mm$

correct the element driving impedances for the desired set of excitations, are listed in Table 4.8.

The above procedure was also repeated for the sets of element excitations obtained for the circumferentially polarised patch arrays and the remaining axially polarised arrays. A self-impedance look-up table was set up for the patch antenna element of each array configuration.

The optimisation algorithm was then used to search for the lengths and feed positions to correct the active driving impedances and consequently the desired null pattern for each array.

For the circumferential polarisation and inter-element spacing of $0.5\lambda_0$, $0.55\lambda_0$ and $0.6\lambda_0$, the active driving impedance of the element in the same direction as the null could not be set to 50Ω. The simulated active driving impedances due to the desired set of excitations for the circumferentially polarised array with $d_\phi = 0.55\lambda_0$, is listed in Table 4.9. The active driving impedances for the desired set of excitations of the axially polarised array with $d_\phi = 0.55\lambda_0$, are also shown for comparison.

Table 4.8: Lengths and feed positions needed to correct the active driving impedances of an axially polarised patch array with $d_\phi = 0.5\lambda_0$

Element	**Length (mm)**	**Feed-position (mm)**
1	73.3	23.45
2	73.4	25.00
3	73.5	23.05
4	72.8	21.30
5	73.6	25.10
6	73.0	22.60
7	73.6	26.10
8	73.1	22.85
9	73.4	24.00
10	73.1	22.85

Table 4.9: Comparison of the active driving impedances for the desired null patterns of the circumferentially and axially polarised patch arrays with $d_\phi = 0.55\lambda_0$

Element	**Circumferential polarisation**	**Axial polarisation**
1	39.4 + j11.3	46.2 + j17.2
2	13.3 + j20.6	46.5 + j13.4
3	50.6 + j15.8	51.2 + j9.90
4	31.7 - j6.30	43.3 + j4.70
5	71.6 + j78.5	49.4 + j24.0
6	35.9 - j1.40	45.7 + j9.10
7	40.1 + j38.3	51.4 + j17.4
8	30.8 - j1.50	42.2 + j11.2
9	34.6 + j26.5	42.2 + j15.4
10	28.2 + j11.4	43.7 + j9.80

For the axially polarised array, with mutual coupling of -20.1 dB between nearest neighbouring elements, the desired input impedance could be found for all 10 elements within the available range of self-impedances. On the other hand, the higher mutual coupling (-13.3 dB) of the circumferentially polarised array contributed to a higher reactance of the driving impedance of the 5th element, which is in the same direction as the null. Consequently, the desired input impedance for this element could not be found within the range of input impedances for the specified patch antenna element configuration. The active driving impedance of this element could therefore not be modified to be exactly 50Ω and the effect of the mutual coupling could not be completely compensated for.

The mutual coupling thus places a constraint on the set of element excitations for which the mutual coupling can be compensated for, using the described compensation technique. This set of element excitations is determined for the desired null pattern and therefore the specifiable characteristics of the null pattern is limited.

A study was therefore conducted to determine the possible null depths of a single null for which the mutual coupling can be compensated for using the specified compensation technique. The element excitation sets for null patterns with various null depths were determined for the circumferentially and axially polarised patch arrays studied in the previous sections. For each specified null depth, it was determined if the desired self-impedances could be found within the available range of self-impedances to compensate for the mutual coupling.

The resulting possible null depths are summarised in Table 4.10 for both polarisations. The study was only conducted for suppression levels up to 40 dB. For all the axially polarised patch arrays with null patterns having null depths of up to 40 dB, the mutual coupling could be compensated for using the described compensation technique. On the other hand, the possible null depths for the null patterns of the circumferentially polarised patch arrays were limited to the values listed in Table 4.10. For null depths larger then the listed values, the mutual coupling could not be compensated for.

For high suppression levels and small inter-element spacing, the mutual coupling in the axially polarised array could be compensated for by using the described mutual coupling compensation technique. On the other hand, the realisable suppression levels were smaller for the circumferential polarisation when the mutual coupling was compensated for using the compensation technique.

Table 4.10: Comparison of possible null depths for circumferentially and axially polarised patch arrays with N=10

Spacing (d_ϕ) (λ_0)	**Circumferential polarisation**	**Axial polarisation**
0.5	-10 dB	-40 dB
0.55	-15 dB	-40 dB
0.6	-15 dB	-40 dB
0.65	-25 dB	-40 dB

4.4 Test cases

4.4.1 Linear patch array test case

A four element microstrip patch array with E-plane coupling was chosen to confirm experimentally the proposed coupling compensation technique. Initially, L_n, W_n and y_n in Figure 4.6 were 62.8mm, 65mm and 12.9mm for all n, respectively. The inter-element spacing was $d = 0.65\lambda_0$ and the self and mutual impedances of the array were computed for different lengths and feed positions using L_n=62.8mm and y_n=12.9mm as the centre variable values of the look-up tables.

A graphical presentation of the variable space for the self impedance is shown on a Smith chart in Figure 4.15. Each impedance curve is formed by keeping L_n constant and varying y_n between 8.9mm and 15.9mm. The optimisation algorithm is constrained to search only within this available self impedance space.

Careful attention should be paid to the element radiation pattern when setting up the look-up tables and variable space. Significant changes in the radiation pattern of the element should be avoided to prevent distortion of the total array radiation pattern. When the probe feed is put too close to the edge of the patch, the probe radiation may alter the element radiation pattern. If the length of the patch is varied too much, the beamwidth of the main beam in the element radiation pattern will be modified. The extent of these effects will vary between patch antenna element configurations.

The optimisation algorithm uses L_n=62.8mm and y_n=12.9mm as the starting values for all n elements to search for the lengths and feed positions where the driving impedances of all the patches are 50Ω. The resulting lengths are: L_1=L_4=63.2mm, $y1$=$y4$=11mm,

L_2=L_3=63.7mm and $y2$=$y3$=8.9mm. Using these parameters, the corresponding self impendances are: Z^s_{11}=Z^s_{44}=48.72-j7.87 and Z^s_{22}=Z^s_{33}=45.08-j14.11.

To verify the simulation results with measurements, both arrays were built and simple cooperate feed networks were designed to excite all patch antennas with equal amplitude and phase. The feed networks consisted of only 50Ω microstrip lines. The S-parameters of both arrays were measured and used in the simulation software to compute the reflection coefficients at the input ports of the feed networks of the arrays. The narrowband arrays built for the measurements were influenced by uncertainties in certain parameters such as the height of the air region, the permittivity of the substrate at high frequencies and some reactance added by the coaxial probes. To compensate for these uncertainties, a single isolated patch was used as a test case, and had to be slightly altered to get good correspondence between simulated and measured results for the single patch. The width had to be increased by 4mm and a width of W_n=69mm was subsequently used for all the patches of both experimental arrays.

Figure 4.16 compares the simulated and measured results for the original uncompensated and compensated arrays. The top views of the uncompensated and compensated arrays are shown in Figures 4.17 and 4.18, respectively. The side view of the compensated array is shown in Figure 4.19. The results show good similarity between the simulated and measured reflection coefficients and the improvement due to compensation technique is clearly visible. The resonant frequency of the compensated array is within 0.1% of 1.8GHz and the measured bandwidth for a VSWR of 1.5 increased from 2.3% to 3.9%, which is an improvement of 69.6% in bandwidth. The measured reflection coefficient at 1.8GHz improved from -17.3dB to -32dB. The technique is thus able to correct the individual driving impedances of the antenna elements and thereby improve the reflection coefficient at the input port of the array feed network.

4.4.2 Cylindrical patch array test case

An axially polarised patch array with N=10 and $d_\phi = 0.5\lambda_0$ was chosen to experimentally confirm the effect of the mutual coupling on the desired null pattern. A copper cylinder with a=127mm and h=2mm was used to mount the array of patches onto.

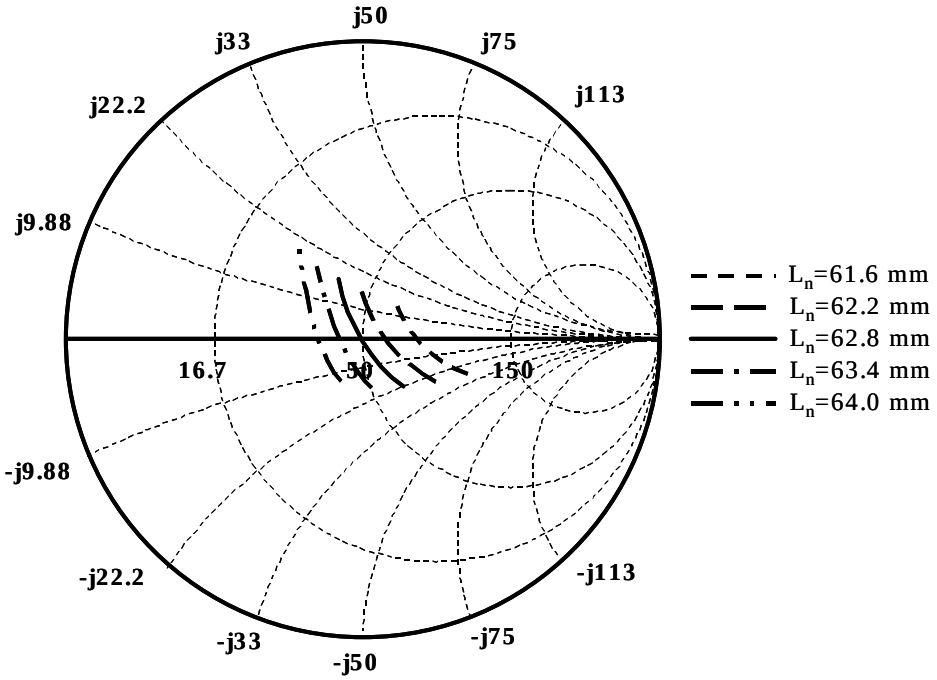

Figure 4.15: Input impedance of the patch antenna element for different L_n and 8.9mm $\leq y_n \leq$ 15.9mm. Figure 4.6 shows the configuration of the array where W_n is 65mm

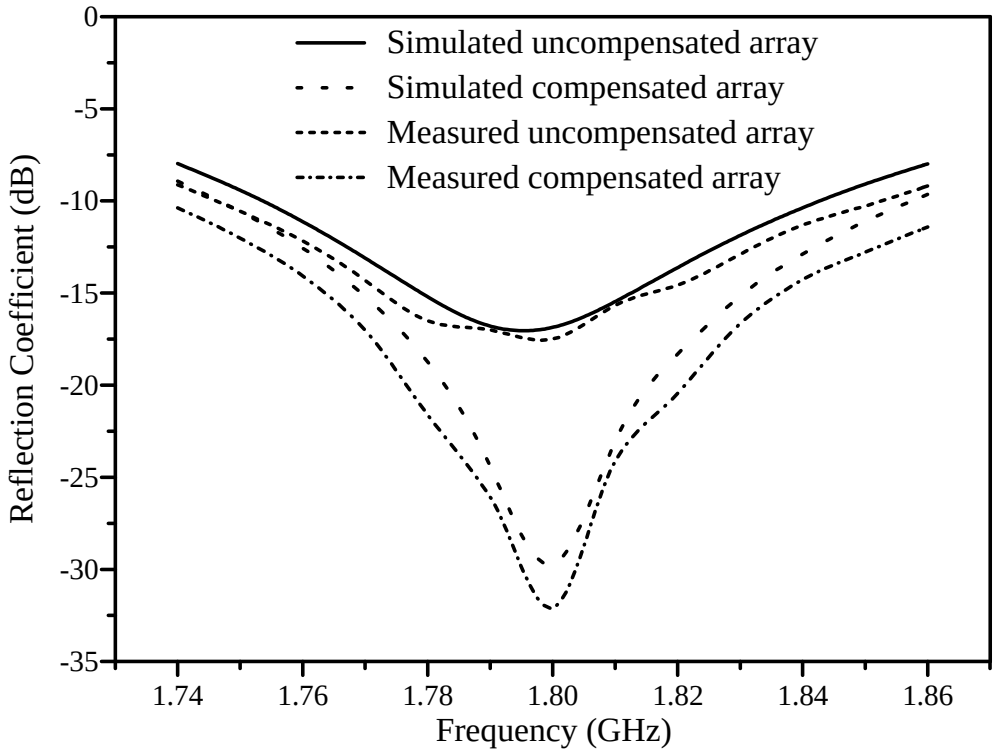

Figure 4.16: Simulated and measured reflection coefficients of the feeding network input ports for the original uncompensated and compensated arrays with $d = 0.65\lambda_0$

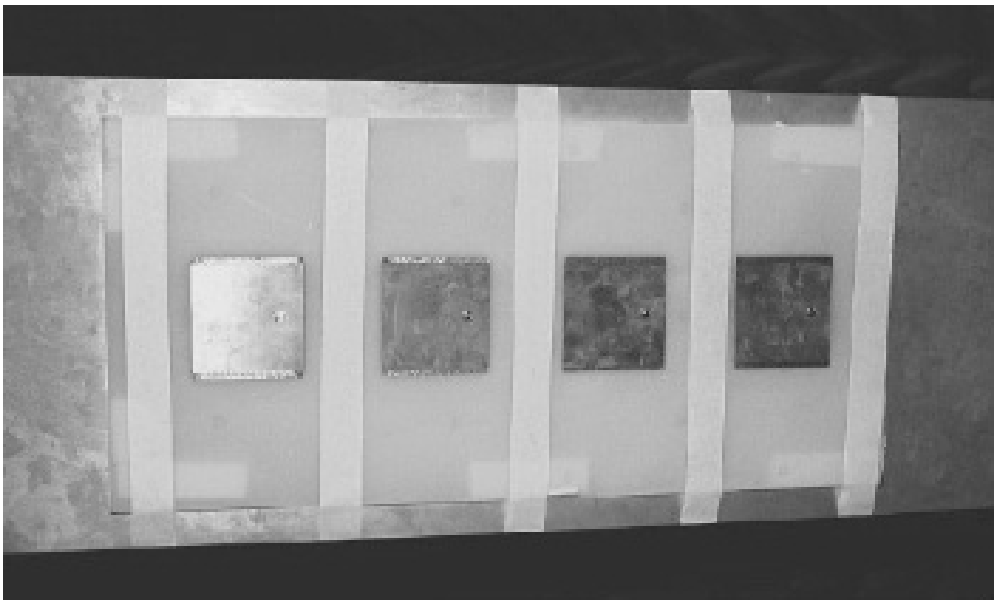

Figure 4.17: Top view of the original uncompensated linear microstrip patch antenna array

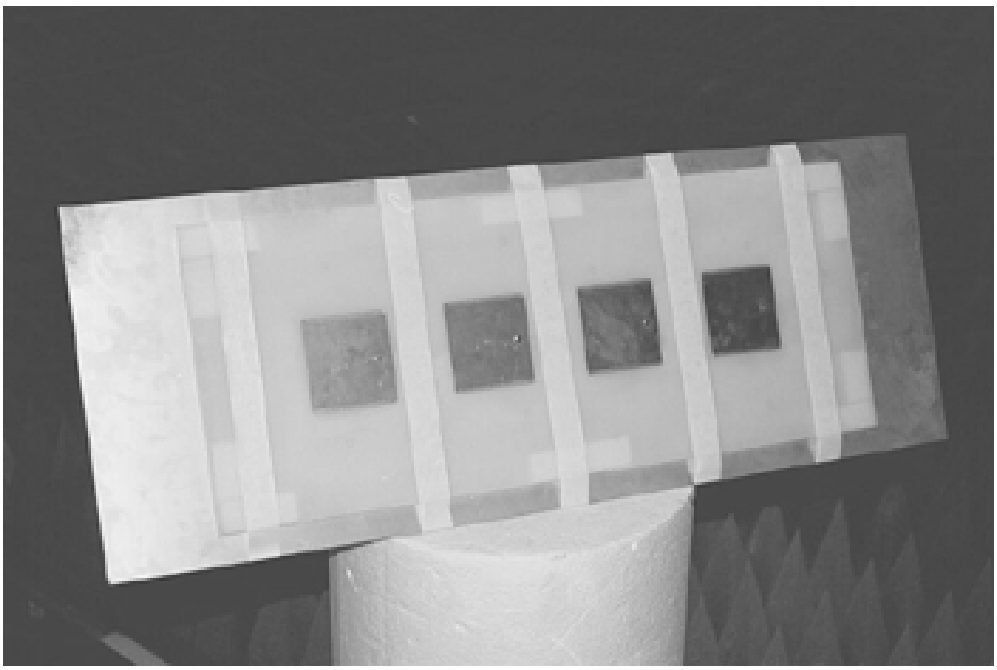

Figure 4.18: Top view of the compensated linear microstrip patch antenna array

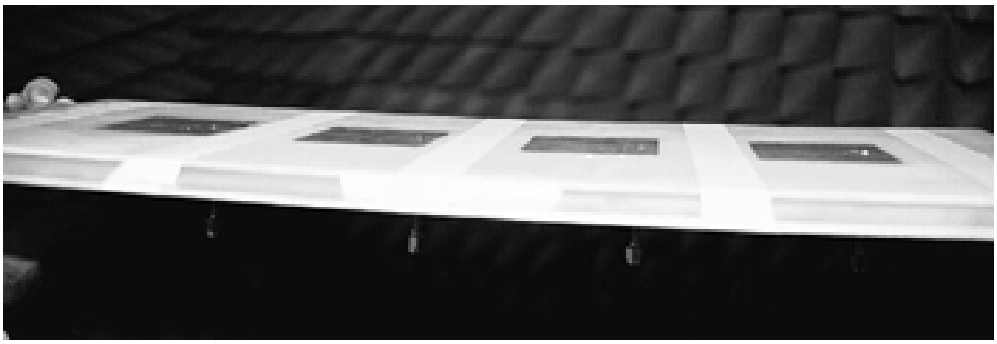

Figure 4.19: Side view of the compensated linear microstrip patch antenna array

The cylindrical patch antenna element was designed for a measured resonant frequency of 1.8 GHz, using the measured reflection coefficient data in paragraph 4.1 for the refinement of the design. The resulting dimensions were L=73.6 mm and W=76 mm, with the feed position at 16.6 mm from the centre of the patch in the z-direction. The resonant frequency and reflection coefficient, obtained from the simulation of the patch element with the FDTD software, were 1.727 GHz and -32.8 dB, respectively.

The cylindrical array was manufactured by etching the patch element array onto the thin layer of FR4 and wrapping it around the cylinder. The 5mm air gap was established by using 5mm polystyrene strips which were also wrapped around the cylinder. To excite the patch elements individually, each element was provided with a probe feed and a coaxial connector.

When the radiation pattern measurements were performed for the first set-up, significant differences were found between the active element patterns. This was due to the slight oval shape of the cylinder. Two PVC discs were then inserted at the bottom and top of the cylinder to ensure that the cylinder maintains a circular shape. The bottom PVC disc also provided the capability for mounting the cylinder on a post and for rotating it around its centre. Figures 4.20 and 4.21 provide the side and top view of the manufactured array, respectively.

The radiation pattern measurement was done in a compact measurement range. The active element pattern was measured for each element by exciting the particular element and terminating the feeds of the rest of the elements with 50Ω loads. The S-matrix of the array was measured using a network analyser in a measurement room partially filled with absorbing material. All measurements were done at 1.8 GHz.

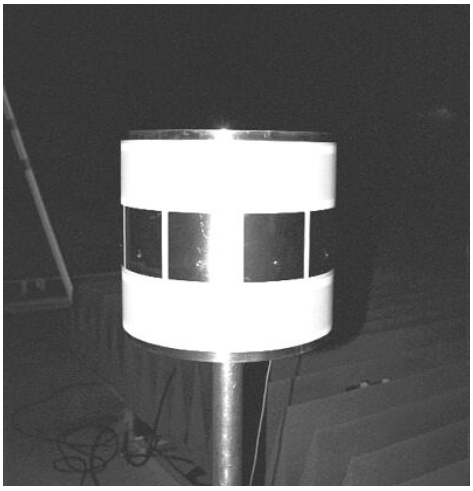

Figure 4.20: Side view of axially polarised microstrip patch array

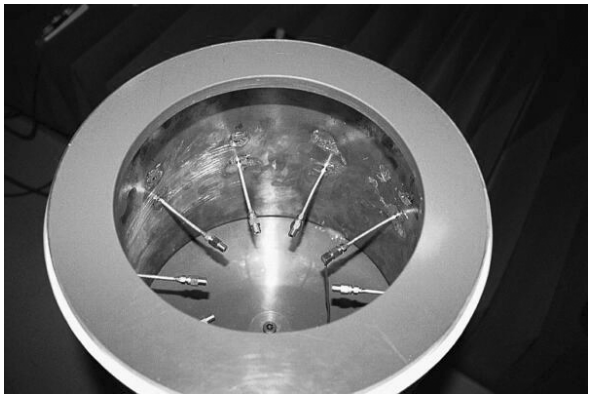

Figure 4.21: Top view of axially polarised microstrip patch array

Without including mutual coupling, the set of excitations for forming a -20 dB null at 180° in an otherwise omni-directional pattern was determined using the simulated radiation patterns of the isolated elements. The ripple was also constrained to 1 dB using the constrained optimisation method. The resulting unconstrained null width was found to be 20.2°. The mutual coupling was then included in the computation of the array pattern by using the simulated array imbedded element patterns and the active driving currents computed for this set of excitations using Equation 2.79. This analysis was repeated for the measured results by using the measured array imbedded element patterns and by computing active driving currents from the measured admittance matrix and the same set of excitations.

Figure 4.22 shows the resulting array patterns for the simulated and measured array

characteristics. The most significant changes in the array radiation pattern when the mutual coupling is included in the analyses, are the decrease in the null depth and the increase in the null width. For the simulated characteristics, the null depth decreased by 5.2 dB, while the null width increased by 3.7°. The null depth decreased by 3.4 dB and the null width increased by 2.9° for the measured array characteristics. The differences between the measured and simulated results are partially caused by the manufacturing tolerances. The input impedances of the antenna elements are sensitive to small variations in the height of the air layer underneath the patch. Any skewness in the probe feed of the patch antenna will also cause the input impedance and the array imbedded element pattern to differ from the simulated results. The differences between the measured and simulated results discussed in paragraph 4.1, also contribute the discrepancies between the simulated and measured results.

For this axially polarised cylindrical array, the length and feed positions of the antenna elements to compensate for the mutual coupling, were found. The look-up table of self-impedances was populated using simulation results. The mutual impedances was assumed to vary little for small changes in the patch lengths and feed positions and was kept constant in the optimisation algorithm. The resulting lengths and feed positions are listed in Table 4.11.

To study the resulting array pattern after the mutual coupling compensation, the cylindrical array was simulated with the modified patch elements. The simulations were done over the bandwidth (for VSWR ≤ 2) of the isolated patch element at 1.696, 1.727 and 1.760 GHz. Figure 4.23 compares the the resulting null pattern before and after the modification of the dimensions of the antenna elements. The resulting ripple was 1.31 dB, while the null depth and null width were -19.5 dB and 20.6°, respectively. To be practical, the lengths and feed positions of the patch elements were only incremented or decremented in steps of 0.1mm. The driving impedances of the patch elements were thus not adjusted to be exactly 50Ω. Small changes in the mutual coupling between the modified antenna elements also contributed to the higher than expected ripple. The null width and null depth compared well to the null width (20.2°) and null depth (-20 dB) when mutual coupling was not included in the analysis.

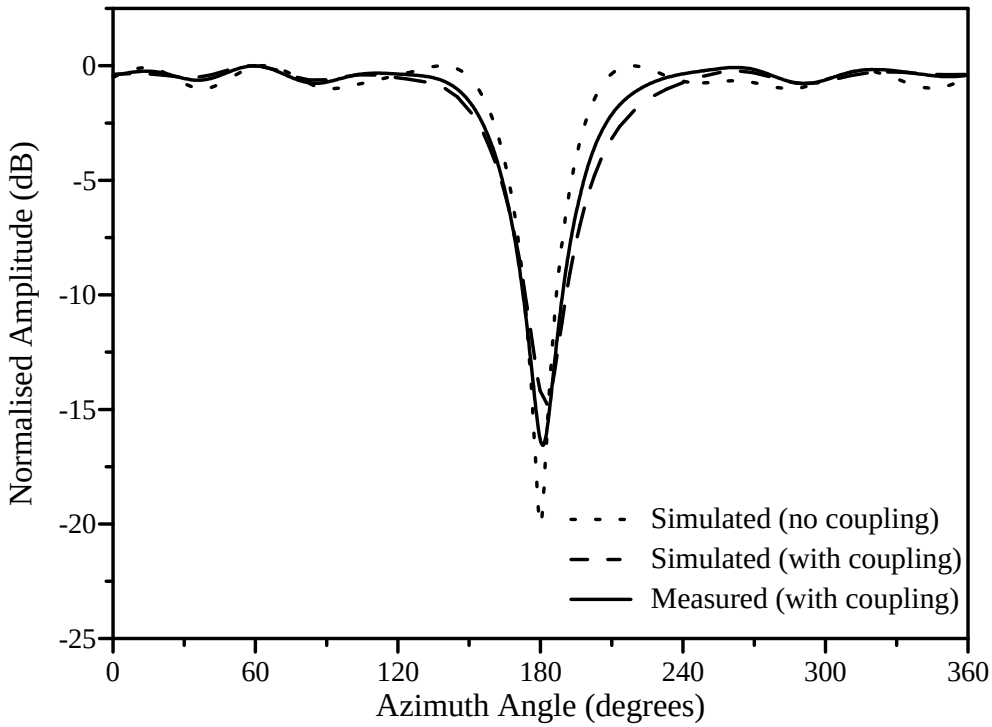

Figure 4.22: Comparison of the resulting null patterns for the simulated and measured array imbedded element patterns and array impedance matrices

Table 4.11: Lengths and feed positions needed to correct the active driving impedances of the axially polarised patch array

Element	**Length (mm)**	**Feed-position from centre (mm)**
1	73.2	17.2
2	73.2	17.2
3	73.4	18.6
4	73.6	16.6
5	72.6	15.0
6	74.0	19.4
7	73.2	16.4
8	73.8	18.9
9	73.0	17.0
10	73.6	18.0

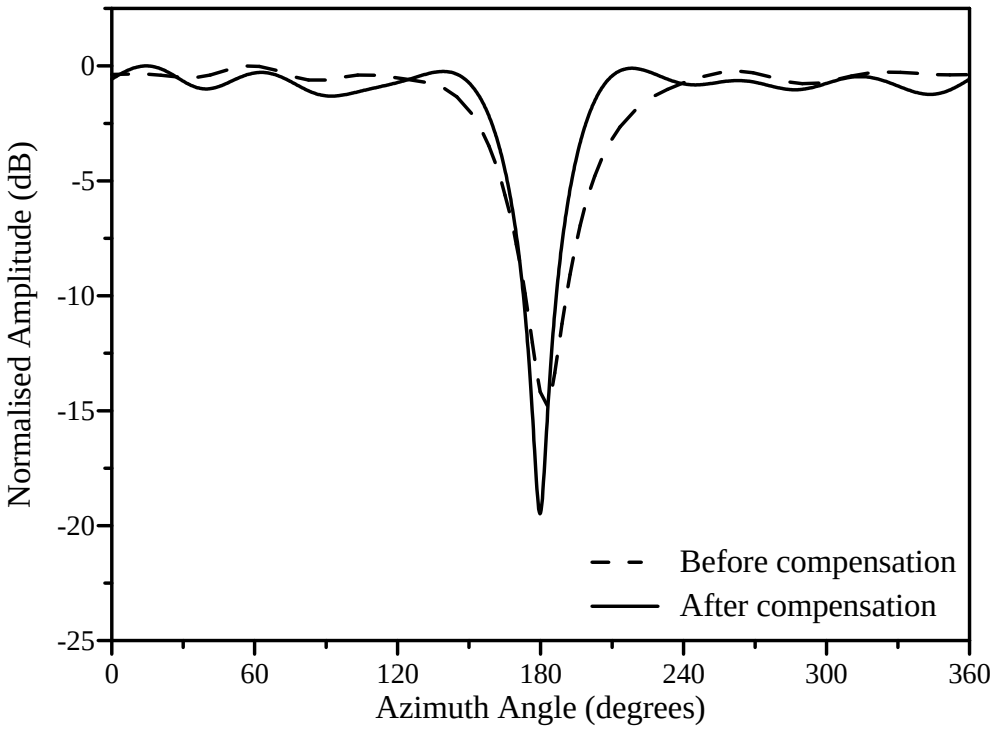

Figure 4.23: Comparison of the resulting null patterns, before and after mutual coupling compensation at 1.727 GHz

Figures 4.24 and 4.25 compare the null patterns before and after compensation at 1.696 and 1.76 GHz, respectively. Table 4.12 compares the characteristics of the null patterns for 1.696, 1.727 and 1.76 GHz before and after the compensation for the mutual coupling. After the coupling compensation technique was applied, the ripple increased by 0.48 and 0.4 dB at 1.696 and 1.76 GHz, respectively. In comparison, the ripple decreased by 0.19 dB and increased by 0.68 dB before the compensation at 1.696 and 1.76 GHz, respectively.

For this axially polarised patch array, the compensation thus limited the increase of the ripple at the higher frequency, but lead to more ripple change at the lower frequency. The ripple at 1.696 and 1.76 GHz, however, only differed by 0.08 dB. The null width and null depth had values close to the those of the desired pattern and changed little over the bandwidth. The null positions were also improved by the compensation technique.

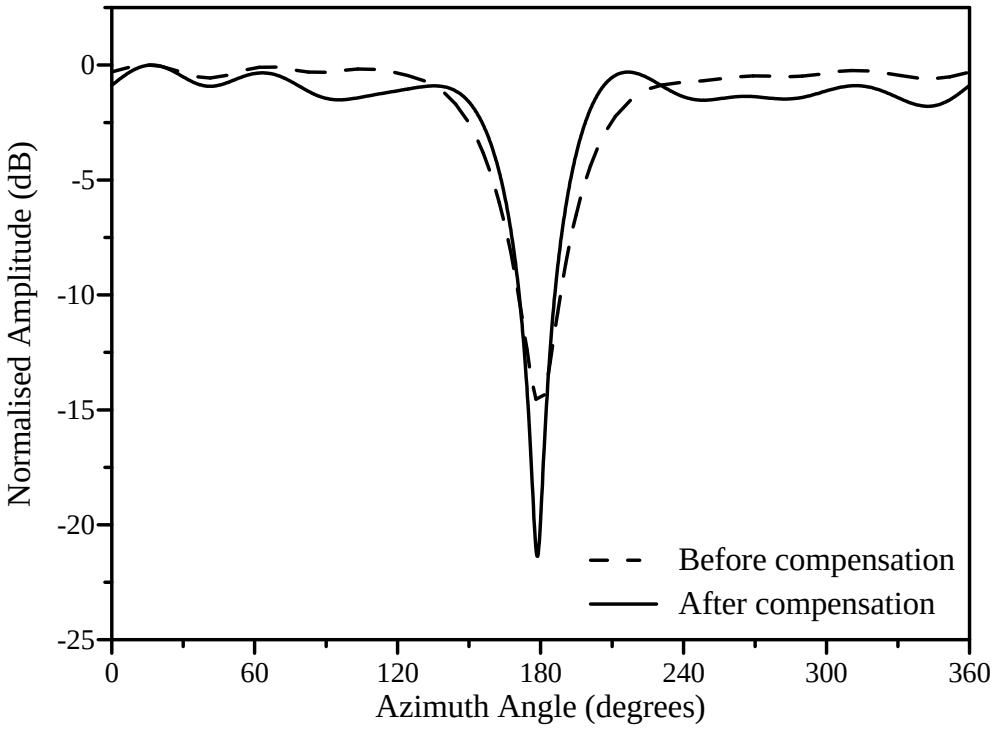

Figure 4.24: Comparison of the resulting null patterns, before and after mutual coupling compensation at 1.696 GHz

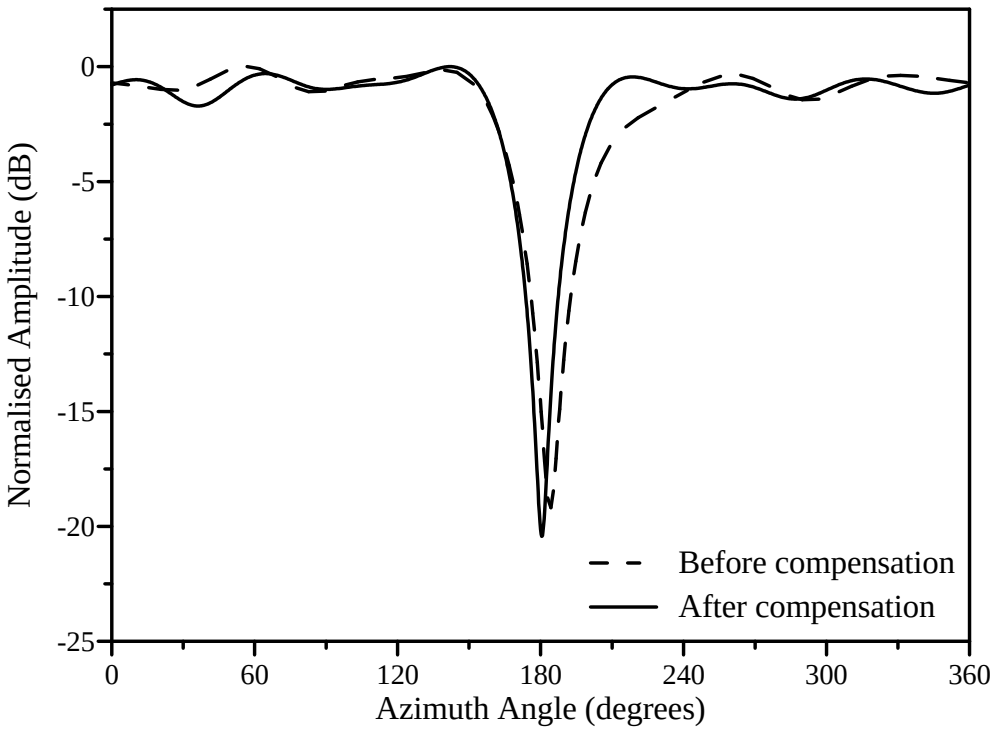

Figure 4.25: Comparison of the resulting null patterns, before and after mutual coupling compensation at 1.760 GHz

Table 4.12: Comparison of null pattern characteristics before and after compensation for the mutual coupling

Frequency (GHz)	**Before compensation**			**After compensation**		
	Ripple (dB)	**Null depth (dB)**	**Null width (°)**	**Ripple (dB)**	**Null depth (dB)**	**Null width (°)**
1.696	0.59	14.8	28.7	1.79	21.4	22.1
1.727	0.78	14.8	28.2	1.31	19.5	20.6
1.760	1.46	19.2	25.3	1.71	20.4	20.2

4.5 Summary

If the resulting element excitations obtained from the null synthesis techniques in the previous chapter, are applied to the cylindrical patch array, the resulting pattern will differ from the desired pattern. This is mainly due to the distortion of the excitations by the mutual coupling between the elements in an array [72, 73].

Before the effect of the mutual coupling on a cylindrical microstrip patch array was investigated, the cylindrical microstrip patch element was designed. A commercial electromagnetic software package applying the Finite Difference Time Domain (FDTD) method [101], was used to obtain simulated results. The approximations used in the simulation of a cylindrical patch antenna were discussed and the effects of these approximations were studied by comparing both simulated and measured results. The investigation was done for axially and circumferentially polarised patch antenna elements. The resulting reflection coefficient characteristics differed slightly from the desired characteristics. The measured shift in the resonant frequency and change in the input impedance could be applied to refine the design of the patch element. For both polarisations, the simulated and measured element radiation patterns compared well within the area of the main beam and differed slightly for the rest of the radiation pattern.

Firstly, the extent to which the mutual coupling affected the bandwidth of a narrowband linear microstrip arrays, was studied. This investigation was conducted in order

to study the improvement in the bandwidth due to the use of a mutual coupling compensation technique. The study was conducted for a four element linear microstrip patch array with a cooperate feed network and the results were compared for different inter-element spacing and polarisations. It was seen that both the minimum of the reflection coefficient at the input port of the feeding network and the resonant frequency are influenced by the mutual coupling. For a horizontally polarised array with E-plane coupling and an inter-element spacing of $0.5\lambda_0$, the resonant frequency was shifted by 2.8%, which is close to the bandwidth of an isolated element. As expected, the effect of the mutual coupling on the bandwidth and resonant frequency was less for larger inter-element spacing. The resonant frequency and bandwidth was less affected for a vertically polarised array with H-plane coupling due to the smaller magnitude of this coupling. The reflection coefficient, however, was -16.5 dB for the smallest inter-element spacing.

It was evident that the characteristics of narrowband arrays were affected by the mutual coupling. A high coupling factor could alter the resonant frequency to such an extent that the active bandwidth falls outside the desired bandwidth of the array. To match the desired and active characteristics of the linear patch arrays, a mutual coupling compensation technique was needed.

During null synthesis, erroneous excitations due to the mutual coupling lead to null filling and null position errors [53, 74]. The nulls introduced in the beam patterns of linear monopole arrays were found to be shifted or filled due to the mutual coupling [74]. Abele [53] studied the effect of the mutual coupling on the null pattern of a cylindrical dipole array and concluded that the coupling needed to be compensated for to prevent distortion of the null pattern characteristics. In this chapter, an investigation into the extent to which the mutual coupling has an influence on the null pattern of a cylindrical microstrip patch array was done.

The coupling in an array has an effect on the array imbedded radiation pattern of the element. Heberling et al. [17, 19] found that the main beam in the array imbedded radiation pattern is broadened by the coupling. In this chapter, the effects of the coupling on the array imbedded element radiation pattern were also investigated for an axially polarised patch array with N =10 and $d_\phi = 0.5\lambda_0$. Both simulated and measured results indicated a broadening in the main beam of the element pattern due to the coupling. It is thus important to use the array imbedded element pattern when

determining the excitation coefficients for a specified array radiation pattern in order to prevent distortion of the resulting array pattern.

For both polarisations, a cylindrical patch array was simulated to study the influence of the mutual coupling on an omnidirectional radiation pattern with a single null. It was seen that the gain ripple in the omni-region, as well as the null depth and width changed due to the coupling. The null position was also influenced. The null positions and null widths were more significantly affected for the circumferential polarisation, than for the axial polarisation. The radiation patterns of axially polarised arrays were less affected by the coupling for small inter-element spacing. This is due to the smaller coupling between the axially polarised patches. For large inter-element spacing, the element excitations were more sensitive to mutual coupling for both polarisations. From this study it was seen that in order to obtain the desired null patterns, the mutual coupling in the cylindrical patch arrays needed to be compensated for.

Given a required set of excitations, the geometries of the array elements can be varied to provide matched and equal driving impedances for all the antenna elements. Yang *et al* [86] proposed a mutual coupling compensation technique to obtain the desired bandwidth and voltage standing wave ratio (VSWR) at the resonant frequency for an electromagnetically coupled (EMC) dipole antenna array. For a given set of excitation voltages, the dipole lengths and dipole offsets from the microstrip feed line were altered to obtain the prescribed driving admittances seen by the feed lines. As a result, a good comparison was also found between the desired and measured radiation patterns. Chen [88, 89] varied the lengths and radii of the dipoles in linear and planar arrays to obtain the desired radiation patterns as well as equal driving impedances for the dipoles.

In this chapter, the above compensation technique was applied to linear and cylindrical microstrip patch antenna arrays. For the patch antenna elements the lengths and feed positions were varied to adjust the self and mutual impedances. The widths and heights of the patch antennae, were kept constant to reduce the dimensionality of the variable space of self-impedances. The self and mutual impedances were computed for linear spaced values of lengths and feed positions and were placed in lookup tables. These tables were used by a least squares optimisation algorithm which interpolated between the impedance values and determined the lengths and feed positions at which the driving impedances of all the patches were equal to 50Ω.

The lengths and feed positions of the cylindrical patch elements were varied to obtain matched driving impedances for a given set of excitations. The computed set of excitations was for a single null in an otherwise omnidirectional array pattern. For an axially polarised array, suitable lengths and feed-positions could be found within the available variable space for all the inter-elements spacing that was studied and null depths up to 40 dB. On the other hand, the higher mutual coupling in the circumferentially polarised patch arrays restricted the null depth for which the coupling could be compensated for using the described technique. For the smallest inter-element spacing studied ($d_\phi = 0.5\lambda_0$), the maximum realisable null depth was found to be 10 dB. As the inter-element spacing was increased, the possible null depth could be increased while still being able to correct the driving impedances by finding suitable lengths and feed positions within the available variable space.

To confirm the proposed coupling compensation experimentally, a four element linear microstrip patch array with E-plane coupling was used. The lookup tables were set up using a commercial electromagnetic software package which utilises the method of moments. The optimisation algorithm was then used to obtain the required lengths and feed positions to correct the driving impedances. A linear array was manufactured with the resulting dimensions to verify the improvement in the reflection coefficient characteristics at the input port of the array. Good agreement was obtained between the simulated and measured reflection coefficients. The compensation technique improved the resonant frequency to be within 0.1% of the desired frequency and the measured bandwidth was increased significantly.

An axially polarised cylindrical patch array was also designed and manufactured to confirm the effects of the mutual coupling on a desired null pattern. The active element patterns as well as the S-matrix were measured. The resulting pattern for the desired set of element excitations was determined using the measurement data and compared to the pattern obtained using simulated data. There was little difference between the null depths and null widths of the two patterns.

For the manufactured cylindrical patch array, the lengths and feed positions of the antenna elements were varied to correct the driving impedances for the desired set of element excitations. To study the resulting array null pattern after the mutual coupling compensation, the cylindrical array was simulated with the modified patch elements over the bandwidth of the isolated patch element. The resulting null patterns were

also compared to the null patterns before the mutual coupling compensation. Over the studied frequency band, the resulting null widths and depths compared well to the null widths and depths of the desired null pattern and varied little. The null positions were also improved over the whole frequency band. When the results at the centre frequency and the lowest frequency were compared, the ripple increased by 0.48 dB. Towards the highest frequency, the ripple increase was limited to 0.4 dB. The resulting gain ripple at the lowest and highest frequency differed by only 0.08 dB for the compensated array. This was an improvement on the ripple variation of 0.87 dB over the bandwidth for the uncompensated array.

For the cylindrical microstrip patch array used in the test case, the effect of the mutual coupling on the null pattern was not severe. If the changes in the null pattern characteristics are not severe and can be tolerated by the system which the antenna is integral to, the mutual coupling compensation is not needed. This can be an advantage, especially when the array is used in an adaptive system.

CHAPTER 5

CONCLUSIONS

The number of both unwanted directional interferences and strong nearby sources, which degrade the performance of a communication system, increase as communication networks expand. The signal-to-interference ratio (SIR) can be improved by using multiple nulls in the directions of the interferences while maintaining omnidirectional coverage in the direction of the users. In this thesis, cylindrical microstrip patch antenna arrays were investigated as an antenna to provide an omnidirectional radiation pattern with nulls at specified angular locations to suppress interference from directional sources.

5.1 Null synthesis using cylindrical microstrip patch arrays

Three null synthesis methods were described and used to provide the omnidirectional array pattern with nulls using the radiation characteristics of the cylindrical microstrip patch antenna elements. In addition, the implementation of the cylindrical microstrip patch array was investigated. The effect of coupling on the resulting null pattern was investigated and a mutual coupling compensation technique was applied to correct the array radiation pattern by adjusting the active driving impedances of the array elements.

Previously, Abele et al. [53] introduced a null synthesis technique for a cylindrical dipole

array. The technique utilised the orthogonal projection method and projected an idealised null pattern onto the orthogonal base of realisable array patterns. The resulting array pattern was an omnidirectional pattern with one or more nulls. Vescovo [56] extended the orthogonal projection method for an arc array with theoretical directional elements. A beam pattern was formed through the projection method and additional nulls were introduced in the pattern with null constraints to reduce the side lobe level. In this study, the null synthesis technique of Abele was extended to incorporate the directional radiation patterns of the cylindrical microstrip patches. The null synthesis technique was then used to form an omnidirectional radiation pattern with nulls at desired locations.

The orthogonal projection method was extended by modifying the orthogonal base for the space of realisable array patterns to include the radiation pattern characteristics of microstrip patches mounted on a conducting cylinder. The orthogonal base was modified for both axially and circumferentially polarised microstrip patch arrays. The unconstrained optimum element excitations obtained from the orthogonal projection method provided an optimal array pattern with the least pattern error. By applying a Hamming window to the sequence excitations before the element excitations were computed, the gain ripple in the omni-region was reduced. The influence of the array configuration on the resulting null pattern characteristics was investigated extensively for both patch array polarisations and a cylindrical array of dipoles. The resulting null pattern characteristics were compared for various numbers of elements and inter-element spacing. In most cases, the microstrip patch arrays yielded better gain ripple in the omni-region of the radiation pattern than dipole arrays.

Since the amplitude and phase of the radiation pattern were optimised simultaneously, the optimal array pattern may not have had the desired characteristics. When a small number of elements was used, the resulting gain ripple in the omni-region was high (more than 2-3 dB). Although the ripple was successfully decreased by using the windowing function of Abele [53], the resulting null width was increased. When maximum omni-coverage and narrow nulls are required, the increase in the null width is a disadvantage. Instead of only minimising the array pattern error, a multi-objective optimisation approach was followed [95–97]. The objective weighting method, previously applied in other fields of computational electromagnetic problems [96,97], was used to improve the amplitude pattern characteristics.

A global performance function was defined by utilising both the amplitude pattern error and the phase pattern error. The optimisation problem was solved by finding the critical ratio of the weights that were assigned to the two errors in the performance function. Each performance function was minimised by using an unconstrained minimisation algorithm [99]. The excitation vector obtained from the orthogonal projection method yielded an optimum radiation pattern with the minimum pattern error and was therefore chosen as the starting vector.

The excitation vector that minimised the performance function formed with the critical weight ratio, was used to form the radiation pattern. The objective weighting method provided a null pattern with a narrower and deeper null and with a higher gain ripple in the omni-region. An increase in the phase pattern error was observed due to the trade-off that existed between the two pattern errors in the performance function. Using this method, deep nulls could be obtained utilising only a small number of elements.

Another way of improving the resulting radiation pattern is to provide control over the individual characteristics. In some applications, the degree of suppression needs to be specified through a controllable null depth. Abele [54] proposed a variable phase step to provide control over the null depth. The accuracy of the resulting null depth depended on the array configuration and the desired null depth. Constrained optimisation provides a method of constraining the different attributes of the amplitude pattern while minimising the array pattern error. A constrained optimisation method was utilised to provide control over the different null pattern characteristics.

Previously, Prasad [45] applied the least squares optimisation method to circular and arc arrays to form a beam pattern with a specified beamwidth. Additional nulls were also placed in the sidelobe region by using null constraints while minimising the mean square difference between the desired pattern and the optimum pattern. The Hook and Jeeves algorithm was also used to perform an iterative search to find the optimum excitation vector while satisfying the null constraints. Ares *et al.* [52] used a simulated annealing technique to produce beam patterns for a circular arc array on a cylinder. A cost function, which could include terms to control the radiation pattern, was minimised. Terms which placed constraints on the excitations, could also be included in the cost function.

A constrained minimisation algorithm [99] was used in this study to yield an excitation vector which minimises the pattern error under the constraints specified for the different

null pattern characteristics (e.g. gain ripple in the omni-region, the null width and null depth). Individual characteristics as well as combinations of characteristics were controllable using the constrained optimisation. Due to the control provided by this method, the pattern characteristics became independent of the number of elements and the inter-element spacing. Multiple nulls with different null depths were also formed, while constraining the gain ripple.

The characteristics of the desired null pattern determine which null synthesis method should be used. When only a low gain ripple is required, the orthogonal projection method with a window function can be used. On the other hand, the objective weighting method can be used to obtain a narrow null when a higher gain ripple is tolerable. The resulting null depth for these two methods will depend on the number of elements as well as the inter-element spacing. The constrained optimisation method can be used to control both the null depth and the ripple, while obtaining a similar null width to that resulting from using the objective weighting method.

The influence of variation in the antenna element configuration on the remaining unconstrained pattern characteristics, while controlling certain null pattern characteristics, was studied. The null pattern characteristics for the axial polarisation were only slightly influenced by a change in the substrate height. The resulting ripple and null width for both polarisations were influenced by a change in the dielectric constant, when the null depth was constrained. The degree to which the unconstrained characteristics of the resulting null pattern changed as the null position was varied, also depended on the polarisation. The sensitivity of the resulting null pattern characteristics to a change in the desired null position or a change in an antenna element characteristic, can be minimised by a careful selection of the element pattern.

5.2 Implementation of cylindrical microstrip patch arrays

A study on the implementation of the cylindrical microstrip patch array was also done. The simulation of the cylindrical microstrip patch element was discussed and both simulated and measured results were compared. The patch antenna elements were simulated and designed using a Finite Difference Time Domain (FDTD) software

package [101]. The resulting reflection coefficient characteristics differed from the desired characteristics due to approximations made in the simulation of the cylindrical patch elements and due to the manufacturing tolerances. For both polarisations, the simulated and measured element radiation patterns compared well within the area of the main beam and differed slightly for the rest of the radiation pattern.

The nulls introduced in the beam patterns of linear monopole arrays were found to be shifted or filled due to mutual coupling [74]. Abele [53] studied the effect of the mutual coupling on the null pattern of a cylindrical dipole array and concluded that the coupling needed to be compensated for to prevent distortion of the null pattern characteristics. In this study, the extent to which the mutual coupling affected the characteristics of both linear and cylindrical narrowband patch arrays, was investigated.

Firstly, the extent to which the mutual coupling affected the reflection coefficient and bandwidth at the input port of a narrowband linear microstrip array, was studied. This investigation was conducted in order to study the improvement in the bandwidth due to the use of a mutual coupling compensation technique. For a narrowband linear microstrip array, both the minimum of the reflection coefficient at the input port of the feeding network and the resonant frequency were influenced by the mutual coupling. For a horizontally polarised array with $d_\phi = 0.5\lambda_0$, a coupling factor of -10.4 dB altered the resonant frequency to such an extent that the active bandwidth fell outside the desired bandwidth of the array. The resonant frequency and bandwidth were less affected for a vertically polarised array due to the smaller magnitude of the coupling ($<$ -16.2 dB).

For the cylindrical microstrip patch arrays, the influence of the mutual coupling on the null patterns was also studied. It was seen that the gain ripple in the omni-region, as well as the null depth, width and position were changed by the coupling. The null positions and null widths were more significantly affected for the circumferential polarisation. For a circumferentially polarised array with $d_\phi = 0.5\lambda_0$, the null position changed by 3.25° and the null width increased by 7.8°. For small inter-element spacing, the radiation patterns of axially polarised arrays were less affected by the coupling. For large inter-element spacing ($d_\phi = 0.7\lambda_0$), the gain ripple in the omni-region changed significantly for both polarisations due to the mutual coupling. The gain ripple changed from 1 dB to 4.63 dB and 2.55 dB for the circumferential and axial polarisations, respectively.

From this study, it was evident that the null patterns of the cylindrical patch arrays were affected by the mutual coupling. To match the desired and active characteristics of the patch arrays, a mutual coupling compensation technique was utilised. Chen [88,89] varied the lengths and radii of the dipoles in linear and planar arrays to obtain the desired radiation patterns as well as equal driving impedances for the dipoles. For the patch antenna elements, the lengths and feed positions were varied to provide matched and equal driving impedances for all the antenna elements given a required set of excitations. The lengths and feed positions at which the driving impedances of all the patches were equal to 50Ω, were determined.

For an axially polarised cylindrical array, suitable lengths and feed-positions were found for all the inter-elements spacing that were studied and null depths up to 40 dB. For small inter-element spacing, the higher mutual coupling in the circumferentially polarised patch arrays restricted the null depth for which the coupling could be compensated for using the described technique. For the smallest inter-element spacing studied ($d_\phi = 0.5\lambda_0$), the maximum null depth for which the coupling could be compensated for was found to be 10 dB. As the inter-element spacing was increased, the possible null depth could be increased while still being able to correct the driving impedances by finding suitable lengths and feed positions within the available variable space.

In the first test case, the compensation technique improved the resonant frequency of a linear microstrip patch array ($N = 4$, $d_\phi = 0.5\lambda_0$) to be within 0.1% of the desired frequency and the measured bandwidth (for VSWR < 1.5) of the array was increased significantly from 2.3% to 3.9%.

For the second test case, an axially polarised cylindrical patch array was used with $N = 10$ and $d_\phi = 0.5\lambda_0$. The lengths and feed positions of the antenna elements were varied to correct the driving impedances for the desired set of element excitations. Over the element bandwidth of 3.7% for VSWR < 2, the resulting null widths and depths compared well to the null widths and depths of the desired null pattern after applying the compensation technique. The null positions were also improved over the whole bandwidth. The resulting gain ripple at the lowest and highest frequency differed by only 0.08 dB for the compensated array. This was an improvement on the ripple variation of 0.87 dB over the bandwidth for the uncompensated array.

The configuration of a cylindrical microstrip patch array thus plays an important role in the null pattern synthesis. The patch antenna element configuration, the inter-element

spacing and the number of elements should all be chosen carefully in order to obtain the desired null pattern as well as the specified driving impedances. The magnitude of the mutual coupling will also influence the choice of the inter-element spacing with the aim of obtaining the desired pattern while compensating for the coupling.

The effect of the mutual coupling on the null pattern was not severe for the cylindrical microstrip patch array used in the test case. The null depth decreased by 3.4 dB and the null width increased by 2.9°, while the ripple and null position varied little. If the changes in the null pattern characteristics are not severe and it can be tolerated by the system which the antenna is integral to, the mutual coupling compensation is not needed. This can be an advantage, especially when the array is used in an adaptive system.

REFERENCES

[1] J. Bartolić, Z. Šipuš, N. Herscovici, D. Bonefačić, and R. Zentner, "Planar and cylindrical microstrip patch antennas and array for wireless communications", *11th Int. Conf. on Antennas Propag.*, Conference Publication, No. 480, pp. 569-573, April 2001.

[2] L.C. Godara, "Applications of antenna arrays to mobile communications, Part I: Performance improvement, feasibility, and system considerations", *Proc. IEEE*, vol. 85, no. 7, pp. 1031-1060, July 1997.

[3] L.C. Godara, "Applications of antenna arrays to mobile communications, Part II: Beam-forming, and direction-of-arrival considerations", *Proc. IEEE*, vol. 85, no. 8, pp. 1195-1245, August 1997.

[4] W.H. Kummer, "Basic array theory", *Proc. IEEE*, vol. 80, no. 1, pp. 127-139, January 1992.

[5] K.R. Carver and J.W. Mink, "Microstrip antenna technology", *IEEE Trans. Antennas Propag.*, vol. 29, no. 1, pp. 2-24, January 1981.

[6] W.F. Richard, Y.T. Lo and D.D. Harrison, "An improved theory for microstrip antennas and applications", *IEEE Trans. Antennas Propag.*, vol. 29, no. 1, pp. 38-46, January 1981.

[7] C.M Krowne, "Cylindrical-rectangular microstrip antenna", *IEEE Trans. Antennas Propag.*, vol. 31, no. 1, pp. 194-199, January 1983.

[8] J. Ashkenazy, S. Shtrikman and D. Treves, "Electric surface current model for the analysis of microstrip antennas on cylindrical bodies", *IEEE Trans. Antennas Propag.*, vol. 33, no. 3, pp. 295-300, March 1985.

[9] I. Jayakumar, R. Garg, B.K. Sarap and B. Lal, "A conformal cylindrical microstrip array for producing omnidirectional radiation pattern", *IEEE Trans. Antennas Propag.*, vol. 34, no. 10, pp. 1258-1261, October 1986.

[10] J.S. Dahele, R.J. Mitchell, K.M. Luk and K.F. Lee, "Effect of curvature on characteristics of rectangular patch antenna", *Electron. Lett.*, vol. 23, no. 14, pp. 748-749, July 1987.

[11] E.V. Sohtell, *Microwave antennas on cylindrical structures*, Ph.D. Thesis, Chalmers University of Technology, Sweden, September 1987.

[12] J. Ashkenazy, S. Shtrikman and D. Treves, "Conformal microstrip arrays on cylinders", *IEE Proc. Microw. Antennas Propag.*, vol. 135, no. 2, pp. 132-134, April 1988.

[13] K. Luk, K. Lee and J.S. Dahele, "Analisys of the cylindrical-rectangular patch antenna", *IEEE Trans. Antennas Propag.*, vol. 37, no. 2, pp. 143-147, February 1989.

[14] T.M. Habashy, S.M. Ali and J.A. Kong, "Input impedance and radiation pattern of cylindrical-rectangular and wraparound microstrip antennas", *IEEE Trans. Antennas Propag.*, vol. 38, no. 5, pp. 722-731, May 1990.

[15] C.M. da Silva, F. Lumini, J.J. da S. Lacava and F.P. Richards, "Analysis of cylindrical array of microstrip rectangular patches", *Electron. Lett.*, vol. 27, no. 9, pp. 778-780, April 1991.

[16] C.F. Huang, "Simple high-frequency diffraction analysis of microstrip antenna on large cylinder", *Electron. Lett.*, vol. 27, no. 13, pp. 1161-1163, June 1991.

[17] D. Heberling, H.J. Scmmitt and W.Brimes, "Experimental investigations on conformal microstrip antenna arrays", *Int. Symp. of Antennas Propag. Soc.*, AP-S Digest, pp. 584-587, June 1991.

[18] F. da Costa Silva, S.B. de Assis Fonseca, A.J.M. Soares and A.J. Giarola, "Analysis of microstrip antennas on circular-cylindrical substrates with a dielectric overlay", *IEEE Trans. Antennas Propag.*, vol. 39, no. 9, pp. 1398-1403, September 1991.

[19] D. Heberling and C. V. Winterfeld, "Investigations on mutual coupling effects in polametric conformal patch arrays", *IEE Int. Conf. on Radar*, pp. 118-121, October 1992.

[20] K. Wong, Y. Cheng and J. Row, "Resonance in a superstrate-loaded cylindrical-rectangular microstrip structure", *IEEE Trans. Antennas Propag.*, vol. 41, no. 5, pp. 814-819, May 1993.

[21] A. Hoorfar, K.C. Gupta and D.C. Chang, "Effects of cylindrical curvature on radiation from a microstrip antenna with a thick cover layer", *Microw. Optic. Tech. Lett.*, vol. 6, no. 13, pp. 762-766, October 1993.

[22] S. Ke and K. Wong, "Input impedance of a probe-fed superstrate-loaded cylindrical-rectangular microstrip antenna", *Microw. Optic. Tech. Lett.*, vol. 7, no. 5, pp. 232-236, April 1994.

[23] W.Y. Tam, A.K.Y. Lai and K.N. Luk, "Cylindrical rectangular microstrip antennas with coplanar parasitic patches", *IEE Proc. Microw. Antennas. Propag.*, vol. 142, no. 4, pp. 300-306, August 1995.

[24] J. Chen and K. Wong, "Mutual coupling computation of cylindrical-rectangular microstrip antennas using cavity-model theory", *Microw. Optic. Tech. Lett.*, vol. 9, no. 6, pp. 323-326, August 1995.

[25] K. Wong, S. Wang and S. Ke, "Measured input impedance and mutual coupling of rectangular microstrip antennas on a cylindrical surface", *Electron. Lett.*, vol. 11, no. 1, pp. 49-50, January 1996.

[26] A. Herschlein, G.Gottwald and W. Wiesbeck, "Patch antennas on finite and infinite cylindrical surface structures", *IEEE Int. Symp. on Phased Array Systems and Technology*, pp. 168-170, October 1996.

[27] J. Jin, A. Berrie, R. Kipp and S. Lee, "Calculation of radiation patterns of microstrip antennas on cylindrical bodies of arbitrary cross section", *IEEE Trans. Antennas Propag.*, vol. 45, no. 1, pp. 126-132, January 1997.

[28] K. Wong and G. Hsieh, "Curvature effects on the radiation patterns of cylindrical microstrip arrays", *Microw. Optic. Tech. Lett.*, vol. 18, no. 3, pp. 206-209, June 1998.

[29] K. Wong, *Design of Nonplanar Microstrip Antennas and Transmission Line*, Wiley Interscience, New York, USA, 1999.

[30] W. Yu, N. Farahat and R. Mittra, "Application of FDTD method to conformal patch antennas", *IEE Proc. Microw. Antennas Propag.*, vol. 148, no. 3, pp. 218-220, June 2001.

[31] H.T. Anastassiu, A.I. Kostaridis, C.G. Biniaris and D.I. Kaklamani, "Analysis of cylindrically conformal microstrip patch arrays via modified method of auxiliary sources", *Electron. Lett.*, vol. 38, no. 25, pp. 1621-1622, December 2002.

[32] E.V. Sohtell, "Microstrip patch phased array on a cylinder", *Int. Symp. Antennas Propag. Soc.*, AP-S Digest, pp. 1152-1155, June 1988.

[33] C. Alakija, "A mobile base station phased array antenna", *IEEE Int. Conf. on Selected Topics in Wireless Comm.*, Conf. Proc., pp. 120-121, June 1992.

[34] D. Löffler, F. Rostan and W. Wiesbeck, "Conformal microstrip patch array for SDMA applications", *Int. Symp. Antennas Propag. Soc.*, AP-S Digest, vol. 3, pp. 1533-1536, July 1997.

[35] D. Löffler, W. Wiesbeck and B. Johannisson, "Conformal aperture coupled microstrip phased array on a cylindrical surface", *Int. Symp. Antennas Propag. Soc.*, AP-S Digest, vol. 2, pp. 882-885, August 1999.

[36] D. Löffler, E. Gschwendtner and W. Wiesbeck, "Design and measurement of conformal antennas on cylindrical and spherical geometries", *AFRICON 1999 Proc.*, vol. 2, pp.1005-1010, October 1999.

[37] M. Kanghou and X. Menglin, "A study of conformal microstrip antenna array on a cylinder", *5th Int. Symp. on Antennas, Propag. and Electomag. Theory*, ISAPE 2000 Digest, pp. 18-21, 2000.

[38] R.J. Allard and D.H. Werner, "A flexible analysis and design approach for body-mounted conformal microstrip antennas", *Int. Symp. Antennas Propag. Soc.*, AP-S Digest, vol. 1, pp. 766-769, 2002.

[39] W.Wiesbeck, M. Younis and D. Löffler, "Design and measurement of conformal arrays", *Int. Symp. Antennas Propag. Soc.*, AP-S Digest, vol. 1, pp. 84-87, 2002.

[40] C.S. Lee, T. Hsieh and P. Chen, "Electrically steerable cylindrical microstrip array antenna", *Microw. Optic. Tech. Lett.*, vol. 36, no. 5, pp. 386-387, March 2003.

[41] J.C. Lim and D.E.N. Davies, "Synthesis of a single null response in an otherwise omnidirectional pattern using a circular array", *Proc. IEEE*, vol. 122, no. 4, pp. 349-352, April 1975.

[42] F. Rostan, G. Gottwald and W. Wiesbeck, "Design and performance of conformal microstrip patch arrays on cylindrical surfaces", *Proc. EuMC*, pp. 1756-1761, Cannes, 1994.

[43] J.C. Lim, "Introduction of a sharp steerable null in an otherwise omnidirectional pattern using a circular array", *Radio and Electron. Eng.*, vol. 47, no. 1/2, pp. 30-32, January 1977.

[44] D.E.N. Davies and M. Rizk, "A broadband experimental null-steering antenna system for mobile communications", *Radio and Electron. Eng.*, vol. 122, no. 4, pp. 349-352, October 1977.

[45] S. Prasad and R. Charan, "On the constrained synthesis of array patterns with applications to circular and arc arrays", *IEEE Trans. Antennas Propag.*, vol. 32, no. 7, pp. 725-730, July 1984.

[46] N. Inagaki, "Null synthesis based on the principle of pattern multiplication", *Electron. Commun. in Japan*, vol. 73, no. 5, pp. 1-11, 1990.

[47] X. Yang and M.H. Er, "Formulation of a single controlled null in an omnidirectional pattern using a circular array", *J. of Elec. Electron. Eng. - IE Aust. and IEEE Aust.*, vol. 12, no. 3, pp. 318-322, September 1992.

[48] M.J. Mismar, "Null steering using the minimax approximation by controlling only the current amplitudes", *Int. J. Electron.*, vol. 78, no. 2, pp. 409-415, 1995.

[49] S.R. Nagesh and T.S. Vedavathy, "A procedure for synthesizing a specified sidelobe topography using an arbitrary array", *IEEE Trans. Antennas Propag.*, vol. 43, no. 7, pp. 742-745, July 1995.

[50] R. Vescovo, "Constrained and unconstrained synthesis of array factor for circular arrays", *IEEE Trans. Antennas Propag.*, vol. 43, no. 12, pp. 1405-1410, December 1995.

[51] R. Vescovo, "Pattern synthesis with null constraints for circular arrays of equally spaced isotropic elements", *IEE Proc. Microw. Antennas. Propag.*, vol. 143, no. 2, pp. 103-106, April 1996.

[52] J.A. Ferreira and F. Ares, "Pattern synthesis of conformal arrays by the simulated annealing technique", *Electron. Lett.*, vol. 33, no. 14, pp. 1187-1189, July 1997.

[53] J. Abele, J. Joubert, J.W. Odendaal, "Introduction of multiple nulls in otherwise omnidirectional pattern of circular dipole array", *Electron. Lett.*, vol. 30, no. 14, pp. 1371-1373, July 1998.

[54] J. Abele, J. Joubert, J.W. Odendaal, "Introduction of multiple nulls with controllable depths in an omnidirectional pattern of a circular array", *Signal Proces.*, vol. 80, pp. 141-149, 2000.

[55] R. Vescovo, "Null synthesis by phase control for antenna arrays", *Electron. Lett.*, vol. 36, no. 3, pp. 198-199, February 2000.

[56] R. Vescovo, "Use of directional elements in the null synthesis for arc arrays", *IEEE Antennas Propag. Soc. Symp. Digest*, pp. 736-739, 1998.

[57] E. Botha, *Contributions to the synthesis of planar and conformal arrays*, Ph.D. Thesis, University of Pretoria, South Africa, August 2000.

[58] C.M. Krowne and A.R. Sindores, "H-plane coupling between rectangular microstrip antennas", *Electron. Lett.*, vol. 16, no. 6, pp. 211-213, March 1980.

[59] C.M. Krowne, "E-plane coupling between two rectangular microstrip antennas", *Electron. Lett.*, vol. 16, no. 16, pp. 635-636, July 1980.

[60] R.P. Jedlicka, M.T. Poe and K.R. Carver, "Measured mutual coupling between microstrip antennas", *IEEE Trans. Antennas Propag.*, vol. 29, no. 1, pp. 147-149, January 1981.

[61] P.H. Pathak and N. Wang, "Ray analysis of mutual coupling between antennas on a convex surface", *IEEE Trans. Antennas Propag.*, vol. 29, no. 6, pp. 911-922, November 1981.

[62] D.M. Pozar, "Input impedance and mutual coupling of rectangular microstrip antennas", *IEEE Trans. Antennas Propag.*, vol. 30, no. 6, pp. 1191-1196, November 1982.

[63] E.H. Van Lil and A.R. Van de Capelle, "Transmission line model for mutual coupling between microstrip antennas", *IEEE Trans. Antennas Propag.*, vol. 32, no. 8, pp. 816-821, August 1984.

[64] A. Benalla and K.C. Gupta, "Multiport network approach for modeling the mutual coupling effects in microstrip patch antennas and arrays", *IEEE Trans. Antennas Propag.*, vol. 37, no. 2, pp. 148-152, February 1989.

[65] L.D. Bamford, P.S. Hall and A.Fray, "Calculation of antenna mutual coupling from far radiated fields", *Electron. Lett.*, vol. 29, no. 14, pp. 1299-1301, July 1993.

[66] S. Ke and K. Wong, "Full-wave analysis of mutual coupling between cylindrical-rectangular microstrip antennas", *Microw. Optic. Tech. Lett.*, vol. 7, no. 9, pp. 419-421, June 1994.

[67] W.Y. Tam, K.Y. Lai and K.M. Luk, "Mutual coupling between cylindrical rectangular microstrip antennas", *IEEE Trans. Antennas Propag.*, vol. 43, no. 8, pp. 897-899, August 1995.

[68] C.Y. Huang and Y.T. Chang, "Curvature effects on the mutual coupling of cylindrical-rectangular microstrip antennas", *Electron. Lett.*, vol. 33, no. 13, pp. 1108-1109, June 1997.

[69] J.Byun, B. Lee and F.J. Harakiewics, "FDTD analysis of mutual coupling between microstrip patch antennas on curved surfaces", *IEEE Antennas Propag. Soc. Symp. Digest*, pp. 886-889, 1999.

[70] T. Su and H. Ling, "On modeling mutual coupling in antenna arrays using the coupling matrix", *Microw. Optic. Tech. Lett.*, vol. 28, no. 4, pp. 231-237, February 2001.

[71] V.B Ertürk and R.G Rojas, "Efficient analysis of input impedance and mutual coupling of microstrip antennas mounted on large coated cylinders", *IEEE Trans. Antennas Propag.*, vol. 51, no. 4, pp. 739-749, April 2003.

[72] M. Rammel, D. Eclercy, A. Reineix and B.Jecko, "Study of the mutual coupling effect on radiated patterns of antenna arrays", *IEE Proc. Microw. Antennas. Propag.*, vol. 144, no. 5, pp. 389-391, October 1997.

[73] I.J. Gupta and A.A. Ksienski, "Effect of mutual coupling on the performance of adaptive arrays", *IEEE Trans. Antennas Propag.*, vol. 31,no. 9, pp. 785-791, September 1983.

[74] K.W. Lo and T.B. Vu, "Minimisation of mutual coupling effect on null steering by using guard elements", *Electron. Lett.*, vol. 23, no. 16, pp. 854-855, July 1987.

[75] K.W. Lo and T.B. Vu, "Simple S-parameter model for receiving antenna array", *Electron. Lett.*, vol. 24, no. 20, pp. 1264-1266, September 1988.

[76] H. Steyskal and J.S. Herd, "Mutual coupling compensation in small array antennas", *IEEE Trans. Antennas Propag.*, vol. 38, no. 12, pp. 1971-1975, December 1990.

[77] D. Eclercy, M. Rammel, A. Reieneix and B. Jecko, "Compensation for the mutual coupling effect on a synthesized pattern array", *Microw. Optic. Tech. Lett.*, vol. 12, no. 1, pp. 50-52, May 1996.

[78] R.S. Adve and T.K. Sarkar, "Elimination of the effect of mutual coupling in an adaptive nulling system with a look direction constraint", *IEEE Antennas Propag. Soc. Symp. Digest*, pp. 1164-1167, 1996.

[79] A.G. Derneryd, "Compensation of mutual coupling effects in array antennas", *IEEE Antennas Propag. Soc. Symp. Digest*, pp. 1122-1125, 1996.

[80] P.N. Fletcher, A.E. Wicks and M. Dean, "Improvement of coupling corrected difference beams in small phased arrays", *Electron. Lett.*, vol. 33, no. 5, pp. 352-353, February 1997.

[81] L.D. Bamford, J.R. James and A.F. Fray, "Minimising mutual coupling in thick substrate microstrip antenna arrays", *Electron. Lett.*, vol. 33, no. 8, pp. 648-650, April 1997.

[82] P. Darwood, P.N. Fletcher and G.S. Hilton, "Mutual coupling compensation in small array antennas", *IEE Proc. Microw. Antennas. Propag.*, vol. 145, no. 1, pp. 1-6, February 1998.

[83] L. Josefsson and P. Persson, "Conformal array synthesis including mutual coupling", *Electron. Lett.*, vol. 35, no. 8, pp. 625-627, April 1999.

[84] G. D'Elia, F. Soldovieri and G. di Massa, "Mutual coupling compensation in a power synthesis technique of planar array antennas, *IEE Proc. Microw. Antennas. Propag.*, vol. 147, no. 2, April 2000.

[85] L. Caccavale, T. Isernia and F. Soldovieri, "Methods for optimal focusing of microstrip array antennas including mutual coupling", *IEE Proc. Microw. Antennas. Propag.*, vol. 147, no. 3, June 2000.

[86] H.Y. Yang, N.G. Alexopoulos, P. M. Lepeltier and G.J. Stern, "Design of transversely fed EMC microstrip dipole arrays including mutual coupling", *IEEE Trans. Antennas Propag.*, vol. 38, no. 2, pp. 145-151, February 1990.

[87] K. Ghorbani and R.B. Waterhouse, "Design of large broadband patch arrays", *IEEE Antennas Propag. Soc. Symp. Digest*, pp. 928-931, 1999.

[88] W. Chen and S.M. Zhang, "Design of dipole arrays with equal element impedances", *Electron. Lett.*, vol. 28, no. 22, pp. 2048-2049, October 1992.

[89] W. Chen, L. Jen and S.M. Zhang, "Planar dipole arrays with equal element input impedances", *Electron. Lett.*, vol. 31, no. 24, pp. 2061-2062, November 1995.

[90] P. Niemand, J. Joubert and J.W. Odendaal, "Multiple null synthesis in an otherwise omnidirectional pattern of a cylindrical microstrip array", *Antennas Propag. 2000 Proc.*, vol. 1, pp. 627, April 2000.

[91] P. Niemand, J. Joubert and J.W. Odendaal, "Cylindrical microstrip array for interference suppression", *SATCAM 2000 Proceedings*, AP/BEM Technical Session, Paper no. 99, September 2000.

[92] P. Niemand, J. Joubert, and J.W. Odendaal, "Null forming synthesis for cylindrical patch arrays, *Microw. Optic. Tech. Lett.*, vol. 32, no. 6, pp. 442-446, March 2002.

[93] P. Niemand, J.W. Odendaal and J. Joubert, "Practical considerations for interference suppression cylindrical arrays", *AFRICON 2002 Proc.*, Paper no. HFTA-7, October 2002.

[94] P. Niemand, J. Joubert and J.W. Odendaal, "Practical considerations for interference suppression cylindrical arrays", *Trans. of SAIEE*, vol. 94, no. 2, pp. 37-39, July 2003.

[95] D.E. Goldberg, *Genetic algorithms in search, optimization, and machine learning*, Addison-Wesley, New York, USA, 1989.

[96] S. Russenschuck, "Pareto optimization in computational electromagnetics", /em Int. Journal of Appl. Electromagnetics in Materials, no. 4, pp. 83-92, 1993.

[97] C.A. Borghi, M. Fabbri, P. Di Barba and A. Savini, "Loney's solenoid multi-objective optimization problem", *IEEE Trans. Magnetics*, vol. 35, no. 3, pp. 1706-1709, May 1999.

[98] R.F. Harrington, *Time-harmonic electromagnetic fields*, MacGraw-Hill, New York, 1961.

[99] Optimization Toolbox, *MATLAB*, Version 5.1.0.421, The Mathworks, Inc., Copyright 1984-1997.

[100] *Ie3d*, Version 5.1, Zeland Software Inc., Copyright 1993-1999.

[101] *Concerto*, Version 2.0, Vector Fields Inc., Copyright 1997-2001.